MODELING BIPHASIC REACTORS, EMULSIONS

AND SELECETION OF SOLVENTS

By

MENELIK NEGASH

Bachelor of Science in Chemical Engineering
Bahir Dar University
Bahir Dar, Ethiopia
2004

Master of Science in Chemical Engineering
Addis Ababa University
Addis Ababa, Ethiopia
2010

Submitted to the Faculty of the
Graduate College of the
Oklahoma State University
in partial fulfillment of
the requirements for
the Degree of
DOCTOR OF PHILOSOPHY
July, 2017

MODELING BIPHASIC REACTORS, EMULSIONS

AND SELECETION OF SOLVENTS

Dissertation Approved:

Dr. Brian Neely

Dissertation Adviser

Dr. Sundararajan Madihally

Dr. Jindal Shah

Dr. Clint Aichele

Dr. Martin Hagan

ACKNOWLEDGEMENTS

I would like to thank Dr. Brian Neely who helped me set a high standard for myself, encouraged me to always struggle to achieve my objectives, and saw the best in me even when I cannot. My regards to him will always stand at the highest position.

I am very grateful to Dr. Sundararajan Madihally with utmost respect for his relentless caring and supporting starting from the first day at OSU. Much of my final semester work, write-ups, and my graduation in general would have been possible due to his help.

My appreciation and utmost respect also goes to my committee members Dr. Clint Aichele, Dr. Martin Hagan and Dr. Jindal Shah. Your patience and help, and the encouragement I received caries me through all the way to the last day and will always remember in the future.

I would also like to thank Dr. Robert L. Robinson. Jr. who introduced me to the world of scientific inquiry, the quest for more evidence and more information, clarity of ideas and, scrutiny of opinions.

My deepest gratitude also passes to Dr. Khaled A. Gasem who opened the door for me to study my PhD at OSU. Although I did not have the privilege to work with him, the few classes I took with him were enough to inspire and gave me strength to go through the hard work that a PhD requires.

My Special thanks also goes to Dr. Solomon Gebreyohannes, Mr. Christian Odaffin, Dr. Sayeed Mohammed for having been like a friend, a brother and a mentor to me.

I would like to thank Mrs. Eilleen Nelson for offering to proof read some of the materials in this work.

Finally, I am very grateful for my family, friends, staff, and faculty for thier contributions towards the success of my PhD work.

Name: MENELIK NEGASH

Date of Degree: July, 2017

Title of Study: MODELING BIPHASIC REACTORS, EMULSIONS AND SELECETION OF SOLVENTS

Major Field: CHEMICAL ENGINEERING

Abstract

Modeling biphasic reactors (BPRs) facilitates understanding the dynamics between the kinetics and component phase distribution between the two partially miscible phases of the reactor. Using experimental results for bio oil upgrading, an algorithm for the modeling of biphasic reactors describing both reaction kinetics and phase separation was implemented using the simulation of a heterogeneous liquid phase hydrogenation of p-hydroxy benzaldehyde to 4-methylcyclohexanol in a water-decalin mixture. The reaction was represented by the Eley-Rideal type surface reaction mechanism. The Non-Random Two-Liquid (NRTL) phase equilibria model and an interfacial mass transfer model based on the two-film theory was used to assess for representation of the component phase distribution. Aspen Plus and Excel-VBA were used for simulation the reactor. Optimizations was performed to estimate the volumetric interfacial area available for mass transfer. Gibbs energy test was performed to confirm if simultaneous reaction and phase distribution is thermodynamically possible.

Quantitative Structure Property Relation (QSPR) based Linear and non-linear models were used to model emulsion properties such as drop size, emulsion fraction, and emulsion type. The model was validated using experimental data, which includes the effects of the water fraction and the organic compounds used on the emulsion properties. The results of the emulsion modeling were used as a basis for selecting a new solvent with the desired emulsion properties such as selective solubility, drop size and type of emulsion, for use in an emulsion formulation and a BPR. QSPR models for emulsion properties, partition and mass transfer coefficient correlation were used to evaluate performances of different solvents for emulsion development for biphasic reactor.

The simulation results showed that biphasic reactor could offer selectivity of reaction in the desired phase, separation of products with increased organic phase solubility, and continuation of the upgrading process in the presence of component phase-distribution. The coefficient of determination values for emulsion property modeling are also comparable or better than values reported for QSPR modeling for other emulsion properties. The importance of emulsion modeling and solvent selection for BPRs was demonstrated successfully.

TABLE OF CONTENTS

Chapter Page

I. INTRODUCTION 1

1.1. Background 1
1.2. Objectives 5
1.3. Thesis organizations 8
REFERENCES 9

II. MODELING AND SIMULATION OF BIOFUEL UPGRADING CATALYTIC BIPHASIC REACTIONS AT THE WATER/OIL INTERFACE; A PHASE EQUILIBRIA APPROACH 11

2.1. Introduction 11
2.2. Methods 14
2.2.1. Simulation strategy 14
2.2.2. Kinetic model derivation 15
2.2.3. Estimation of kinetic parameters 19
2.2.4. Thermodynamic property model 20
2.2.5. Sources of NRTL binary parameters 21
2.2.6. Simulation in Aspen Plus using user defined kinetic models in Excel-VBA 22
2.2.7. Activity coefficient and Gibbs energy test 23
2.3.Results and discussion 24
2.3.1. Model prediction and simulation results 25
2.3.2. Gibbs energy analysis 36
2.3.3. Activity coefficient analysis 27
2.4.Conclusions 28
REFERENCES 37

III. MODELING AND SIMULATION OF BIOFUEL UPGRADING CATALYTIC BIPHASIC REACTIONS AT THE WATER/OIL INTERFACE; A MASS TRANSFER APPROACH 39

3.1. Introduction 39
3.2. Methods 42
3.2.1. Simulation strategy 42
3.2.2. Kinetic model derivation 44
3.2.3. Kinetic parameter determination 46

3.2.4. Mass transfer model derivation....47
3.2.5. Mass transfer parameters estimation....51
3.2.6. Calculation of water and decalin solubility....54
3.2.7. Optimization of mass transfer module....54
3.2.8. Activity coefficient and Gibbs energy test....55
3.3. Results and discussion....57
3.3.1. Model and simulation results....57
3.3.2. Gibbs Energy analysis....59
3.3.3. Activity coefficient analysis....59
3.4. Conclusions....60
REFERENCES....61

IV. MODELING AND SIMULATION OF BIOFUEL UPGRADING CATALYTIC BIPHASIC REACTIONS AT THE WATER/OIL INTERFACE; A MASS TRANSFER APPROACH....69

4.1. Introduction....69
4.2. Methods....71
4.2.1. Available data....71
4.2.2. Data classification....73
4.2.3. Descriptor reduction....74
4.2.4. Prediction models for ADF and EF....74
4.2.5. Prediction model for effects of water cut on ADS....74
4.2.6. Prediction models for ET....75
4.3. Results and discussion....76
4.3.1. ADS modeling....76
4.3.2. EF modeling....76
4.3.3. ET modeling....77
4.3.4. Modeling effect of water cut on ADS....78
4.3.5. Descriptors used for model development....78
4.4. Conclusions....79
REFERENCES....90

V. SOLVENT SELECTION FOR BIPHASIC REACTORS....92

5.1. Introduction....92
5.2. Methods....94
5.2.1. Preselection of solvents....94
5.2.2. Solvent screening algorithm....94
5.2.3. Emulsion property model development....94
5.2.4. Calculation of partition coefficients....95
5.2.5. Calculation of mass transfer constants....95
5.3. Results and discussion....99
5.3.1. Emulsion property modeling results....99
5.3.2. Estimation of diffusivity....100
5.3.3. Estimation partition coefficients....100

5.3.4. Estimation of mass transfer coefficients 101
5.4. Conclusions 101
6. REFERENCES 110

VI. CONCLUSIONS AND RECOMMENDATIONS 112

6.1. Conclusions 112
6.1.1. Modeling and simulation of biofuel upgrading catalytic biphasic reaction at the water/oil interface; a phase equilibria approach 113
6.1.2. Modeling and simulation of biofuel upgrading catalytic biphasic reaction at the water/oil interface; a mass transfer approach 115
6.1.3. Modeling effects of solvent type and water cut on emulsion characteristics using quantitative structure property relationship (QSPR)
6.1.4. Solvent selection for biphasic reactors 116
6.2. Recommendations 117

APPENDICES 119
A. Regression of NRTL binary parameters 119
B. *A priori* prediction of NRTL parameters 123
C. Molar Enthalpy and Molar Gibbs Energy change for each reaction 124
D. Best descriptor values used for the emulsion property model 126
E. Rate equations using Euler's method 127

LIST OF TABLES

Table Page

2.1. Prototype reactor operating conditions 29
2 2. Source of NRTL binary parameters for the simulations 29
2.3. Regressed kinetic parameters and mass transfer coefficients 30
2.4. Changes in chemical compositions from experiments in a biphasic reactor 30
2 5. Predictions results obtained using different NRTL binary parameter sources 31
3.1. Prototype reactor operating conditions 61
3.2. RMSE comparison for simulation result of Biphasic reactor modeling with phase equilibria and mass transfer. 61
4.1. Effect of solvent type on emulsion properties 80
4.2. Effect of water fraction on droplet size of the emulsion.....81
4.3. Five best descriptors used in the QSPR model for emulsion fraction 82
5.4. Solvents selected for evaluation of mass transfer coefficient for BPR.....110
5.5. Solvent database used for building emulsion property model 103
5.6. Effect of Reynold number and mass transfer direction on mass transfer coefficient 104
5.7. Emulsion property model results for target solvents. 105
5.8. Partition coefficient estimation using UNIFAC and regression by Aspen Plus .106
5.9. Diffusivity calculation results for p-cresol and 4-MECH in all solvents using the Sitaraman correlation 107
5.10. Results of mass transfer coefficient calculations for mass transfer from the aqueous phase to organic phase. 108

LIST OF FIGURES

Figure Page

1.1. Overview of project formulation strategy....4
2.1. Schematic showing various steps used in modeling a biphasic reactor....31
2.2. Thermodynamic model parameter data matrix....32
2.3. Schematic for the biphasic reactor simulation....32
2.4. Simulation results using UNIFAC a priori predicted (top), UNIFAC- Aspen Plus LLE (middle), UNIFAC- Aspen Plus LLE-Regressed (bottom) NRTL binary parameters....33
2.5. Simulation results using QSPR a priori predicted (top), QSPR - Aspen Plus LLE (middle), QSPR- Aspen Plus LLE- Regressed (bottom) NRTL binary parameters....34
2.6. Simulation results for Gibbs energy of the mixture and change in Gibbs energy 35
2.7. Simulation results for activity coefficient (γ) of components using UNIFAC-Aspen Plus LLE-Regressed NRTL parameters for aqueous phase (left) and organic phase (right). 35
2.8. Simulation results for activity coefficient (γ) of reacting components using QSPR- Aspen Plus LLE-Regressed (OU) NRTL parameters for aqueous phase (left) and organic phase (right). 36
3.1. Schematic showing various steps used in modeling a biphasic reactor....62
3.2. Solubility model representations for mole fractions of water in decalin rich (left) and decalin in water rich (right)....62
3.3. Algorithm for optimization of the mass transfer model for biphasic reactor 63
3.4. Simulation results for the biphasic reactor; before reaction starts (top), before mass transfer starts (middle), after mass transfer (bottom)....64
3.5. Simulation results for activity coefficient (γ) of reacting components using QSPR-Aspen Plus-Regressed NRTL parameters 65
3.6. Gibbs energy plot for the reactor mixture, and aqueous and organic phase mixtures....65
3.7. Gibbs energy change due to mass transfer (left) and chemical reaction (right) ..66
3.8. Gibbs energy change due to both mass transfer and chemical reaction against time 66
4.1. Microscope image of toluene ((left) and p-xylene (right) (40wt%water)....83
4.2. Graphical representation of experimental data for effect of water cut on drop size. for cyclic hydrocarbon (left). cyclic branched hydrocarbon (right). 83
4.3. Flowchart for the algorithm of SQR model for emulsion properties....84
4.4. Graphical representation of a feed forward perceptron network. 84

4.5. QSPR drop size model representation (left) and prediction (right) 85
4.6. Comparison of ensemble average drop size (ADS) model representations against experimental data.....85
4.7. Comparison of QSPR ADS model predictions with experimental data using best using LOO –CV for Ensemble training average (left) and Ensemble test set (right).....85
4.8. Comparison of QSPR emulsion fraction model predictions with experimental data using best model. Training data set (left). Test data set (right).....86
4.9. Comparison of emulsion fraction (EF) ensemble model prediction against experimental data.....87
4.10. Comparison of EF experimental data with representation (left) and prediction (right) using ensemble models with leave-one out cross validation.....87
4.11. Output of the perceptron neuron emulsion type (ET) model.....88
4.12. Training performance of the perceptron network using training data 70%.....88
4.13. Model results for effects of water cut on ADS 88
4.14. LOO-CV results for effects of water cut on ADS.....89
4.15. Model results for effects of water cut on ADS with exponential transformation of water cut.....89
5. 1. Algorithm for solvent selection and screening for biphasic reactor 108
5. 2. Comparison of experimental data against model prediction for ADS and EF of solvents.....109

CHAPTER I

INTRODUCTION

1.1. Rationale

Although bio-oil from fast pyrolysis is being used commercially as a fuel for stationary engines, significant upgrading is required for bio-oils to be used as a fuel for transportation purposes [1]. The bio-oil contains diverse functional groups including acids, alcohols, aldehydes, esters, oxygenates, sugars, furans, phenols, guaiacols and syringols [2, 3]. Upgrading of the bio-oil can be performed by reducing the oxygen content of the bio-oil to increase the calorific value and reducing the amount of highly reactive compounds to improve the chemical and storage stability of the biofuel [2-7].

Different works have demonstrated that biphasic reactors, which have the advantage of simultaneous chemical reaction and product separation, could be applicable to bio-oil upgrading [2, 6, 8]. Conventional reaction processes employ reaction and separation in different unit operation, requiring additional operations such as recycling for process optimization. This may increase the production cost and energy demands of chemical processes such as bio-oil upgrading. Unlike conventional reactors, biphasic reactors employ reactions in an emulsion of aqueous and organic liquid mixtures while phase distribution of reacting components between the two immiscible phases is occurring simultaneously. In this study, a typical bio-oil upgrading with biphasic reactors, which

employ catalytic surface reactions in a Pickering emulsion of aqueous and organic liquids with simultaneous mass transfer of reacting components across the interface, is used as a case study. Developing effective modeling and simulation techniques of biphasic reactors could bring many advantages to the growing application of biphasic reactors in bio-oil upgrading. First, modeling and simulation can be applied to predict the dynamics of compositions in the biphasic reactors and reduce the need for costly and sometimes difficult experimental data collection. Second, a reliable simulation would allow development and optimization of a viable process; specifically, simulation would facilitate studies on the effect of variations in catalysts, organic solvents, operating conditions, and feed stocks more readily.

In modeling reactions in biphasic reactors, both a kinetic model for the transformation of materials with the chemical reaction and a mass transfer model for multi-phase component phase distribution is required. For reactions involving heterogeneous catalysis, different kinetic models such as Eleyi – Redeal or Langmuir-Hinshelwood isotherm could be used to describe the reaction mechanism [9]. The proposed reaction mechanism should be tested using experimental data, and the model that best represents the experimental data is used in the final biphasic reactor model. Different modeling approaches could also be used to represent the component phase distribution in the biphasic reactor. The first approach is to use a thermodynamic phase equilibria model such as the Non Random-Two Liquid (NRTL) model. NRTL model is widely used to predict the liquid-liquid equilibrium component phase distribution of partially, as well as, completely miscible fluids [10].

The alternative approach is to represent component phase distribution using models based on interfacial mass transfer resistance, such as the two-film theory. Interfacial mass transfer models are used to represent mass transfer occurring in emulsions where adequate mixing is involved such as biphasic reactors [11-15]. The advantage and disadvantage of using different models could be compared and will be helpful to explain the biphasic reactor process from

different perspectives. For example, the presence of phase selectivity in some reactions in a biphasic medium could be well explained by the mass transfer resistances occurring inside and across the phases in the emulsion [8]. Assessing the effect of emulsion drop size, emulsion type (water in oil or oil in water), and partition coefficient on the rate of mass transfer could be better realized by the mass transfer model as the variables appears directly in the model equation [11, 15, 16].

A complete understanding of a biphasic reactor can be obtained by further developing predictive models for effects of solvent type and water fraction of the biphasic medium on emulsion properties such as droplet size, emulsion fraction, and emulsion type. Predicting the emulsion fractions and the size of droplets in the biphasic medium is important in estimating the interfacial area available for the reaction and mass transfer. The biphasic medium could be water in oil (oil being the continuous phase and water being the dispersed phase in the form of droplets) or oil in water depending on the reactor operating parameters and emulsion components. Further, the dispersed phase droplet size also depends on the water fraction and solvent type and reactor operating parameters such as mixing rate and temperature [17]. The rate of reaction and mass transfer between phases is dependent on the catalytic area available for reaction and the interfacial area available for mass transfer, respectively. Therefore, an accurate prediction of emulsion properties enhances our ability in selecting solvents for formulating emulsions with the desired properties in general and estimating and evaluating the performance of emulsions in the biphasic reactors in particular. **Figure 1.1** shows the integral approach employed in this dissertation work.

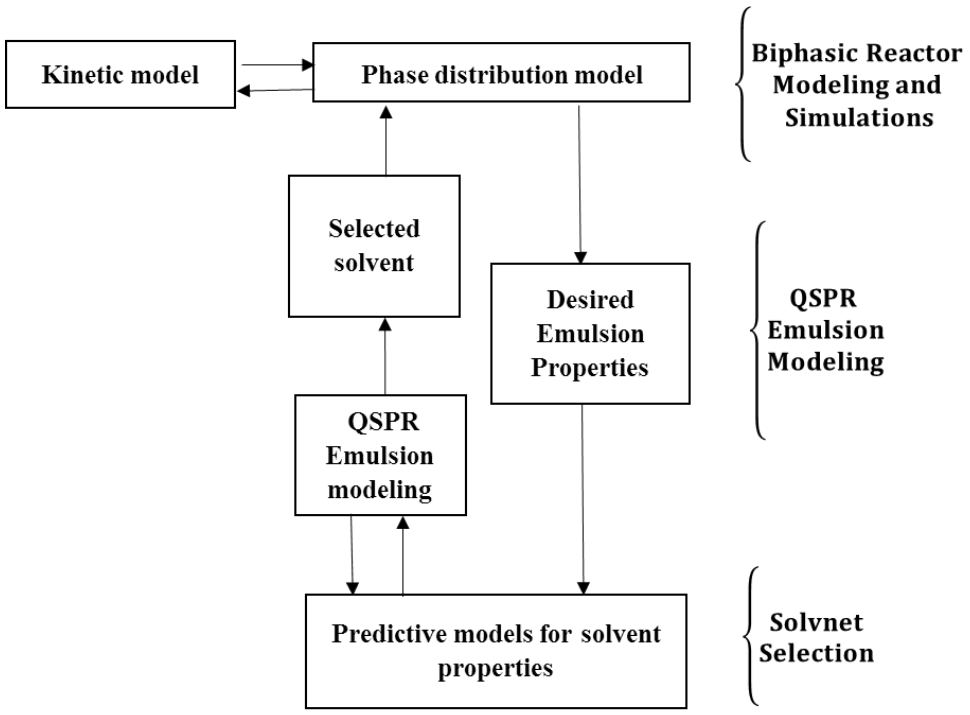

Figure 1.1. Overall project formulation strategy

Linear and nonlinear QSPR techniques can be used to model emulsion properties such as drop size, emulsion fraction, and emulsion type. QSPR techniques have been used to model different physical and thermodynamic properties such as LLE binary parameters, partition coefficients, and activity coefficients in the literature [18-21]. Partition coefficient and solubility of reacting species in the biphasic mediums determines the rate and direction of mass transfer in the biphasic reactor. Therefore, developing a predictive model capable of selecting a solvent is important for designing a biphasic reactor with improved performance. The Computer-Aided Molecular Design (CAMD) procedure, which was developed by the the Oklahoma State University Thermodynamics Research Group [21, 22], can be used to identify a new solvent for formulating emulsions with a set of desired properties. A database of potential solvents with structures similar to those solvents used in developing the QSPR emulsion models should be collected and a scoring criteria established for selecting a suitable solvent.

The major technical challenge for this project is discovering available experimental data for phase equilibria binary parameters for all systems at the reactor operating temperatures and measurement of the actual interfacial area of emulsions available for mass transfer. To overcome these challenges, regression models and *a priori* prediction models will be used to estimate binary parameters. Further, optimization techniques will be employed to estimate the effective interfacial area available for mass transfer.

1.2. Objectives

i. Modeling and simulation of biofuel upgrading catalytic biphasic reaction at the water/oil interface; a phase equilibria approach

Modeling of biphasic reactors requires devising mathematical representations for the composition dynamics due to material transformation by the chemical reaction and a component distribution between the aqueous and organic phases of the reactor. The main objective of Chapter 2 is to develop a novel approach to represent the component phase distribution with liquid-liquid phase equilibria and devise a heterogeneous chemical reaction mechanism for representation of the material transformation for the catalyst surface reaction in the liquid phase. This work has the following specific objectives:

i. Develop an algorithm for modeling and simulation of a biphasic reactor with a liquid-liquid thermodynamic phase equilibria model to represent the component phase distributions between the two phases in the biphasic reactor.
ii. Estimate the binary interaction parameters of the thermodynamic model using available ternary equilibrium data and *a priori* prediction for ternary compounds lacking experimental equilibrium data.
iii. Assess the effect of *a priori* prediction of liquid-liquid phase equilibria binary parameters using QSPR-NRTL and UNIFAC models.

iv. Devise a kinetic model to represent bio-oil upgrading heterogeneous chemical reaction. Validate the kinetic model and the overall biphasic reactor model using biphasic reactor composition data.

v. Develop and implement a simulation strategy using Excel-VBA and Aspen Plus to estimate the composition dynamics of the biphasic reactor for the entire reaction time and validate the model using biphasic reactor experimental data.

vi. Use an activity coefficient and Gibbs energy test to validate assumptions taken to develop the biphasic reactor model.

ii. Modeling and simulation of biofuel upgrading catalytic biphasic reaction at the water/oil interface; a phase equilibria approach

Mass transfer models can be used to represent phase distributions if we assume that there is a significant interfacial mass transfer resistance that would affect the relative rate of reaction in the respective phases of the reactor. This approach facilitates the explanation of the persistence of phase selectivity of reaction and offers an expression in which emulsion properties such as drop size and partition coefficient are used. The main objective of Chapter 3 is to build a biphasic reactor with a mass transfer model that includes the following specific objectives:

i. Develop an algorithm for modeling and simulation of biphasic reactors with a mass transfer model to represent component phase distribution between the two phases in the biphasic reactor.

ii. Develop and implement a simulation strategy using Excel-VBA and Aspen Plus to estimate the composition dynamics of the biphasic reactor for the entire reaction time using the new models.

iii. Develop an optimization strategy to estimate the amount of fractional area available for mass transfer between the droplet and continuous phase of the biphasic reactor.

iv. Validate the overall biphasic reactor model using the biphasic reactor composition data and assess the advantages of the new approach.

v. Use an activity coefficient and Gibbs energy test to validate assumptions taken to develop the assumption used to develop the biphasic reactor model.

iii. Modeling effects of solvent type and water cut on emulsion characteristics using a quantitative structure property relationship (QSPR) model

Developing an ability to predict emulsion characteristics is important for formulation of emulsions with desirable properties. The main objective of Chapter 4 is to develop QSPR models capable of reliable prediction for emulsion properties such as average droplet size, emulsion fraction, and emulsion type with solvent type and water cut as independent variables. The specific objectives of this chapter includes the following:

i. Generate and optimize molecular structures for the solvents used in developing the equilibrium and mass transfer models. Calculate molecular descriptors for QSPR model building.
ii. Devise a descriptor reduction strategy that will be used for final model development
iii. Develop linear and non-linear QSPR models capable of predicting effect of solvent type on average droplet size and emulsion fraction.
iv. Develop QSPR models capable of predicting the effect of solvent type on emulsion type.
v. Develop a QSPR model capable of predicting effect of solvent type and water fraction on average droplet size.

iv. Predictive models for solvent selection for biphasic reactor

Biphasic reactors employ a mixture of aqueous and organic solvents as a medium to carry out reactions and may employ component phase separation of products due to increased solubility in the organic phase. The type of organic solvent largely affects the interfacial area available for mass transfer, type of emulsions, mas transfer constants, and partition coefficient of solutes that are taking part in the reactions process. Hence, the main objectives of Chapter 5 is to devise and implement a strategy for selecting and screening solvents for enhanced phase distribution of

solutes from the aqueous phase to the organic phase of the biphasic reactor with the following specific objectives:

i. To employ the QSPR models for average drop size, emulsion fraction, and emulsion type to rank solvents based on the total area available for mass transfer
ii. Identify solvents that create a Water/Oil emulsion with, where the organic phase is the continuous phase.
iii. Estimate the partition coefficients/solubility of solutes in the biphasic reactor medium using infinite dilution activity coefficient models and evaluate solvents based on the overall score obtained using the screening criteria set above.

1.3. Thesis organization

This thesis is organized in a manuscript style with one introduction, four independent works, and conclusions and recommendations. The introduction part contains the background, the rationale, and the objective of this work. The second chapter concerns modeling and simulation of a biphasic reactor, using a phase equilibria approach to represent the component interfacial mass transfer. In the third chapter, the biphasic reactor is modeled and simulated using a two-film theory model for representing the interfacial mass transfer. The fourth chapter discusses the work on modeling of emulsion properties such as droplet size, emulsion type and emulsion fraction. The fifth chapter focuses on identifying a solvent using Computer-Aided-Molecular-Design (CAMD) techniques. Finally, recommendations and conclusions are given in the last chapter of the thesis work.

REFERENCES

1. Lehto, J., et al., *Review of fuel oil quality and combustion of fast pyrolysis bio-oils from lignocellulosic biomass.* VTT Technology 2013. **87. 79 p.**
2. Mahfud, F., F. Ghijsen, and H. Heeres, *Hydrogenation of Fast Pyrolyis Oil and Model Compounds in a Two-Phase Aqueous Organic System Using Homogeneous Ruthenium Catalysts.* Journal of Molecular Catalysis A: Chemical, 2007. **264**(1-2): p. 227-236.
3. Huber, G.W., S. Iborra, and A. Corma, *Synthesis of Transportation Fuels from Biomass: Chemistry, Catalysts, and Engineering.* Chemical Review, 2006. **106**(9): p. 4044-4098.
4. Mahfud, F.H., *Exploratory Studies on Fast Pyrolysis Oil Upgrading*, in *Faculty of Mathematics and Natural Sciences*. 2007, University of Groningen. p. 158.
5. Resasco, D.E., et al., *Furfurals as Chemical Platform for Biofuels Production*, in *Heterogeneous in Biomass to Chemicals and Fuels*, D. Kubička and I. Kubičková, Editors. 2011, Research Signpost. p. 155-188.
6. Simonetti, D.A. and J.A. Dumesic, *Catalytic Strategies for Changing the Energy Content and Achieving C-C Coupling in Biomass-Derived Oxygenated Hydrocarbons.* ChemSusChem, 2008. **1**(8-9): p. 725-733.
7. Czernik, S. and A.V. Bridgwater, *Overview of Applications of Biomass Fast Pyrolysis Oil.* Energy & Fuels, 2004. **18**(2): p. 590-598.
8. Resasco, D.E., *Carbon nanohybrids used as catalysts and emulsifiers for reactions in biphasic aqueous/organic systems.* Chinese Journal of Catalysis, 2014. **35**(6): p. 798-806.
9. Fogler, H.S., *Elements of Chemical Reaction Engineering*. 4th ed. 2006, Upper Saddle River, NJ: Prentice Hall PTR.
10. Renon, H. and J.M. Prausnitz, *Local Compositions in Thermodynamic Excess Functions for Liquid Mixtures.* American Institute of Chemical Engineers, 1968. **14**(1): p. 135-144.
11. Tudose, R.Z. and G. Apreotesei, *Mass Transfer Coefficients in Liquid–liquid Extraction.* Chemical Engineering and Processing: Process Intensification, 2001. **40**(5): p. 477-485.
12. Pugazhenthi, G. and A. Kumar, *Modeling of the Mass Transfer Effect in Biphasic Enzyme Membrane Reactor for Hydrolysis of Olive Oil*, in *International Journal of Food Engineering*. 2008.
13. Kundu, A., et al., *Mass Transfer Characteristics in Gas-liquid-liquid System.* The Canadian Journal of Chemical Engineering, 2003. **81**(3-4): p. 640-646.

14. Kalaichelvi, P. and T. Murugesan, *A correlation for overall mass transfer coefficients in rotating disc contactors.* Bioprocess Engineering, 1998. **19**(5): p. 381-384.
15. Melgarejo-Torres, R., et al., *Mass Transfer Coefficient Determination in Three Biphasic Systems (Water–ionic liquid) Using a Modified Lewis Cell.* Chemical Engineering Journal, 2012. **181–182**: p. 702-707.
16. Rudose, R.Z. and G. Lisa, *The determination of individual mass transfer coefficients in liquid-liquid extraction.* Chem. Ind. , 2003. **57**(9): p. 393-398.
17. Weston, J.S., et al., *Silica Nanoparticle Wettability: Characterization and Effects on the Emulsion Properties.* Industrial & Engineering Chemistry Research, 2015. **54**(16): p. 4274-4284.
18. Neely, B.J., et al., *Nonlinear Quantitative Structure-property Relationship Modeling of Skin Permeation Coefficient.* Journal of Pharmaceutical Sciences, 2009. **98**(11): p. 4069-4084.
19. Yerramsetty, K.M., B.J. Neely, and K.A.M. Gasem, *A Non-Linear Structure-Property Model For Octanol-Water Partition Coefficient.* Fluid phase equilibria, 2012. **332**: p. 85-93.
20. Gebreyohannes, S., et al., *Improved QSPR Generalized Interaction Parameters for the Nonrandom Two-Liquid Activity Coefficient Model.* Fluid Phase Equilibria, 2013. **339**: p. 20-30.
21. Godavarthy, S.S., et al., *Design of Improved Permeation Enhancers for Transdermal Drug Delivery.* Journal of Pharmaceutical Sciences, 2009. **98**(11): p. 4085-4099.
22. Golla, S., et al., *Virtual Design of Chemical Penetration Enhancers for Transdermal Drug Delivery.* Chemical Biology & Drug Design, 2012. **79**(4): p. 478-487.

CHAPTER II

MODELING AND SIMULATION OF BIOFUEL UPGRADING CATALYTIC BIPHASIC REACTIONS AT THE WATER/OIL INTERFACE; A PHASE EQUILIBRIA APPROACH

2.1. Introduction

The bio-oil obtained through biomass fast pyrolysis is a complex amalgam of compounds with diverse functional groups including acids, alcohols, aldehydes, esters, oxygenates, sugars, furans, phenols, guaiacols, syringols, and a significant amount of water [2, 3]. Pyrolysis oil can be used as a fuel for transportation with significant upgrading [7, 23-26], which includes reducing the oxygen content of the bio-oil to increase calorific value and reducing the amount of highly reactive compounds to improve chemical and storage stability [2-7].

Biphasic catalytic reactors can be used to upgrade the pyrolysis oil. Since bio-oils contain diverse compounds in a mixture of oil and water, an efficient upgrading may require phase selective catalysis and separation of water-soluble compounds. This means that a biphasic catalytic reactor can target specific reactions in the water phase and facilitate separation of components from the water phase to the oil phase if the upgrading reactions resulted in decreased solubility of biofuel compounds in the oil phase [2, 24, 27]. In cases where the upgrading involves a series of multiple reactions, the ability to catalyze the reactions in both phases of the biphasic reactor could offer a unique opportunity in completing the upgrading process even in the presence of component phase distribution. Biphasic reactors for bio-oil upgrading employ catalysts such as solid acid catalysts on on metal-supported nanoparticles [24, 27, 28] or zeolites [29, 30] to selectively

catalyze the target reactions in the organic and aqueous phases. Some examples of biphasic catalytic reaction systems are water/decalin [28, 29], water/dodecane [31], and water/toluene [2].

Modeling and simulation of biphasic reactors for bio-oil upgrading can facilitate understanding of the composition dynamics and optimization of the bio-oil upgrading. A thorough understanding of the process could lead to optimizing operating parameters for higher selectivity and yield. The objective of the current work was to construct a reaction-constrained, multi-component phase equilibrium algorithm to model a typical biphasic reaction system encountered in the upgrading of bio-oil to biofuel. The computational strategy employed calls for (a) kinetic models to describe the reactions occurring at the interphase utilizing reactants in the organic and the aqueous phases (the reaction step), and (b) generalized phase equilibrium models to determine the component distribution into the aqueous and organic phases (the separation step).

The hydrogenation of p-hydroxybenzaldehyde to 4-methylcyclohexanol in a water/decalin biphasic catalytic reaction system was used to demonstrate the efficacy of the simulation algorithm and the generalized phase equilibrium modeling. The hydrogenation of p-hydroxybenzaldehyde (p-BAL) to 4-methylcyclohexanol (4-MECH), a typical reaction in the upgrading of bio-oil from fast pyrolysis, was selected as a case study. The analysis of the reaction pathway from unpublished work completed by co-authors at the University of Oklahoma (OU) showed the hydrogenation of p-BAL to occur as a series of three reactions. Hydrogenation of p-hydroxybenzaldehyde to p-hydroxybenzyl alcohol is followed by hydrogenation and dehydration to form p-cresol, which undergoes further hydrogenation to finally form 4-methyl cylohexanol. In summary, the reaction-phase distribution pathway can be described as follows:

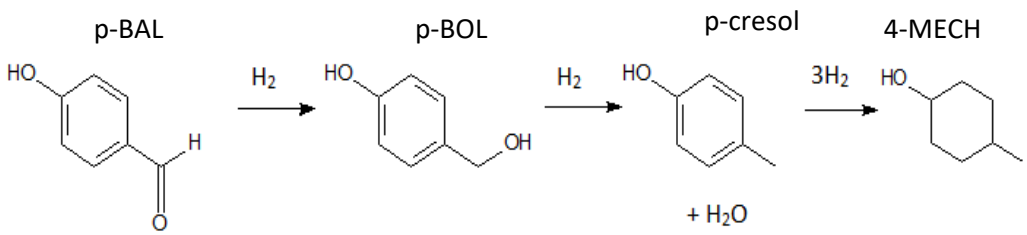

$$R_{Water} \underset{k_{-pR}}{\overset{k_{pR}}{\rightleftharpoons}} R_{Oil}$$

$$R_{Water} \xrightarrow{k_o} P_{Water}$$

$$R_{Oil} \xrightarrow{k_o} P_{Oil}$$

where R is any reacting component, P is the corresponding product, and k_{pR} and k_o are mass transfer coefficient and rate constants, respectively. Since p-BAL and p-BOL have limited solubility in the organic phase, the first two reactions occur predominantly in the aqueous phase. Whereas, p-cresol and 4-MECH are strongly soluble in both phases, and the change in the concentration of these two chemicals due to component phase distribution is significant.

In modeling biphasic systems, both heterogeneous reaction kinetics for material transformations and multi-phase (vapor-liquid-liquid) equilibrium modeling for determining the phase compositions are required. Thus, beyond the need for reliable kinetic models, accurate liquid-liquid and vapor-liquid equilibrium models of mixtures encountered in the process are essential. For reactions involving heterogeneous catalysis, the Eley-Rideal mechanism can be used to describe the reaction mechanism [9]. The Nonrandom-Two Liquid (NRTL) thermodynamic model is used widely to predict the liquid-liquid equilibrium distribution of partially, as well as completely miscible fluids [10, 32]. In the absence of experimentally regressed NRTL interaction parameters, *a priori* prediction by UNIQUAC Functional Group Activity Coefficient (UNIFAC) is used in Aspen Plus [33]. Gebreyohannes [20] showed that generalized Quantitative Structure-Property Relationship (QSPR) modeling could also be used to provide *a priori* prediction of NRTL binary parameters. Therefore, the efficacy of *a priori* prediction of the parameters by UNIFAC and QSPR would be assessed in the simulation of the

biphasic reactor. In the current work, a novel approach to model and simulate biphasic reactors was developed and experimental data was used to evaluate the model.

2.2. Methods

2.2.1. Simulation strategy

The computational strategy and the procedure for implementation of the simulation of a biphasic reaction system is described in detail in the following sections. The kinetic and the thermodynamic models used in the reaction and phase separation, respectively, are constructed and combined in the simulation of the biphasic reactor model. To facilitate the modeling of the biphasic reactor, two simplifying assumptions were made.

1. No headspace is present in the reactor, which assumes the thermodynamic effect of hydrogen gas on the liquid phases is negligible, as hydrogen saturates the phases.
2. Mass transfer of the components in each phase and through the oil/water interface is not the rate-limiting step. This is a result of the enhanced interfacial area of water/oil emulsions stabilized by amphiphilic nanohybrid catalysts, which favors mass transfer between the two phases [27, 28].

The computational strategy for modeling the phase equilibrium of catalytic processes implemented in this study is outlined in **Figure 2.1**.

The algorithm for modeling the multi-component kinetically constrained reactions in a biphasic catalytic reactor consists of the following steps:

(a) the reaction kinetics (rate laws and their constants) on each side of the amphiphilic catalyst at the interface of the phases are determined;

(b) for a given time increment, the reaction rate constraints are applied to the mass balance calculations; i.e., an account is made of all reactants and products and their respective masses;

(c) as the components from the reactions separate preferentially between the phases, liquid-liquid equilibrium calculations are performed on the compositions at the reaction temperature and pressure to reflect component phase distribution;

(d) the re-distributed components constitute the new reaction feed composition for the next time increment of an updated Step b; and

(e) the process continues iteratively until the set of solutions for the distribution of the components in each coexisting phase as a function of time is obtained for the entire reaction time.

2.2.2. Kinetic model derivation

The kinetic model was derived using the Eley-Ridealmechanism [9] for the rate expression in terms of the concentrations of p-BAL, p-BOL, p-cresol, and 4-MECH.

The following assumptions were made in the derivation of the reaction mechanism: (a) molecular adsorption of p-BAL, (b) non-competitive molecular adsorption of hydrogen gas, (c) single reactant binding site, (d) all adsorption sites are alike, (e) irreversible surface reaction is the rate-determining step, and (f) reversible desorption of the products. These are comparable assumptions to those employed by other investigators [9, 34, 35].

The elementary steps for the hydrogenation of p-BAL to 4-MECH can be depicted by **Equations (1.1-1.8)**, in which **•S** represents an active site and the species A, B, C, D and S represent p-BAL, p-BOL, p-cresol, 4-MECH and catalyst, respectively.

Adsorption : $A + S \underset{k_{-A}}{\overset{k_A}{\rightleftharpoons}} A \bullet S$ **(1.1)**

Surface Reaction 1 : $A \bullet S + H_2 \underset{k_{-R1}}{\overset{k_{R1}}{\rightleftharpoons}} B \bullet S$ **(1.2)**

Desorption 1 : $D \bullet S \underset{k_{-D1}}{\overset{k_{D1}}{\rightleftharpoons}} D + S$ **(1.3)**

Surface Reaction 2 : $B \bullet S + H_2 \underset{k_{-R2}}{\overset{k_{R2}}{\rightleftharpoons}} C \bullet S + H_2O$ **(1.4)**

Desorption 2 : $\mathrm{C} \bullet S \underset{k_{-D2}}{\overset{k_{D2}}{\rightleftharpoons}} C + S$ **(1.5)**

Surface Reaction 3 : $C \bullet S + 2H_2 \underset{k_{-R3}}{\overset{k_{R3}}{\rightleftharpoons}} D \bullet S$ **(1.6)**

Desorption 3 : $\mathrm{D} \bullet S \underset{k_{-D3}}{\overset{k_{D3}}{\rightleftharpoons}} D + S$ **(1.7)**

H_2 *Adsorption :* $2H_2 + 2S \underset{k_{-H2}}{\overset{k_{H2}}{\rightleftharpoons}} 2H \bullet S$ **(1.8)**

As hydrogen gas is in excess, the partial pressure of hydrogen can be considered constant during the entire reaction period. Then, the rate expressions for the adsorption and desorption steps become: [35].

$$r_{H_2ads} = k_{H_2} P_{H_2} C_S^{\,2} - k_{-H_2} P_{H \bullet S}^{\,2} \quad \textbf{(1.9)}$$

$$r_{Ads} = k_A C_A C_S - k_{-A} C_{A \bullet S} \quad \textbf{(1.10)}$$

$$r_{Des_1} = k_{D_1} C_{B \bullet S} - k_{-D_1} C_B C_S \quad \textbf{(1.11)}$$

$$r_{Des_2} = k_{D_2} C_{C \bullet S} - k_{-D_2} C_C C_S \quad \textbf{(1.12)}$$

$$r_{Des_3} = k_{D_3} C_{D \bullet S} - k_{-D_3} C_D C_S \quad \textbf{(1.13)}$$

With the surface reactions being the limiting reactions,

$$r_{SR_1} = k_{R_1} C_{A \times S} P_{H_2} - k_{-R_1} C_{B \times S} \quad \textbf{(1.14)}$$

$$r_{SR_2} = k_{R_2} C_{B \times S} P_{H_2} - k_{-R_2} C_{C \times S} \quad \textbf{(1.15)}$$

$$r_{SR_3} = k_{R_3} C_{C\times S} P_{H_2}^3 - k_{-R_3} C_{D\times S} \quad \textbf{(1.16)}$$

From the Pseudo Steady-State Hypothesis [9], **Equations (1.9-1.13)** become:

$$P_{H\bullet S} = \left(\frac{k_{H_2}}{k_{-H_2}} \right)^{1/2} P_{H_2}{}^{1/2} C_S \quad \textbf{(1.17)}$$

$$C_{A\bullet S} = \frac{k_A}{k_{-A}} C_A C_S \quad \textbf{(1.18)}$$

$$C_{B\bullet S} = \frac{k_{-D_1}}{k_{D_1}} C_B C_S \quad \textbf{(1.19)}$$

$$C_{C\bullet S} = \frac{k_{-D_2}}{k_{D_2}} C_C C_S \quad \textbf{(1.20)}$$

$$C_{D\bullet S} = \frac{k_{-D_3}}{k_{D_3}} C_D C_S \quad \textbf{(1.21)}$$

Applying Site Balance, the total concentration of the active sites, is

$$C_{SO} = C_S + C_{A\cdot S} + C_{B\cdot S} + C_{C\cdot S} + C_{D\cdot S} + P_{H\cdot S} \quad \textbf{(1.22)}$$

$$C_{SO} = C_S \left[1 + K_A C_A + K_B C_B + K_C C_C + K_D C_D + K_{H_2}^{1/2} P_{H_2}^{1/2} \right] \quad \textbf{(1.23)}$$

$$C_S = \frac{C_{SO}}{\left[1 + K_A C_A + K_B C_B + K_C C_C + K_D C_D + K_{H_2}^{1/2} P_{H_2}^{1/2} \right]} = \frac{C_{SO}}{\Theta_V} \quad \textbf{(1.24)}$$

As in conventional Eley-Rideal derivation, assuming irreversible surface reactions and substituting for CS, CA·S, CB·S, CC·S, and CC·S in the respective limiting reactions gives the following rate expressions for a single phase.

$$r_A = -\frac{k_{R_1} C_{SO} K_A P_{H_2}}{\Theta_V} C_A = -\frac{k_1 K_A}{\Theta_V} C_A \quad \textbf{(1.25)}$$

$$r_B = \frac{k_1 K_A}{\Theta_V} C_A - \frac{k_2 K_B}{\Theta_V} C_B \quad \textbf{(1.26)}$$

$$r_C = \frac{k_2 K_B}{\Theta_V} C_B - \frac{k_3 K_C}{\Theta_V} C_C \quad \textbf{(1.27)}$$

$$r_D = \frac{k_3 K_C}{\Theta_V} C_C \quad \textbf{(1.28)}$$

Where

$$k_1 = k_{R_1} C_{SO} P_{H_2}, \quad K_A = \frac{k_A}{k_{-A}}, \quad k_2 = k_{R_2} C_{SO} P_{H_2}, \quad K_B = \frac{k_{-D_1}}{k_{D_1}}$$

$$k_3 = k_{R_3} C_{SO} P_{H_2}{}^3, \quad K_C = \frac{k_{-D_2}}{k_{D_2}}, \quad K_D = \frac{k_{-D_3}}{k_{D_3}}, \quad \text{and } K_{H_2} = \frac{k_{H_2}}{k_{-H_2}}$$

Applying the complete mass balance for the biphasic system by accounting for the transfer of mass between the phases, however, provides the complete rate expressions for the biphasic reactions. The mass transfer section in our model is represented by phase equilibria separation. In multi component phase equilibria calculations, the value of the partition coefficient may be dependent on composition and may not remain constant, as it is shown in the equations.

$$r_{A-Oil} = \frac{dC_{A-Oil}}{dt} = -\frac{k_1 K_A C_{A-Oil}}{\Theta_V} - k_{pA_{-1}} C_{A-Oil} + k_{pA_1} C_{A-Water} \quad \textbf{(1.29)}$$

$$r_{A-Water} = \frac{dC_{A-Water}}{dt} = -\frac{k_1 K_A C_{A-Water}}{\Theta_V} + k_{pA_{-1}} C_{A-Oil} - k_{pA_1} C_{A-Water} \quad \textbf{(1.30)}$$

$$r_{B-Oil} = \frac{dC_{B-Oil}}{dt} = \frac{k_1 K_A C_{A-Oil}}{\Theta_V} - \frac{k_2 K_B C_{B-Oil}}{\Theta_V} - k_{pB_{-1}} C_{B-Oil} + k_{pB_1} C_{B-Water} \quad \textbf{(1.31)}$$

$$r_{B-WATER} = \frac{dC_{B-Water}}{dt} = \frac{k_1 K_A C_{A-Water}}{\Theta_V} - \frac{k_2 K_B C_{B-Water}}{\Theta_V} + k_{pB_{-1}} C_{B-Oil} - k_{pB_1} C_{B-Water} \quad \textbf{(1.32)}$$

$$r_{C-Oil} = \frac{dC_{C-Oil}}{dt} = \frac{k_2 K_B C_{B-Oil}}{\Theta_V} - \frac{k_3 K_C C_{C-Oil}}{\Theta_V} - k_{pC_{-1}} C_{C-Oil} + k_{pC_1} C_{C-Water} \quad \textbf{(1.33)}$$

$$r_{C-Water} = \frac{dC_{C-Water}}{dt} = \frac{k_2 K_B C_{B-Water}}{\Theta_V} - \frac{k_3 K_C C_{C-Water}}{\Theta_V} + k_{pC_{-1}} C_{C-Oil} - k_{pC_1} C_{C-Water} \quad \textbf{(1.34)}$$

$$r_{D-Oil} = \frac{dC_{D-Oil}}{dt} = \frac{k_3 K_C C_{C-Oil}}{\Theta_V} - k_{pD_{-1}} C_{D-Oil} + k_{pD_1} C_{D-Water} \quad \textbf{(1.35)}$$

$$r_{D-Water} = \frac{dC_{D-Water}}{dt} = \frac{k_3 K_C C_{C-Water}}{\Theta_V} + k_{pD_{-1}} C_{D-OIL} - k_{pD_1} C_{D-Water} \quad \textbf{(1.36)}$$

$$\Theta_V = 1 + K_A C_{A-Total} + K_B C_{B-Total} + K_C C_{C-Total} + K_D C_{D-Total} + K_{H_2}^{1/2} P_{H_2}^{1/2} \quad \textbf{(1.37)}$$

The above differential equations **(Equations 1.30-1.37)** are then solved for a given time increment using numerical approximations by Euler's method to obtain the new product distribution. The complete equation based on the Euler's method is given in **Appendix E.**

2.2.3. Estimation of kinetic parameter

The discretized rate equations obtained for the kinetic model derivation based on the Euler's method were fitted to the experimental concentration data for a single phase. The sum of squared deviations (SSD) minimization with nonlinear least-square regression analysis was used in the fitting of the reaction rate and adsorption constants. The equilibrium adsorption constants were fitted to the experimental data, while ensuring that the adsorption constant value of p-hydroxybenzaldehyde was higher than the value for the other species, and the adsorption constant of hydrogen was very small. This follows experimental trends observed in the hydrogenation of aldehydes [34, 35] The operating conditions and specifications for the reactor are provided in **Table 2.1** and experimental biphasic reactor composition data taken at different intervals of the reaction time is provided in **Table 2.4** in the results and discussion section.

2.2.4. Thermodynamic property model

The thermodynamic model used for the liquid-liquid phase equilibria (LLE) calculation is the nonrandom two-liquid (NRTL) activity coefficient model [10, 36]. This model was chosen for

its applicability to systems with partial and complete miscibility [32]. Further, the NRTL model has been shown to provide reasonable generalized predictions for LLE systems that are within 2-3 times the regression errors [20]. The NRTL activity coefficient model is described by the following equations:

$$ln(\lambda_1) = x_2^2\left[\tau_{21}\left(\frac{G_{21}}{x_1 + x_2 G_{21}}\right)^2 + \left(\frac{\tau_{12}G_{12}}{\left(x_2 + x_1 G_{12}\right)^2}\right)\right] \quad \textbf{(1.38)}$$

$$ln(\lambda_2) = x_1^2\left[\tau_{12}\left(\frac{G_{12}}{x_2 + x_1 G_{12}}\right)^2 + \left(\frac{\tau_{21}G_{21}}{\left(x_1 + x_2 G_{21}\right)^2}\right)\right] \quad \textbf{(1.39)}$$

The model parameters are defined as:

$$G_{12} = exp(-\alpha_{12}\tau_{12}), \quad G_{21} = exp(-\alpha_{12}\tau_{21})$$

$$\tau_{12} = \frac{g_{12} - g_{22}}{RT} = \frac{a_{12}}{T}, \qquad \tau_{21} = \frac{g_{21} - g_{11}}{RT} = \frac{a_{21}}{T}$$

Where, γ is the activity coefficient of components, x is the mole fraction of components, α_{12} is the non-randomness factor in the mixture and are the two adjustable parameters, g is an energy parameter characterizing interactions between the molecules of same liquid molecules and different liquid molecules in the NRTL model, R is the universal gas constant, and T is the mixture temperature. The extended version of the NRTL model with temperature dependent terms is used by Aspen Plus [33].

2.2.5. Sources of NRTL binary parameters

Figure 2.2 shows three different sources of NRTL binary parameters used in the simulations. Experimental binary data for two systems were obtained from the Aspen Plus LLE database [33]. NRTL parameters for five binary systems were regressed from two ternary experimental data sets collected by the co-authors at OU. For compounds lacking experimentally regressed NRTL binary interaction parameters, the efficacy of using *a priori* predictions by a

theory-based approach involving UNIQUAC Functional Group Activity Coefficient, (UNIFAC) [37] and generalized Quantitative Structure-Property Relationship (QSPR) [20, 38] modeling is assessed.

The regression of binary parameters was performed using LLE ternary data for water/decalin/p-cresol and water/decalin/4-MECH systems. Concentration data for p-cresol and 4-MECH was available at 30, 40, 50, and 60°C. The concentrations of decalin and water were calculated by a solubility model, which was developed using separate solubility data for the water/decalin system. Then NRTL binary parameters regressed at each temperature were used to develop a linear model and predict binary parameter values at the reactor temperature of 150°C. The regression results of the binary parameters were sensitive to initial values. Therefore, average values of parameters for temperatures between 30-60°C were regressed using Aspen Plus. The average regressed parameters were then modified to provide a concentration-based phase distribution ratio approximately equal to the experimentally determined ratio at 60°C, which is 1.7 and 3.2 for p-cresol and 4-MECH, respectively. These results were then used as initial values to obtain binary parameters at 60°C by regression. For 50°C, the results at 60°C were used as initial values, and this computational scheme of using the higher temperature parameters as initial values was continued for the lower temperatures to 30°C. Experimental ternary equilibrium mole fraction data for two systems, solubility data for water and decalin are provided in Appendix A in **Tables A1 and Table A2**. **Figure A1** also compares experimental solubility data against model prediction which is discussed in detail in chapter 3. Similarly, regressed and predicted NRTL binary parameters and *a priori* predicted NRTL binary parameters using UNIFAC and QSPR are given in Table A3, A4 and Table B5 in Appendix B respectively.

2.2.6. Simulation in Aspen Plus using user defined kinetics in Excel-VBA

The algorithm used for modeling the multi-component kinetically constrained phase distribution in a biphasic catalytic reactor described in Section 2.1 is implemented by using Excel-VBA, and Aspen Plus. The computational strategy employed and the process flow sheet used to represent the biphasic reactor system in Aspen Plus are shown in **Figures 2.3** and **2.4**, respectively. An Excel-VBA code was written to solve the kinetic equations numerically represented by the Euler method (**Equations 1.30-1.37**). The reactors, REACTOR1 and REACTOR2, in **Figure 2.4** represent the reactions in the organic and aqueous phase, respectively. ASPEN Simulation Workbook (ASW) is used to facilitate the flow of information between Excel-VBA and Aspen Plus. The initial amount of water, decalin, and p-BAL used in the experiment was specified in Aspen Plus, and the implementation started by performing a phase separation calculation in the decanter. Then, the component concentration and mass balance results of the organic and aqueous phase were sent to the kinetic module in Excel VBA. The computational result of the kinetics module in Excel-VBA was sent to the mixer in Aspen Plus and then to the decanter where computation of phase distribution denotes the initiation of the next time step. A one-minute step size was chosen for the simulation to minimize simulation time. Higher step sizes increase the error; however, there was no significant improvement in simulation representation with lower step sizes. The closure of the mass balance was checked on each iteration of the computation.

The effect of NRTL binary parameters on the prediction results was investigated using three case studies based on the source of the phase equilibrium binary parameters. The first case (Case I) used NRTL model binary parameters obtained from UNIFAC and QSPR-NRTL. The second case (Case II) includes NRTL binary parameters for two systems obtained from the ASPEN LLE database in addition to the *a priori* predicted binary parameters employed in Case I. Thus, a combination of parameter sources are used: UNIFAC- Aspen Plus LLE or QSPR- Aspen

Plus LLE. In the third case (Case III), NRTL binary parameters for five binary systems predicted at 150°C (using a linear regression model based on data from OU) were also employed in addition to the parameters used in Case II. The specific parameter source for each case study is shown in **Table 2.2.**

2.2.7. Activity coefficients and Gibbs energy minimization analysis

For reactions involving phase equilibria, rate equations are expressed as a function of activates instead of concentrations. The reaction system operates in the range of infinite dilution activity coefficients where the overall reacting systems is composed of less than two percent of the reactor content. Therefore, the activity coefficients of the chemical components in each phase were tracked to check if a significant change in activity value occurred. Aspen Plus was used to evaluate activity coefficients based on **Equation 1.40.**

$$\gamma_i = \frac{y_i \mathrm{P}}{x_i p_i^{sat}} \qquad \textbf{(1.40)}$$

Where, γ_i is activity coefficient of component i

P is total pressure of the system

p^{sat} is partial pressure of the component i at saturation or vapor pressure

x_i, *and* y_i *are* mole fraction of component i in the liquid and vapor phase respectively.

For a closed system of given initial feed, temperature, and pressure, reactions occur as the Gibbs free energy proceeds to a minimum. Gibbs energy of the system should be evaluated to see if the aqueous and organic phase reactions and component mass transfer result in minimizing the Gibbs Energy of the mixture with time for each phase locally, and the overall reactor, globally. The pseudo-equilibrium assumptions in the biphasic reactor model for reactions in each phase and mass transfer of components between phases after each time increment are (a) local

equilibrium at the interface (where the reactions occur), and (b) a global equilibrium in the bulk phases of the reactor.

Equations 1.41 to 43 are used to calculate the Gibbs energy of mixing for the organic phase, aqueous phase and the overall reactor values, respectively

$$\Delta G_{mix(Oil)} = RT \sum_{i(Oil)}^{n} x_{i(Oil)}\, lnx_{i(Oil)}\, \gamma_{i(Oil)} \quad \textbf{(1.411)}$$

$$\Delta G_{mix(Water)} = RT \sum_{i(Water)}^{n} x_{i(Water)}\, lnx_{i(Water)}\, \gamma_{i(Water)} \quad \textbf{(1.42)}$$

$$\Delta G_{mix(Reactor)} = RT \sum_{i(Reactor)}^{n} x_{i(Reactor)}\, lnx_{i(Reactor)}\, \gamma_{i(Reactor)} \quad \textbf{(1.43)}$$

These values are deviations from the respective values of Gibbs energy of ideal mixtures for each system given by **Equation 1.44**.

$$G_{system} = G_{ideal} + \Delta G_{mix} = \sum_{i}^{n} H_{i(Ideal)} + T \sum_{i}^{n} S_{i(Ideal)} + \Delta G_{mix} \quad \textbf{(1.44)}$$

Aspen Plus was used to calculate all the Gibbs energy values.

2.3. Results and discussion

The experimental results show that bio-oil upgrading resulted in a product, 4-MECH, which has less oxygen content and higher solubility in the organic phase. The compositional result of the biphasic semi-continuous batch reactor is given in **Table 2.5** and **Figures 2.5** and **2.6.** The first two components in the reaction series have limited solubility in the oil phase, and the partition coefficient for the third component, p-cresol, and the forth component, 4-MECH, is 3.3 and 5.7, respectively, at the reaction temperature. The presence of phase transfer is demonstrated with the compositional change evidenced by the fact that the reaction starts with 0.14 g of p-BAL in the water phase and ends with 0.05 g of p-cresol and 0.03 g of 4-MECH in the

organic phase, which indicates that above 50% of the total initial reactant mass migrates to the organic phase, as shown in **Table 2.2**.

The modeling and simulation of p-hydroxybenzaldehyde hydrogenation to 4-methylcyclohexanol in a biphasic reaction system involved kinetically constrained reactions and phase equilibria computations. The effect of the thermodynamic model parameters on the equilibrium property predictions shows how various sources of NRTL model parameters affect the distribution of the components in the phases. For validating the model and algorithm, the rate of reaction is analyzed along with the Gibbs energy profile and the activity coefficients. As the reactions progress with time, the rate of reactions and the Gibbs energy profile give a picture of the concurrent reaction and redistribution of the components in the reaction.

The surface reaction and adsorption equilibrium constants obtained using the nonlinear regression in Excel-solver are shown in Table 2.3.

2.3.1. Model predictions and simulation results

The effect of the thermodynamic model and LLE binary parameter sources on the simulation results was investigated by comparing the three case studies. As the reaction progressed, the experimental composition data was compared with the simulation results. The estimated errors in the experimental measurements were tracked using error bars of ±5% on the concentration data.

In Case I, **Figures 2.5** and **2.6** (top) show the distribution of the components when *a priori* predicted NRTL parameters by the UNIFAC and QSPR NRTL models are used. The model predictions show significant deviations from the experimental results especially in the decalin phase. This could be attributed to the inability of the UNIFAC model to capture appropriately the thermodynamic behavior of LLE systems and to account for the temperature

dependence of the properties [20, 39]. This case, however, serves as the base case for comparison of simulation result improvements realized in Case II and III.

The simulation results incorporating additional NRTL binary parameters obtained from the ASPEN LLE database (Case II) demonstrate prediction improvements for p-BAL and p-BOL. The use of binary parameters for p-cresol and p-BOL did not result in improvements to either the p-cresol or p-BOL predictions. Since both p-BOL and p-cresol are present in decalin in the infinite-dilution range, and the distribution of p-BOL and p-cresol may be highly affected by the presence of larger quantities of water and decalin, changes in the simulation results are insensitive to changes to the parameter values. The improvements obtained by using regressed NRTL binary parameters can be observed in **Figures 2.4** and **2.5** (middle).

Our results showed that binary parameters regressed from experimental data resulted in the most accurate representations. *A priori* predicted NRTL parameters using UNIFAC and QSPR models represent alternative methods for calculation of the parameters when experimental data is unavailable. (Case III) provides the best-case scenario. The overall prediction improvements obtained in case III can be seen in **Figure 2.4** and **2.5 (**bottom), and **Table 2.5**.

2.3.2. Gibbs Energy minimization analysis

For a given closed system, reactions occur as the Gibbs free energy proceeds to a minimum. A method of validating the biphasic reactor model is to track the change in Gibbs energy of the system to ensure that both reactions in the aqueous and organic phase and component phase distribution as the reaction progresses, results in a lower local and overall Gibbs energy, respectively. The heat of reaction and Gibbs energy change based on molar values for the three reactions, and the biphasic reactor mixtures are provided in Appendix C in **Tables C.1 and Table C.2** respectively. The heat of reaction for all reactions is found to be exothermic. The product of the first reaction has a higher Gibbs energy than the reactants; however, products of

the second and third reaction have higher but negative overall Gibbs energy change than the first reaction. A positive Gibbs energy change is possible for individual reactions, as long as the Gibbs energy change is negative for the overall reaction. For example, Wang et al. showed that in the production of lactic acid from cellulose, the Gibbs energy change of one of the intermediate reactions is positive while the Gibbs energy change for the overall reaction is negative [40].

Figure 2.7 presents the overall dynamics of the Gibbs free energy change in the biphasic reactor. The Gibbs energy of mixture for the organic and aqueous phase reactors decreases with reaction at each discreet time iteration. Further, the Gibbs energy for both the organic and aqueous phase, as well as the biphasic reactor mixtures, also decreases with time. The decline of Gibbs energy shows the progress of the reaction, as well as component phase distribution toward local equilibrium at the interface and global equilibrium in the reactor, which validates our simulation assumptions.

2.3.3. Activity coefficient analysis

The reaction rates could be expressed in terms of activities, which are products of the concentration of the species and their activity coefficients; however, for reacting systems where the activity coefficients are relatively constant through the course of the reactions, activity coefficients may become part of the rate constant and can be omitted from the rate expression [9, 41, 42]. To investigate the behavior of the activity coefficients of the components as the reactions progress, the values for each component was generated over the reaction time, and the changes in between time increment iterations were found to be less than 1%.

Figures 7 and **8** provide the plot of activity coefficient of the reacting components as the reaction progresses with time. The expectation was that the activity coefficients would remain constant at equilibrium as the components are in the infinite-dilution region. From the figures, the activity coefficients of the reacting species are observed to remain relatively constant throughout

the reaction, validating the use of concentrations of the species in the derivation of the reaction rate law.

2.4. Conclusions

An algorithm proposed for modeling a biphasic reactor was implemented successfully. Hydrogenation of p-hydroxybenzaldehyde to 4-methylcyclohexanol in a decalin/water biphasic system was used as a prototype of a biphasic reactor model involving phase equilibria with kinetically constrained catalytic reactions. Kinetic modeling of the reaction using the Eley-Rideal mechanism fit the experimental data. Aspen Plus and Aspen Simulation Workbook were useful in constructing and testing the biphasic reactor model. Both QSPR-NRTL and UNIFAC models could be used to determine LLE binary parameters when binary parameters regressed from experimental data are not available. Model validation tests for the biphasic reactor using rate of reaction, Gibbs energy and activity coefficient analyses showed that the reactor modeling is reasonable, as the trends observed in the simulation of the biphasic reactor model coincide with the experimental observations.

Acknowledgments

This study was financially supported by the U.S. Department of Energy, DOE/EPSCOR (Grant DE-SC0004600).

Table 2.1. Prototype reactor operating conditions

Operating Conditions	
Temperature °C	150
Pressure	400 psi H_2
Catalyst Type	5% Ru/SWNT MCM-41
Catalyst weight	15 mg
Reaction time, min	30 - 90
Reaction volume, ml	Decalin: 25 ± 0.1
	Water: 25 ± 0.1
	p-BAL: 150 ± 0.5 mg
Reactor Volume, ml	100

Table 2.2. Source of NRTL binary parameters for the simulations

Sources of binary parameters			Sources of binary parameters		
			Case I	Case I	Case III
1	decalin	p-BAL	QSPR/UNIFAC	QSPR/UNIFAC	QSPR/UNIFAC
2	decalin	p-BOL	QSPR/UNIFAC	QSPR/UNIFAC	QSPR/UNIFAC
3	water	p-BAL	QSPR/UNIFAC	QSPR/UNIFAC	QSPR/UNIFAC
4	p-BAL	p-BOL	QSPR/UNIFAC	QSPR/UNIFAC	QSPR/UNIFAC
5	p-BAL	p-cresol	QSPR/UNIFAC	QSPR/UNIFAC	QSPR/UNIFAC
6	p-BAL	4-MECH	QSPR/UNIFAC	QSPR/UNIFAC	QSPR/UNIFAC
7	p-BOL	4-MECH	QSPR/UNIFAC	QSPR/UNIFAC	QSPR/UNIFAC
8	p-cresol	4-MECH	QSPR/UNIFAC	QSPR/UNIFAC	QSPR/UNIFAC
9	decalin	water	QSPR/UNIFAC	QSPR/UNIFAC	Regressed(OU)
10	decalin	p-cresol	QSPR/UNIFAC	QSPR/UNIFAC	Regressed(OU)
11	decalin	4-MECH	QSPR/UNIFAC	QSPR/UNIFAC	Regressed(OU)
12	water	p-cresol	QSPR/UNIFAC	QSPR/UNIFAC	Regressed(OU)
13	water	4-MECH	QSPR/UNIFAC	QSPR/UNIFAC	Regressed(OU)
14	water	p-BOL	QSPR/UNIFAC	Aspen Plus	Aspen Plus
15	p-BOL	p-cresol	QSPR/UNIFAC	Aspen Plus	Aspen Plus

Table 2.3. Regressed kinetic parameters and mass transfer coefficients

Rate Constants (mM/min)		Adsorption Constants (mM^{-1})		Partition Coefficients		Mass Transfer Coefficients (m/s)	
K_1	24.1	$K_{p\text{-}BAL}$	0.0050	$k_{p\ p\text{-}BAL}$	-	$k_{p\text{-}BAL1}$	0
K_2	5.5	$K_{p\text{-}BOL}$	0.0050	$k_{p\ p\text{-}BOL}$	-	$k_{p\text{-}BAL\text{-}1}$	0
K_3	13.3	$K_{p\text{-}cresol}$	0.0008	$k_{p\ p\text{-}cresol}$	3.3	$k_{p\text{-}BOL1}$	0
		$K_{p4\text{-}MECH}$	0.0003	$k_{p\ 4\text{-}MECH}$	5.7	$k_{p\text{-}BOL\text{-}1}$	0
		K_{H2}	0.0003			$k_{p\text{-}cresol\text{-}1}$	0.012
						$k_{p\text{-}cresol\text{-}1}$	0.004
						$k_{4\text{-}MECH1}$	0.04
						$k_{4\text{-}MECH\text{-}1}$	0.007

Table 2.4. Changes in chemical compositions from experiments in a biphasic reactor

Time	Aqueous phase(mM/l)				Organic phase(mM/l)			
(Min)	p-BAL	p-BOL	p-Cresol	4-MeHOL	p-BAL	p-BOL	p-Cresol	4-MeHOL
0	47.0	0.0	0.0	0.0	0.0	0.0	0.0	0.0
10	20.9	23.4	0.8	0.0	0.0	0.0	1.6	0.0
25	5.9	30.7	1.1	0.0	0.0	0.0	8.1	0.0
45	2.2	25.7	4.2	0.6	0.0	0.0	12.5	2.2
90	1.4	10.8	8.9	1.6	0.0	0.0	16.1	6.8

Table 2.5. Predictions results obtained using different NRTL binary parameter sources

Parameter source	RMSE (mmol/L)								
	Water phase				Organic phase				Overall
	p-BAL	p-BOL	p-cresol	4-MECH	p-BAL	p-BOL	p-cresol	4-MeCH	
UNIFAC	1.87	1.69	7.01	0.68	0.23	0.67	6.14	0.36	9.71
UNIFAC – Aspen LLE	1.86	2.14	6.09	1.72	0.24	0.10	5.28	1.33	8.82
UNIFAC – Aspen LLE-Regressed	0.80	0.41	1.50	0.62	0.00	0.24	1.30	0.28	2.30
QSPR	3.65	1.74	6.85	2.45	0.90	1.19	7.98	3.07	12.0
QSPR – Aspen LLE	3.64	1.08	6.82	2.42	0.90	0.33	8.07	3.08	11.3
QSPR – Aspen LLE-Regressed	1.37	0.56	1.10	0.11	1.23	0.03	1.19	0.78	2.63

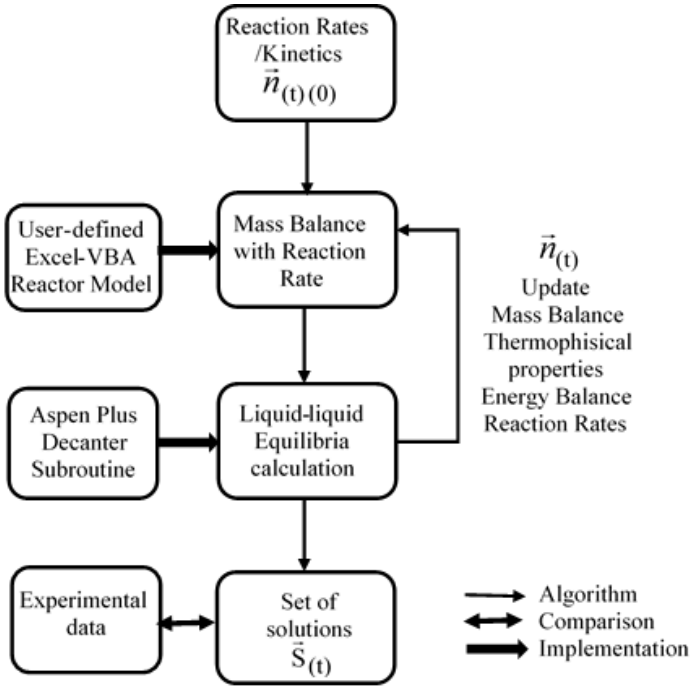

Figure 2.1. Schematic showing various steps used in modeling a biphasic reactor

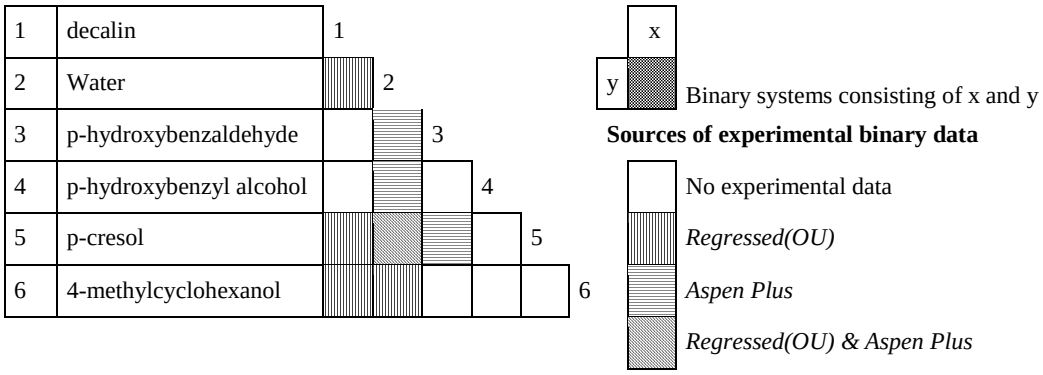

Figure 2.2. Thermodynamic model parameter data matrix

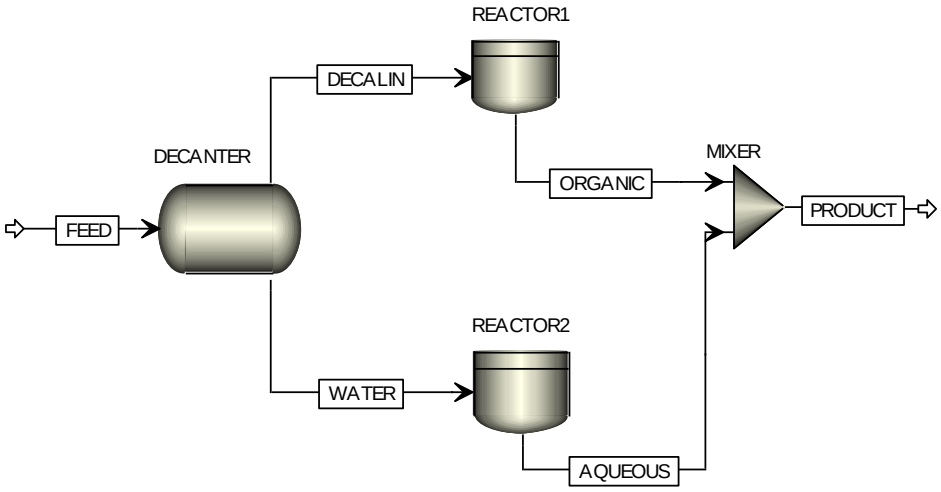

Figure 2.3. Schematic for the biphasic reactor simulation

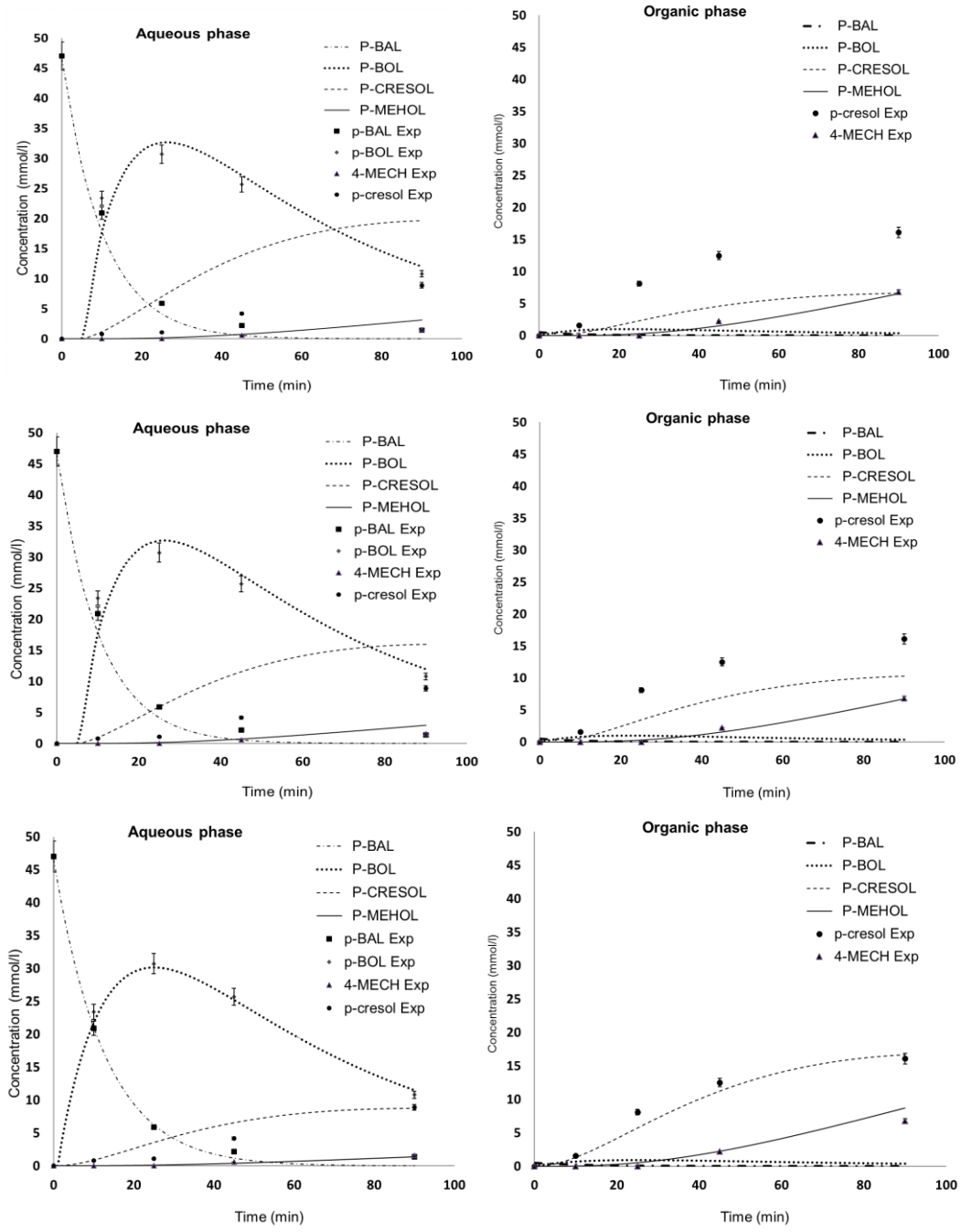

Figure 2.4. Simulation results using UNIFAC *a priori* predicted (top), UNIFAC- Aspen Plus LLE (middle), UNIFAC- Aspen Plus LLE-Regressed (bottom) NRTL binary parameters

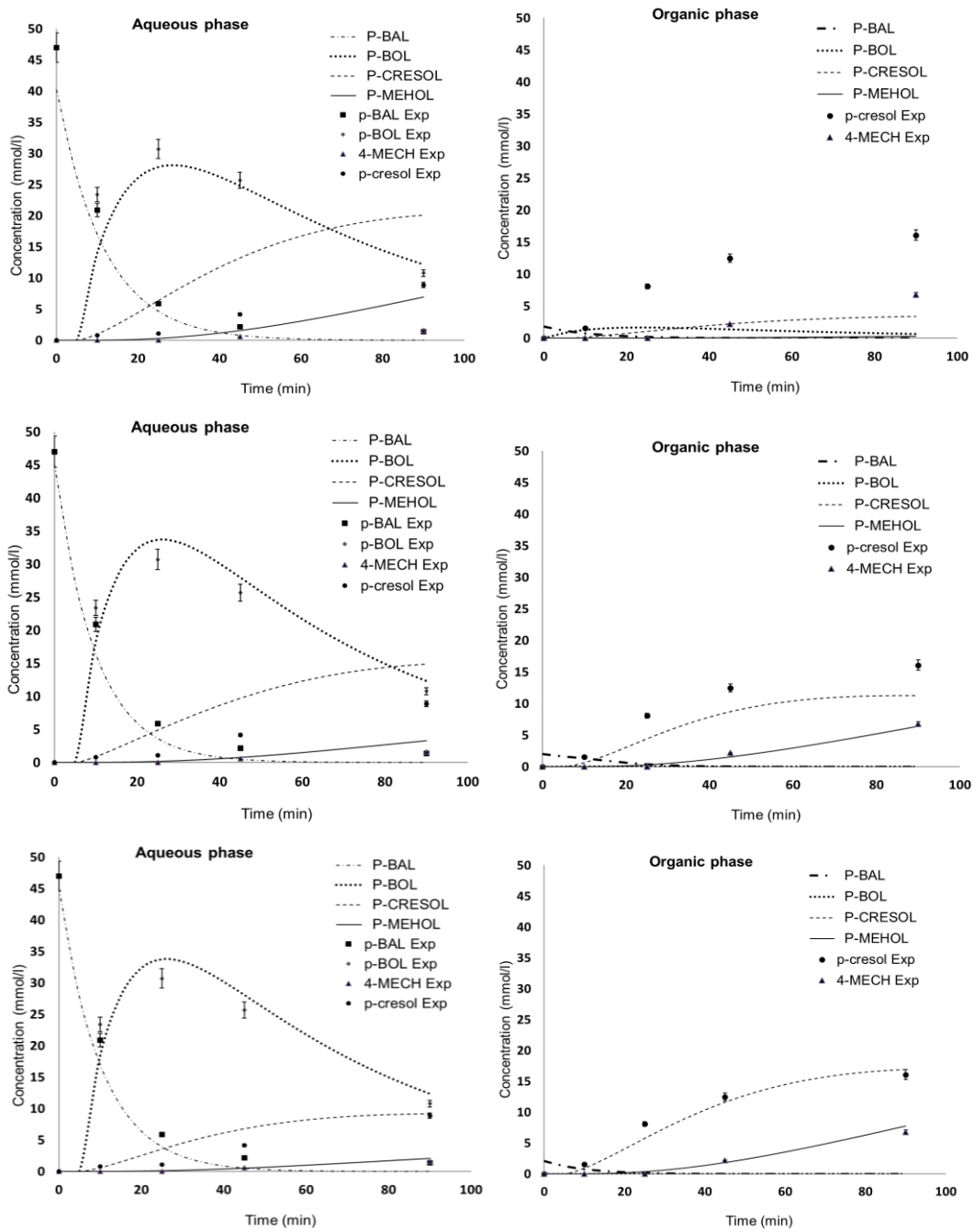

Figure 2.5. Simulation results using QSPR *a priori* predicted (top), QSPR - Aspen Plus LLE (middle), QSPR- Aspen Plus LLE- Regressed (bottom) NRTL binary parameters

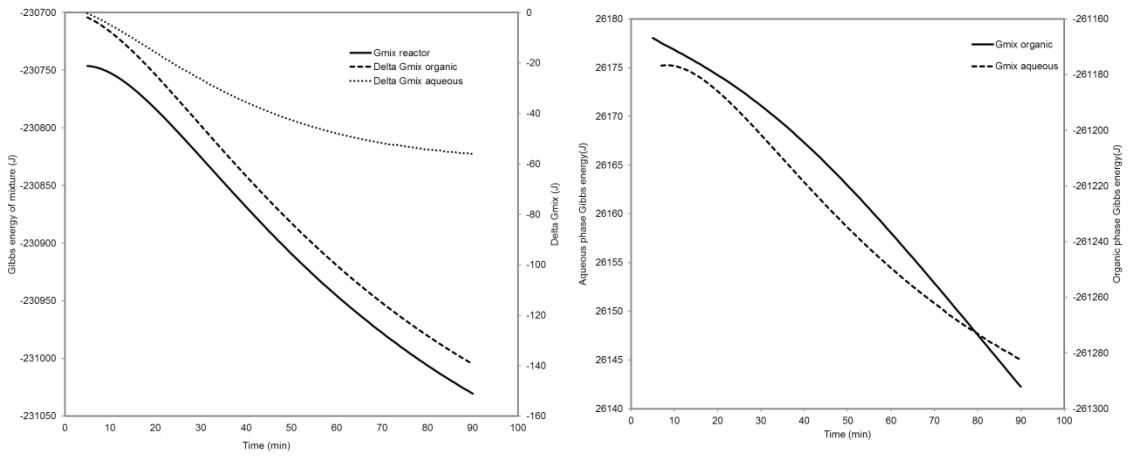

Figure 2.6. Simulation results for Gibbs energy of the mixture and change in Gibbs energy

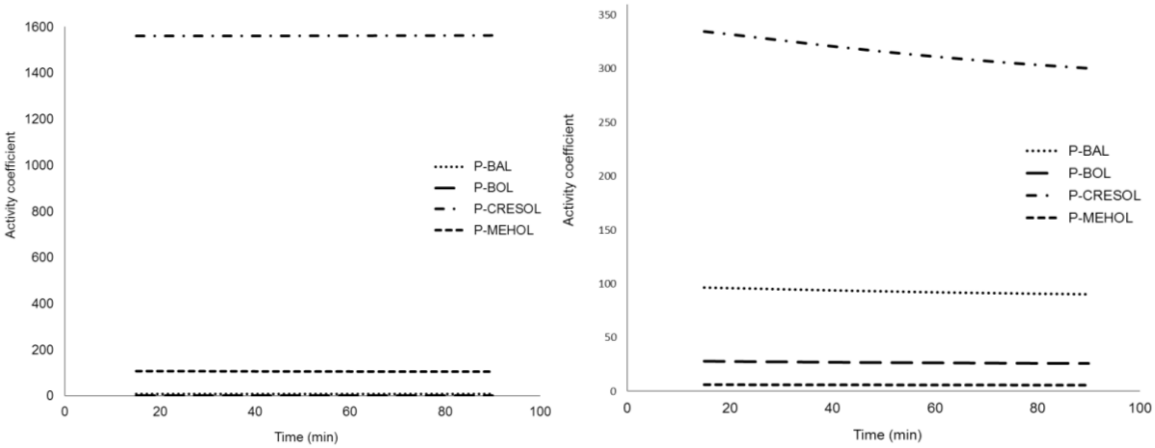

Figure 2.7. Simulation results for activity coefficient (γ) of components using UNIFAC-Aspen Plus LLE-Regressed NRTL parameters for aqueous phase (left) and organic phase (right).

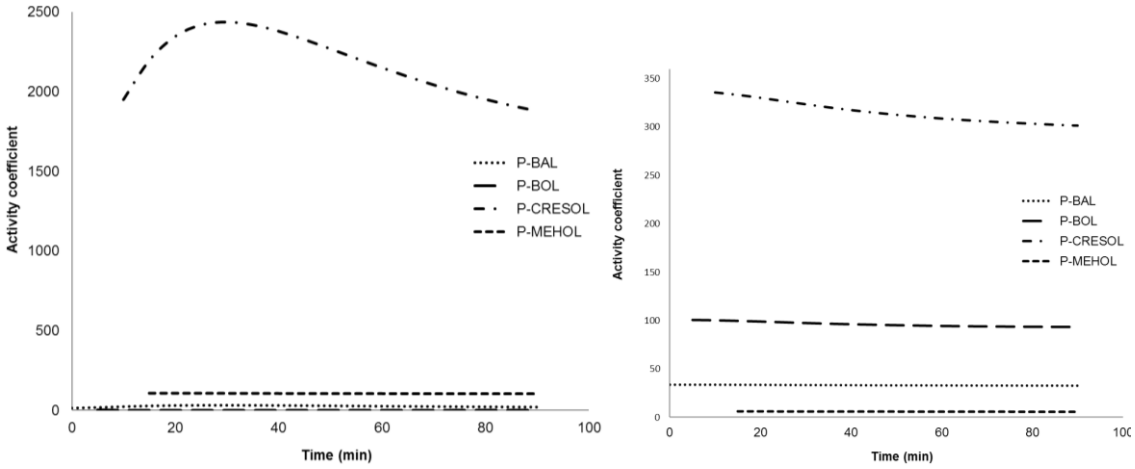

Figure 2.8. Simulation results for activity coefficient (γ) of reacting components using QSPR-Aspen Plus LLE-Regressed (OU) NRTL parameters for aqueous phase (left) and organic phase (right).

REFERENCES

1. Mahfud, F., F. Ghijsen, and H. Heeres, *Hydrogenation of Fast Pyrolyis Oil and Model Compounds in a Two-Phase Aqueous Organic System Using Homogeneous Ruthenium Catalysts.* Journal of Molecular Catalysis A: Chemical, 2007. **264**(1-2): p. 227-236.
2. Huber, G.W., S. Iborra, and A. Corma, *Synthesis of Transportation Fuels from Biomass: Chemistry, Catalysts, and Engineering.* Chemical Review, 2006. **106**(9): p. 4044-4098.
3. Mahfud, F.H., et al., *The Application of Water-Soluble Ruthenium Catalysts for the Hydrogenation of the Dichloromethane Soluble Fraction of Fast Pyrolysis Oil and Related Model Compounds in a Two Phase Aqueous–Organic System.* Journal of Molecular Catalysis A: Chemical, 2007. **277**(1-2): p. 127-136.
4. Crossley, S., et al., *Solid Nanoparticles that Catalyze Biofuel Upgrade Reactions at the Water/Oil Interface.* Science, 2010. **327**(5961): p. 68-72.
5. Czernik, S. and A.V. Bridgwater, *Overview of Applications of Biomass Fast Pyrolysis Oil.* Energy & Fuels, 2004. **18**(2): p. 590-598.
6. Domine, M.E., et al., *Coprocessing of Oxygenated Biomass Compounds and Hydrocarbons for the Production of Sustainable Fuel.* ChemSusChem, 2008. **1**(3): p. 179-181.
7. Santhanaraj, D., et al., *Gluconic Acid from Biomass Fast Pyrolysis Oils: Specialty Chemicals from the Thermochemical Conversion of Biomass.* ChemSusChem, 2014. **7**(11): p. 3132-3137.
8. Mahfud, F.H., *Exploratory Studies on Fast Pyrolysis Oil Upgrading*, in *Faculty of Mathematics and Natural Sciences*. 2007, University of Groningen. p. 158.
9. Resasco, D.E., et al., *Furfurals as Chemical Platform for Biofuels Production*, in *Heterogeneous in Biomass to Chemicals and Fuels*, D. Kubička and I. Kubičková, Editors. 2011, Research Signpost. p. 155-188.
10. Simonetti, D.A. and J.A. Dumesic, *Catalytic Strategies for Changing the Energy Content and Achieving C-C Coupling in Biomass-Derived Oxygenated Hydrocarbons.* ChemSusChem, 2008. **1**(8-9): p. 725-733.
11. Zapata, P., et al., *Condensation/Hydrogenation of Biomass-Derived Oxygenates in Water/Oil Emulsions Stabilized by Nanohybrid Catalysts.* Topics in Catalysis, 2012. **55**(1): p. 38-52.
12. Faria, J., M.P. Ruiz, and D.E. Resasco, *Phase-Selective Catalysis in Emulsions Stabilized by Janus Silica-Nanoparticles.* Advanced Synthesis & Catalysis, 2010. **352**(14-15): p. 2359-2364.
13. Zapata, P.A., et al., Hydrophobic Zeolites for Biofuel Upgrading Reactions at the

Liquid–Liquid Interface in Water/Oil Emulsions. Journal of the American Chemical Society, 2012. **134**(20): p. 8570-8578.
14. Perego, C. and A. Bosetti, *Biomass to fuels: The role of zeolite and mesoporous materials.* Microporous and Mesoporous Materials, 2011. **144**(1–3): p. 28-39.
15. Morita, T., H.J. Lim, and I. Karube, *Enzymatic hydrolysis of polysaccharides in water-immiscible organic solvent, biphasic systems.* Journal of Biotechnology, 1995. **38**(3): p. 253-261.
16. Fogler, H.S., *Elements of Chemical Reaction Engineering*. 4th ed. ed. 2006, Upper Saddle River, NJ: Prentice Hall PTR.
17. Renon, H. and J.M. Prausnitz, *Local Compositions in Thermodynamic Excess Functions for Liquid Mixtures.* American Institute of Chemical Engineers, 1968. **14**(1): p. 135-144.
18. Prausnitz, J.M., R.N. Lichtenthaler, and E.G. de Azevedo, *Molecular Thermodynamics of Fluid-Phase Equilibria*. 1998: Prentice Hall.
19. Aspen Technology, I., *Aspen Plus 8.2*. 2013.
20. Gebreyohannes, S., et al., *Improved QSPR Generalized Interaction Parameters for the Nonrandom Two-Liquid Activity Coefficient Model.* Fluid Phase Equilibria, 2013. **339**: p. 20-30.
21. Rioux, R.M. and M.A. Vannice, *Hydrogenation/Dehydrogenation Reactions: Isopropanol Dehydrogenation overCopper Catalysts.* Journal of Catalysis, 2003. **216**(1–2): p. 362-376.
22. Sitthisa, S., et al., *Kinetics and Mechanism of Hydrogenation of Furfural on Cu/SiO2 Catalysts.* Journal of Catalysis, 2011. **277**(1): p. 1-13.
23. Resasco, D.E., et al., *Center for Interfacial Reaction Engineering - EPSCoR Implementation Award*. 2007, DOE/EPSCoR.
24. Aspen Technology, I., *Aspen Physical Property System: Physical Property Methods*. V7.0 ed. 2008, Burlington, MA 01803, USA: Aspen Technology, Inc. 129.
25. Ravindranath, D., et al., *QSPR Generalization of Activity Coefficient Models for Predicting Vapor–Liquid Equilibrium Behavior.* Fluid Phase Equilibria, 2007. **257**(1): p. 53-62.
26. Magnussen, T., *UNIFAC Parameter Table for Prediction of Liquid-Liquid Equilibria*. DECHEMA. 1981, Frankfurt am Main 97, Wesf Germany: Postfach 97 01 46.
27. Wang, Y., et al., *Chemical Synthesis of Lactic Acid from Cellulose Catalysed by Lead(II) Ions In Water*, in *Nature Communications*. 2013, Nature Publishing Group, a division of Macmillan Publishers Limited. All Rights Reserved. p. 2141.
28. Kline, W.E. and H.S. Fogler, *Dissolution Kinetics: Catalysis by Salts.* Journal of Colloid and Interface Science, 1981. **82**(1): p. 103-115.
29. Kline, W.E. and H.S. Fogler, *Dissolution kinetics: Catalysis by Strong Acids.* Journal of Colloid and Interface Science, 1981. **82**(1): p. 93-102.
30. Ruiz, M.P., et al., *Nanostructured Carbon–Metal Oxide Hybrids as Amphiphilic Emulsion Catalysts.* ChemSusChem, 2011. **4**(7): p. 964-974.

CHAPTER III

MODELING AND SIMULATION OF BIPHASIC REACTORS WITH CATALYTIC SURFACE REACTIONS AT THE WATER/OIL INTERFACE; A MASS TRANSFER APPROACH

3.1. Introduction

Biphasic reactors can employ catalytic surface reactions in a Pickering emulsion of aqueous and organic liquids with simultaneous mass transfer of reacting components inside each phase and across the interface [1]. These important features of biphasic reactors could help reduce or eliminate the need of downstream processes for product separation [2, 3]. By optimizing the operating parameters of biphasic reactors, improving selectivity and yield, and controlling rate of reactions could be possible. This requires a thorough understanding of the biphasic reactor operations including the kinetics of reactions, mass transfer of components, and the interaction between them. Therefore, process modeling and simulation could be used to quantify and predict the effect of reaction, as well as, mass transfer on the composition dynamics of the biphasic reactor. A specific example of biphasic reactor application used in this study is the upgrading of biofuels from fast pyrolysis of lignocellulosic materials by refining oxygenated derivatives using nanohybrid amphiphilic catalysts [4].

The hydrogenation of p-hydroxy benzaldehyde (p-BAL) to 4-methylcycolohexanol (4-MECH), a typical biofuel upgrading reaction, was used as a case study to develop and validate

the model. The intermediate products are p-hydroxy benzyl alcohol (p-BOL) and p-cresol. The reactor operates at 150 ˚C and constant supply of H_2 at 400 psi in a 100 ml semi- bacth biphasic reactor of equal volumes of organic and aqueous phases. Amphiphilic metal-supported single walled carbon nanotube (5 Ru/SWNT-SiO_2 MCM-41) was used as both as a catalyst and emulsion stabilizing agent. The active metal catalysts were preferentially deposited on the hydrophilic and hydrophobic side of nanohybrids so that catalysts could appear on both sides of the interface. The catalyst preparations and experimental procedures for similar reactions are described in previous studies by Crossly et al. [1]. The experiment was carefully designed so that there will be components with different solubilities in both phases and mass transfer exists between the two phases as discussed in Faria and Zapata et al. [22, 23]. The presence of chemical reaction on both phases of the reactor and partitioning of components due to phase distribution between the organic and aqueous phases in the mixture was also confirmed in similar studies by Crossley et al. [1] and Ruiz et al.[24]. The reaction pathway for the model reaction is given as follows.

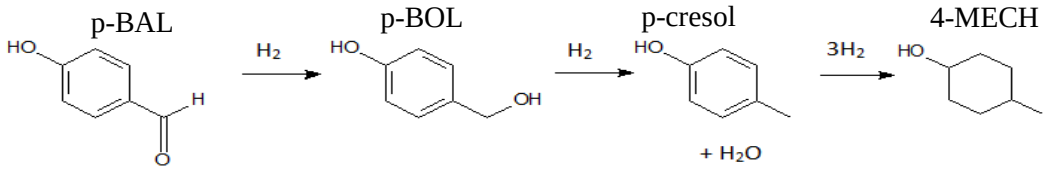

$$R_{Water} \underset{k_{-pR}}{\overset{k_{pR}}{\rightleftharpoons}} R_{Oil}$$

$$R_{Water} \xrightarrow{k_o} P_{Water}$$

$$R_{Oil} \xrightarrow{k_o} P_{Oil}$$

where R is any reacting component, P is the corresponding product, and k_{pR} and k_o are mass transfer coefficient and rate constants, respectively.

Different modelling approaches may be used to represent the reaction- phase separation scheme, depending on the operating parameters of the biphasic reactor and the assumptions taken to simplify system modeling. For heterogeneous catalysis, Langmuir-Hinshelwood or Eleyi-Rdeal

models can be used to describe the reaction mechanism [5]. Different steps could be rate limiting in the reaction mechanism. For example, Madon et al. [6] showed that chemisorption of dissolved hydrogen molecules was the rate limiting step in the liquid phase hydrogenation of cyclohexene over Pd catalyst. However, the surface reaction might be a rate-controlling step if there is efficient mass transfer of hydrogen to the surface of the catalyst [5, 7-9]. If the mass transfer resistance within and between the phases is reduced due to high solubility of components and lower droplet size (high interfacial area) and adequate mixing, the phase distribution ratio might approximate the equilibrium partition coefficient. In this case, phase equilibria might be used to represent the component phase separation. Our previous work attempted to model the same system with a phase equilibria assumption [10]. However, the presence of phase selectivity in some reactions in a biphasic medium could be well explained by the mass transfer resistances occurring inside and across each phase in the emulsion [11]. Assessing the effect of emulsion drop size, emulsion type (water in oil or oil in water), and partition coefficient on the rate of mass transfer could be better realized by the mass transfer model as the variables appear directly in the model equations [12-14].

Different studies have reported on modelling of biphasic reactors with mass transfer resistance. A diffusional model is used when there is mass transfer within the phase in a stagnant region with some boundary conditions (Hu, Wang et al. 2008, Pugazhenthi and Kumar 2008) while interfacial mass transfer resistance is used for modeling of mass transfer in emulsion where adequate mixing is involved [3, 12, 14-19]. Further, in most of the literature in modeling interfacial mass transfer, the reaction is usually occurring in a single phase, and mass transfer is usually considered in one direction. This work, however, focuses on modelling biphasic reactors with heterogeneous chemical reactions in both phases and stabilized by solid nano particles with possible mass transfer in both directions. A mass transfer approach to model and simulate biphasic reactors was proposed and experimental data from hydrogenation of p-hydroxy

benzaldehyde to 4-methylcelohexanol was used to evaluate the performance of the proposed model.

Evaluation of thermodynamic properties such as activity coefficients for chemical reaction and Gibbs energy of the system is important to validate the underlying assumptions taken to develop the model. A Gibbs energy test could be used to justify the presence of reaction on both sides, the direction of mass transfer and if the overall simulation goes toward minimizing the organic phase, aqueous phase and overall rector mixture Gibbs energy. Further, since the reaction is taking place in both phases with interfacial mass transfer, simultaneous calculation of the mass and energy balances should be performed to validate the composition changes due to reactions and phase transfer. This requires intensive calculations of thermos-physical properties at each time step of the reaction with possible multiple iterations during the entire reaction time. The use of commercial thermos-physical property calculation software such as Aspen Plus [20], could be used and integrated to the biphasic reactor model. The Non-Random-Two-Liquid (NRTL) phase equilibria model could be used to evaluate the required thermodynamic properties for liquid systems with limited solubility [21].

This work provides significance in two aspects. First, the model will increase our understanding of the interaction between mass transfer and kinetics in biphasic reactors, where surface reactions occur at the water/oil interface. Secondly, we demonstrated successful integration of the commercial software Aspen Plus with the biphasic reactor model. Biphasic reactor models, with sensitive model parameters to small changes, could benefit from the highly rigorous calculations provided by the commercial simulation software.

3.2. Methods

3.2.1. Simulation strategy

The computational procedure used in the implementation of modelling and simulation of the biphasic reactor was based on three main assumptions. First, a saturated hydrogen with the

liquid phase was assumed at the beginning of reaction and the semi continuous system was treated as a batch reaction operating under the same temperature and pressure for the purpose of mass balance and Gibbs energy calculation. The effect of solvent on reaction rate is assumed minimal, such that the reaction mechanism and kinetic parameters in both phases is the same. Rate of reaction is evaluated with average concentration of reacting species, and the species activity coefficient term is assumed to remain constant throughout the reaction time.

The algorithm used in the implementation of modeling and simulation of the catalytic process and the associated interfacial mass transfer using Excel-VBA and Aspen Plus is outlined in **Figure 3.1**. The implementation starts with devising a rate mechanism for the heterogeneous reaction and mass transfer separately. Then, the parameters for the kinetic and mass transfer models are determined. The reaction kinetics and the mass transfer mathematical model code were written and implemented in VBA. Microsoft Excel and Aspen simulation workbook were used to facilitate information flow between VBA and Aspen Plus. Gibbs Energy, concentrations, activity coefficients and other necessary themo-phsycal properties were calculated in Aspen Plus using the nonrandom two liquid (NRTL) [21] thermodynamic liquid-liquid equilibrium model.

The procedure for the model implementation using Aspen Plus with reactor and mass transfer model user defined interfaces on VBA-Excel calls for,

(a) at time t=0s, all stream properties for each phase such as composition, mole fraction, activity coefficient, mass and energy balance, mixture Gibbs energy for each phase and the overall reactor is evaluated using Aspen Plus and the results are sent to Excel through Aspen Simulation Workbook (ASW).

(b) at time t=0s, the kinetics in both phases is evaluated independently in the user defined reactor module in VBA-Excel.

(c) the resulting composition values in Aspen Plus is then updated through ASW. Then, the procedure in part (a) is repeated with the new composition value.

(d) then determination of mass transfer directions and rate of mass transfer using the two film theory model is performed using user defined models in VBA-Excel. Products p-cresol and 4-MECH are soluble in both phases and preferentially distribute between the two phases depending on their relative compositions in each phases.

(e) the new composition values in both phases in Aspen Plus are updated through ASW, and stream and mixture property calculations in part (a) are performed.

(f) at time t=t+Δt, reaction kinetics are evaluated based on the new reaction feed composition for the next time increment (Δt) of an updated Step b; and

(g) the process continues iteratively until the set of solutions for the distribution of the components in each coexisting phase as a function of time is obtained for the entire reaction time.

3.2.2. Kinetic model derivation

The kinetic model derived for this study is given in **Equation 3.1-3.5**. The following assumptions were made in the derivation of the reaction mechanism: (a) molecular adsorption of p-BAL, (b) non-competitive molecular adsorption of hydrogen gas, (c) single reactant binding site, (d) all adsorption sites are alike, (e) the irreversible surface reaction between adsorbed molecules and the hydrogen in the gas phase is the rate-limiting step, and (f) reversible desorption of the products.

$$r_A = -\frac{k_{R_1} C_{SO} K_A P_{H_2}}{\Theta_V} C_A = -\frac{k_1 K_A}{\Theta_V} C_A \qquad \textbf{(3.1)}$$

$$r_B = \frac{k_1 K_A}{\Theta_V} C_A - \frac{k_2 K_B}{\Theta_V} C_B \quad \textbf{(3.2)}$$

$$r_C = \frac{k_2 K_B}{\Theta_V} C_B - \frac{k_3 K_C}{\Theta_V} C_C \quad \textbf{(3.3)}$$

$$r_D = \frac{k_3 K_C}{\Theta_V} C_C \quad \textbf{(3.4)}$$

$$\Theta_V = 1 + K_A C_{A-TOTAL} + K_B C_{B-TOTAL} + K_C C_{C-TOTAL} + K_D C_{D-TOTAL} + K_{H_2}^{1/2} P_{H_2}^{1/2} \quad \textbf{(3.5)}$$

Where

$$k_1 = k_{R_1} C_{SO} P_{H_2}, \quad K_A = \frac{k_A}{k_{-A}}, \quad k_2 = k_{R_2} C_{SO} P_{H_2}, \quad K_B = \frac{k_{-D_1}}{k_{D_1}}$$

$$k_3 = k_{R_3} C_{SO} P_{H_2}{}^3, \quad K_C = \frac{k_{-D_2}}{k_{D_2}}, \quad K_D = \frac{k_{-D_3}}{k_{D_3}}, \quad \text{and } K_{H_2} = \frac{k_{H_2}}{k_{-H_2}}$$

A is p-hydroxybenzaldehyde (p-BAL)

B is p-hydroxybenzylalcohol (p-BOL)

C is p-cresol (p-cresol)

D is 4-methylcyclohexanol (4-MECH)

H_2 is hydrogen gas

K is equilibrium adsorption constants (mM^{-1})

k is rate constant (mM/min)

Θ_V is available catalyst surface fraction

Applying the complete mass balance for the biphasic system by accounting for the transfer of mass between the phases provides the complete rate expressions for the biphasic reactions. The mass transfer section in our model is represented by phase equilibria separation. In

multi component phase equilibria calculations, the value of the partition coefficient may be dependent on composition and may not remain constant, as it is shown in the model equations.

$$r_{A-Oil} = \frac{dC_{A-Oil}}{dt} = -\frac{k_1 K_A C_{A-Oil}}{\Theta_V} - k_{pA_{-1}} C_{A-Oil} + k_{pA_1} C_{A-Water} \quad \textbf{(3.6)}$$

$$r_{A-Water} = \frac{dC_{A-Water}}{dt} = -\frac{k_1 K_A C_{A-Water}}{\Theta_V} + k_{pA_{-1}} C_{A-Oil} - k_{pA_1} C_{A-Water} \quad \textbf{(3.7)}$$

$$r_{B-Oil} = \frac{dC_{B-Oil}}{dt} = \frac{k_1 K_A C_{A-Oil}}{\Theta_V} - \frac{k_2 K_B C_{B-Oil}}{\Theta_V} - k_{pB_{-1}} C_{B-Oil} + k_{pB_1} C_{B-Water} \quad \textbf{(3.8)}$$

$$r_{B-WATER} = \frac{dC_{B-Water}}{dt} = \frac{k_1 K_A C_{A-Water}}{\Theta_V} - \frac{k_2 K_B C_{B-Water}}{\Theta_V} + k_{pB_{-1}} C_{B-Oil} - k_{pB_1} C_{B-Water} \quad \textbf{(3.9)}$$

$$r_{C-Oil} = \frac{dC_{C-Oil}}{dt} = \frac{k_2 K_B C_{B-Oil}}{\Theta_V} - \frac{k_3 K_C C_{C-Oil}}{\Theta_V} - k_{pC_{-1}} C_{C-Oil} + k_{pC_1} C_{C-Water} \quad \textbf{(3.10)}$$

$$r_{C-Water} = \frac{dC_{C-Water}}{dt} = \frac{k_2 K_B C_{B-Water}}{\Theta_V} - \frac{k_3 K_C C_{C-Water}}{\Theta_V} + k_{pC_{-1}} C_{C-Oil} - k_{pC_1} C_{C-Water} \quad \textbf{(3.11)}$$

$$r_{D-Oil} = \frac{dC_{D-Oil}}{dt} = \frac{k_3 K_C C_{C-Oil}}{\Theta_V} - k_{pD_{-1}} C_{D-Oil} + k_{pD_1} C_{D-Water} \quad \textbf{(3.12)}$$

$$r_{D-Water} = \frac{dC_{D-Water}}{dt} = \frac{k_3 K_C C_{C-Water}}{\Theta_V} + k_{pD_{-1}} C_{D-OIL} - k_{pD_1} C_{D-Water} \quad \textbf{(3.13)}$$

$$\Theta_V = 1 + K_A C_{A-Total} + K_B C_{B-Total} + K_C C_{C-Total} + K_D C_{D-Total} + K_{H_2}^{1/2} P_{H_2}^{1/2} \quad \textbf{(3.14)}$$

The model differential equations (**Equations 3.6-3.14)** are then solved for a given small time increment using numerical approximations by Euler's method to obtain the new product distribution. The complete equation based on the Euler's method is provided in Appendix E (**Equations E.1 –Equation E.9**).

3.2.3. Kinetic parameter determination

The operating conditions and specifications for the reactor are provided in **Table 3.1**, and experimental biphasic reactor composition data taken at different intervals of the reaction time is shown **Table 2.4** chapter 2 and discussed in the results and discussion section.

The discretized rate equations obtained for the kinetic model derivation based on the Euler's method were fitted to the experimental concentration data for a single phase. The sum of squared deviations (SSD) minimization with nonlinear least-square regression analysis was used in the fitting of the Langmuir–Hinshelwood rate law. The equilibrium adsorption constants were fitted to the experimental data, while ensuring that the adsorption constant value of p-hydroxybenzaldehyde was higher than the value for the other species, and the adsorption constant of hydrogen was very small. This follows experimental trends observed in the hydrogenation of aldehydes [21, 22].

3.2.4. Mass transfer model derivation

Effects of mass transfer limitation on Hydrogen

Since emphasis is given to the probable limiting nature of mass transfer in the biphasic medium, considering the options where mass transfer limitation of hydrogen gas might play a role in determining the rate of the first or all reactions in the series is important. For example, the study of hydrogenation of cyclohexane on the Pt and Al catalyst by Bodart showed that chemisorption of hydrogen was found to be the rate limiting step while Gonzo showed that desorption of products was the rate limiting step [8]. In this case the rate of reaction will be first order to that dissolved hydrogen concentration in the first case while the rate was proportional to the square root of dissolved hydrogen concentration in the second case as shown in **Equation 3.15** and **Equation 3.16**.

Madon, et al.[6] showed the mechanism for liquid phase hydrogenation reaction on supported platinum in a gradientless slurry reactor can be given as follows

Step 1. H_2 (g) ←→ H_2 (l)

Step 2. H_2 (l) ←→ H_2(p)

Step 3. H_2(p) +**→ 2H*

Step 4. R + ** ←→ *R*

Step 5. *R* + H* ←→ RH* + **

Step 6a. RH* + H* ←→ RH_2 +**

Step 6b. RH_2** → RH_2 +** desorption

In the above rate mechanism, the reaction rate can be assumed to be the rate of chemisorption of hydrogen (step 3), which is assumed to be the limiting (irreversible) reaction step, giving rise to a first order reaction with respect to dissolved hydrogen in the liquid,

$$r = r_3 \approx kC_{H_2} \quad \textbf{(3.15)}$$

Gonzo and Boudart [8] analyzed the reaction mechanism for the catalytic hydrogenation of cyclohexane for gas-phase and liquid-phase reaction on supported palladium. They found that step 6, which is the product desorption step, to be the rate limiting step. Accordingly, the rate equation drived for the proposed mechanism was given as follows.

$$r = r_6 \approx k(C_{H_2})^{1/2} \quad \textbf{(3.16)}$$

The concentration of reacting species in the rate equations for the aqueous phase and organic phase will be substituted by the hydrogen concentration expression C_{H2} if we assume that mass transfer of hydrogen is limiting in the reaction step.

Model derivation

The theoretical approach for the rigorous mass transport calculation in biphasic medium should consist of mass transfer due to diffusion inside each liquid phase and the distribution of molecules from one liquid phase to another due to the interfacial mass transfer. Since the reaction is taking place at the interface, there will be a concentration gradient within the droplet and the continuous phase unless the gradient is assumed insignificant due to solubility and mixing of the reacting components.

Inside each phase, the flux of a species in terms of chemical potential gradient can be calculated by the following equations.

$$\frac{dJ_{C(Oil)}}{dt} = \frac{D_{C(Oil)}C_{C(Oil)}}{RT}\frac{d\mu_{C(Oil)}}{dr} \quad \textbf{(3.17)}$$

$$\frac{dJ_{D(Oil)}}{dt} = \frac{D_{D(Oil)}C_{D(Oil)}}{RT}\frac{d\mu_{D(Oil)}}{dr} \quad \textbf{(3.18)}$$

$$\frac{dJ_{C(Water)}}{dt} = \frac{D_{C(Water)}C_{C(Water)}}{RT}\frac{d\mu_{C(Water)}}{dr} \quad \textbf{(3.19)}$$

$$\frac{dJ_{D(Water)}}{dt} = \frac{D_{D(Water)}C_{D(Water)}}{RT}\frac{d\mu_{D(Water)}}{dr} \quad \textbf{(3.20)}$$

Where

J is the mass flux (M/m^2)

D is the diffusion coefficient (m^2/s)

R is the universal constant (J / M. K.)

r is the radius of droplet (m)

x is the average distance between two droplets (m)

c is the concentration of species (M/liter)

μ is the chemical potential of species (J/M)

The concentration of a species is assumed to be dilute (in the range of mmol/liter) enough so that the relative movements of other species in the medium do not affect significantly the flux and chemical potential gradient of that given species.

The diffusional equations should be solved with the kinetics and interfacial mass transfer flux equations. Individual (for A, B, C, and D) kinetic equations at each phase, given in the kinetic model section, and mass transfer of C and D across the interface should be solved simultaneously. The equations for interfacial mass transfer are,

$$N_C = K_{m(O/W)}a(\phi_C C_{C(Water)} - C_{C(Oil)}) \approx K_{m(W/O)}a(C_{C(Water)} - (1/\phi_C)C_{C(Oil)})$$

$$N_D = K_{m(O/W)}a(\phi_C C_{D(Water)} - C_{D(Oil)}) \approx K_{m(W/O)}a(C_{D(Water)} - (1/\phi_D)C_{D(Oil)})$$

Where

$C_{A(Oil)}$ is the concentration of A in the oil phase *(mol/m^3)*

a is the specific area of the droplet (*1/m*)

ϕ is the partition coefficient of species between the oil phase and water phase

$K_{m(O/W)}$ is the overall mass transfer coefficient of a species when mass transfer is from oil phase to water phase (*m/s*)

N_A is the flux of species A form oil phase to water phase due to mass transfer (*mol/(m^3s)*)

Initial and boundary conditions for the equations above can be given as the following:

Initial conditions

At t=0s and r=r

$C_{A(Water)}$ *=47mmol/liter,* $C_{B(Water)}$ *=0,* $C_{C(Water)}$ *=0,* $C_{D(Water)}$*=0*

$C_{A(Oil)}$*=0,* $C_{B(Oil)}$*=0,* $C_{C(Oil)}$*=0,* $C_{D(Oil)}$*=0*

Boundary conditions I

At t=t, r=0μm, and d=½*l, (where l is the estimated average thickness of the continuous phase between two adjacent droplets)

$$\frac{dN_{A(Water)}}{dt} = \frac{dN_{B(Water)}}{dt} = \frac{dN_{C(Water)}}{dt} = \frac{dN_{D(Water)}}{dt} = 0$$

$$\frac{dN_{A(Oil)}}{dt} = \frac{dN_{B(Oil)}}{dt} = \frac{dN_{C(Oil)}}{dt} == \frac{dN_{D(Oil)}}{dt} = 0$$

Boundary conditions II

Different modeling scenarios can be envisioned depending on the assumptions taken for the mass transfer equations. For example, mass transfer resistance across the interface can be much higher than diffusional mass transfer resistance within the phase. In this case no concentration gradient can be assumed in each phase. Another assumption may be that diffusional mass transfer resistance in each phase is higher than mass transfer resistance across the interface. Each assumption results in implications in simplifying the equations used for the mass transfer in

modeling the biphasic reactor. For example, one of the following two cases might be used as boundary conditions at the interface,

a. if interphase mass transfer resistance is insignificant

$$\phi * C_{C(Water)} = C_{C(Oil)})$$

b. if interphase mass transfer resistance is significant

$$N_C = K_{m(O/W)} a(\phi_C C_{C(Water)} - C_{C(Oil)}) \approx K_{m(W/O)} a(C_{C(Water)} - (1/\phi_C) C_{C(Oil)})$$

$$N_D = K_{m(O/W)} a(\phi_C C_{D(Water)} - C_{D(Oil)}) \approx K_{m(W/O)} a(C_{D(Water)} - (1/\phi_D) C_{D(Oil)})$$

Furthermore, the assumption that the interface mass transfer is significant or much higher than the diffusional resistance leads to the assumption that the concentration of species across each phase is constant and the diffusional equations can be removed from the mass transfer model. Further, this assumption has implications for the kinetics equations too. The concentration gradient of species within the phases dissipates due to the mixing effect and solubility of components. Hence, the average concentration value for each phase can be used in evaluating the reaction kinetic and mass transfer models.

3.2.5. Estimation of mass transfer parameters

The mass transfer across the aqueous-organic phase boundary can be calculated using the two-film theory which states that the mass transfer across the boundary is proportional to the mass transfer coefficient, interfacial area of the emulsion, the driving force which is the bulk concentration difference between the droplet, and the continuous phase and partition coefficient.

The overall mass transfer coefficient and mass transfer of species A could be given by **Equation 3.21** or **Equation 3.22**.

(a) when the mass transfer direction is from oil phase to water phase

$$\frac{1}{K_{mA_{(O/W)}} a} = \frac{1}{k_{mA_{(O)}} a} + \frac{\phi_{(A)}}{k_{mA_{(W)}} a}$$

$$N_A = K_{mA_{(O/W)}} a\left(C_{A(Oil)} - \phi_{(A)} C_{A(Waterr)}\right) \quad \textbf{(3.21)}$$

(b) when the mass transfer direction is from water phase to oil phase

$$\frac{1}{K_{mA_{(W/O)}} a} = \frac{1}{\phi_{(A)} k_{mA_{(O)}} a} + \frac{1}{k_{mA_{(W)}} a}$$

$$N_A = K_{mA_{(W/O)}} a\left(\frac{C_{A(Oil)}}{\phi_{(A)}} - C_{A(Water)}\right) \quad \textbf{(3.22)}$$

where

$C_{A(Oil)}$ is the concentration of A in the oil phase *(mol/m^3)*

a is the specific area of *(1/m)*

ϕ is the partition coefficient of species between the oil phase and water phase

$K_{m(O/W)}$ is the mass overall mass transfer coefficient of species in when mass transfer is from the oil phase to the water phase (*m/s*)

N_A is the flux of species A from the oil phase to the water phase due to mass transfer (*mol/(m^{3}s)*)

$k_{m(O)}$ is the mass transfer coefficient of species in the oil phase (*m/s*)

The use of the equations given above is dependent on the direction of mass transfer. If component A is transferred from the organic phase to aqueous phase, then equation two can be used. If the opposite is true, then equation one will be used.

3.2.6. Calculation of diffusion constant

For systems involving the interaction between polar and nonpolar components, a correlation developed by Sitaraman et al [26] could be used to estimate the diffusion coefficient, as given by **Equation 3.23**.

$$D_{AB} = 16.19 * 10^{-14} \left(\frac{M_B^{1/2} \Delta H_B^{1/3} T}{\mu_B V_A^{1/2} \Delta H_A^{0.3}} \right) \quad \textbf{(3.23)}$$

Where

M is the molecular weight (*g*)

ΔH is the change of enthalpy of vaporization (*J/M*)

μ is the viscosity of solute in the solvent

V is the molecular volume of the solute (m^3)

T is temperature of the solution (K)

Diffusivity estimates for p-cresol and 4-MECH in the water and decalin phase by **Equation 24** are 2.62E^{-09}, 2.81E^{-09} and 3.61E^{-09}, 3.27E^{-09} $\frac{\boldsymbol{m^2}}{\boldsymbol{s}}$,respectively.

3.2.1.1. Calculation of mass transfer constant ($\boldsymbol{k_m}$)

Calculation of the mass transfer constant of Solute A in Solvent B can be performed using empirical correlations. Tudose and Apreotesei [14] use **Equation 3.24** to estimate the overall mass transfer coefficient for a water/acetone/carbon tetrachloride ternary system in a Lewis cell where acetone was allowed to diffuse from water to carbon tetrachloride and vice versa. Apreotesei et al [27] furthered the work with inclusion of two additional ternary systems (water-acetone-chloroform, and water-acetone-toluene) to develop a generalized mass transfer coefficient correlation which will be used for both cases of mass transfer direction change and at different mixing condition.

$$S_h = b \, \mathrm{Re}_{ag}^{\ p} \, S_c^{\ n} \left(\frac{D_{AW}}{D_{AO}} \right)^2 \phi^r \quad \textbf{(3.24)}$$

where,

$$S_h = \frac{dk_{mW}}{D_{AW}}\ ,\ S_C = \frac{\gamma}{D_{AW}}\ ,\ Re_{ag} = \frac{nd^2\rho}{\mu}$$

D is the diffusion coefficient, n=1/3, p=1/2 and power for the mixing Reynold number (Re_{ag}) and the partition coefficient ϕ have different values depending on stirred phase solute transferred direction.

The fraction of the volumetric interfacial area available for mass transfer is impacted by the presence of catalyst at the interface, effects of surface deformation, effects of adhesion, and cohesion at the surface.

3.2.6. Calculation of water and decalin solubility

The solubility model of decalin in the water phase and vice versa was developed from experimental data collected by procedures similar to those used to collect the ternary equilibrium data. The water and decalin solubility at different temperatures is shown in **Figure 3.2** and **Table A.2** in Appendix A. Exponential regression in solver-excel is used to develop the solubility model, which is then used to predict the composition of decalin and water in the opposite phases at the reactor temperature.

3.2.7. Optimization of the mass transfer module.

Not all the interfacial area between the droplet and the continuous phases can be available for mass transfer due to the presence of the carbon nano hybrid emulsion stabilizers and catalysts at the water/oil interface. Estimating the interfacial area requires estimating variables such as contact angle, the average number of catalysts surrounding a single droplet, and the degree of surface tension, deformation and similar factors. For this reason, an optimization procedure for the simulation of the biphasic reactor was developed to estimate the fraction of the droplet area available for mass transfer.

The direct heuristic search optimization by Rinehart [28] was modified and used for optimization of the mass transfer model. This search algorithm starts with the initial values and

jumps to the next values of decision variables (DV) in the steepest direction. The DV is expanded by 25% when the search minimizes the objective function (OF) or contracted by the same factor if the search fails.

The objective function for this optimization is the sum of root mean-square-error (RMSE), average absolute deviation (AAD), and %AAD for both the organic and aqueous phase. Using the combination of different weighted OF helps to balance the bias due to the relative difference in the organic and aqueous phase composition values and the lower and higher composition values at different reaction times.

Experimentally determined droplet size was used as the initial guess for determining fractional surface area available for mass transfer by the optimizer. The specific interfacial area of a spherical droplet used as initial value is calculated as shown in **Equation 3.25** below.

Area and volume of a droplet (diameter = 40 μm)

$$a = \frac{A_{dropelt}}{V_{dropelt}} = \frac{\pi(20x10^{-6})^2 m^2}{\pi(20x10^{-6})^3 m^3} = 60x10^6 m^{-1} \quad \textbf{(3.25)}$$

3.2.8. Activity coefficients and Gibbs energy minimization analysis

For reactions involving phase equilibria, rate equations are expressed as a function of activities instead of concentrations. The reaction system operates in the range of infinite dilution where the overall reacting system is composed of less than two percent of the reactor content. Therefore, the activity coefficients of the chemical components in each phase was tracked to check if there is significant change in activity values. Aspen Plus was used to evaluate activity coefficients based on the equation.

$$\gamma_i = \frac{y_i \mathrm{P}}{x_i p_i^{sat}} \quad \textbf{(3.26)}$$

where

γ_i is the activity coefficient of component i

P is the total pressure of the system

p^{sat} is the partial pressure of component i at saturation or vapor pressure

x_i, and y_i are the mole fractions of component i in the liquid and vapor phase, respectively.

For a closed system of given initial feed, temperature, and pressure, reactions occur as the Gibbs free energy proceeds to a minimum. A method of validating the model is to track the change in Gibbs energy of the system, as the reaction progresses, to ensure that reactions in the aqueous and organic phase and the component mass transfer results in minimizing the Gibbs Energy of the mixture in each phase, locally, and the overall reactor, globally. The pseudo-equilibrium assumptions in the biphasic reactor model for reactions in each phase and mass transfer of components between phases after each time increment are

(a) local equilibrium at the interface, where the reactions occur, and

(b) a global equilibrium in the bulk phase of the reactor.

Equations 27-29 are used to calculate the Gibbs energy of mixing for the organic phase, aqueous phase, and the overall reactor values.

$$\Delta G_{mix(Oil)} = RT \sum_{i(Oil)}^{n} x_{i(Oil)} \, lnx_{i(Oil)} \, \gamma_{i(Oil)} \quad \textbf{(3.27)}$$

$$\Delta G_{mix(Water)} = RT \sum_{i(Water)}^{n} x_{i(Water)} \, lnx_{i(Water)} \, \gamma_{i(Water)} \quad \textbf{(3.28)}$$

$$\Delta G_{mix(Reactor)} = RT \sum_{i(Water)}^{n} x_{i(Reactor)} \, lnx_{i(Reactor)} \, \gamma_{i(Reactor)} \quad \textbf{(3.29)}$$

These values are deviations from the respective values of Gibbs energy of ideal mixtures for each system given by **Equation 3.30**.

$$G_{system} = G_{ideal} + \Delta G_{mix} = \sum_{i}^{n} H_{i(Ideal)} + T \sum_{i}^{n} S_{i(Ideal)} + \Delta G_{mix} \quad \textbf{(3.30)}$$

Aspen Plus was used to calculate the Gibbs energy values.

3.3. Results and discussion

The simulation results showed that biphasic reactors with reactions and mass transfer on both phases could be modeled and simulated with reasonable accuracy. The contribution of reaction, as well as, mass transfer to the organic and aqueous phase composition dynamics of the biphasic reactor was quantified and the resulting composition prediction was compared with the experimental data. The assumption of mass transfer between the two phases and the direction of transport is also supported by the Gibbs energy test.

Equations 3.31 and **3.32** show the result of the nonlinear regression performed in Excel and **Figure 3.2** shows the corresponding curve fittings. The models were used to calculate mole fractions of water and decalin at the reactor operating temperature of 150°C.

$$X_W = 2.38*10^{-5}*e^{0.016T} \quad \textbf{(3.31)}$$

$$X_D = 3.00*10^{-11}*e^{0.026T} \quad \textbf{(3.32)}$$

Table 3.2 shows the comparison between the simulation results and the experimental data for the biphasic reactor in the case study. Simulation results of the biphasic reactor against experimental data is also depicted in **Figure 3.3 and 3.4**. Since both p-BAL and p-BOL are not soluble in the decalin phase, predictions for the two chemicals reflect only the results of the devised kinetic mechanism of the surface reaction. Composition curves for p-cresol and 4-MECH reflects effects of both reaction and mass transfer. The R-squared value for p-BAL and p-BOL is approximately 0.98 and 1, respectively. In the prediction curve, the concentration of p-BAL continues to decrease to zero although the experimental data shows about 1 mmol/l still unconsumed by the reaction. This might be due to the small quantity of p-BAL not present at the surface of the reaction; therefore, a low adsorption process might control the rate of reaction at this stage. The prediction accuracy of the p-Cresol and 4-MECH was largely dependent on the assumption taken to approximate the fractional area available for mass transfer.

Measuring or estimating the surface tension between the catalyst and the organic and aqueous molecules, surface area coverage by the catalyst (angle of contact and the local number of catalyst at the interface), and the relative superficial velocity of the droplet against the continuous phase is beyond the scope this work. Those assumptions, however, play a considerable role in explaining the component distribution of p-cresol at the early stage of the reaction. For example, the phase distribution ratio (PDR) of p-cresol grows from zero to 2.0 at the beginning of the reaction to the experimental value of 7.8. Since formation of p-cresol is supposed to be limited to the aqueous phase, then there must be another reason other than mass transfer that could explain a partition coefficient higher than the equilibrium value. One possible explanation is that p-cresol was washed away from the hydrophilic catalyst surface by the organic phase due to a higher mixing effect on the continuous phase. Therefore, a more reasonable result of the kinetic-mass transfer reactor model could be obtained after this early reactor stage at 25 minutes.

The direction of mass transfer for 4-MECH is from the water phase to the decalin phase with increasing distribution ratio throughout the 90 minutes of reaction time. Further analysis of the simulation shows a reversal of mass transfer direction around 100 minutes. For p-cresol, the distribution ratio increases to 3.2, i.e. the equilibrium partition coefficient value at around 18 minutes to a maximum value of 8.2 at approximately 31 minutes. A higher distribution coefficient than the partition coefficient could be explained by a) phase migration of p-creosl starts as soon as p-cresol was formed in the water phase and the distribution ratio starts to increase toward the equilibrium value, b) the reaction of p-cresol to 4-MECH increases faster in the water phase at this time which further increases the distribution ratio to the maximum value observed in the simulation and experiment, and c) having enough time for p-cresol to reach the catalyst surface in the decalin phase, the p-cresol concertation starts to drop and due to a higher concertation of p-cresol in the organic phase the reaction is faster which decreases the distribution ration below the partition coefficient value before mass transfer occurs. Therefore, depending on

the relative rate of reaction and mass transfer, the prediction curve might be above or below the experimental values because the delay time that mass transfer may take time to respond the change in mass transfer direction and other factors. The results however showed that modeling and simulation of the biphasic reactor gives insights in how to improve selectivity and yield.

The activity coefficient results are plotted in **Figure 3.6**. The activity coefficient values of the reacting components do not change significantly except for p-cresol in the organic phase, which changes about 18% over the 90 minute reaction period. Depending on the sensitivity of the calculation, activity coefficients could be used in the rate reaction calculation. However, any underestimate of conversion of p-cresol to 4-MECH in the organic phase will be compensated by partition of p-cresol and 4-MECH either to the organic phase or aqueous phase depending on the relative concentration of component at the specific time.

The Gibbs energy of the Biphasic reactor at the three different states, namely before and after the reaction and after the mass transfer is discussed using **Figures 3.6- 3.8. Figure 3.6** shows that the overall mixture Gibbs energy of the biphasic reactor and mixture Gibbs energy of the organic phase and aqueous phase decreases with time. Further, the Gibbs energy change for each reaction (delta R Aqueous and delta R organic) at each reaction time step remains below zero, which is in agreement with the kinetics that reaction occurs in both phases throughout the 90 minutes reaction time. The aqueous phase Gibbs energy change for reaction returns a small positive number while for the organic phase the value opposite with a magnitude close to the aqueous phase (**Figure 3.7**). Since the reactions occur in the same reactor, the energy might transfer from the aqueous phase to the organic phase.

The figure confirms that the change in Gibbs energy for both the aqueous and organic phase due to mass transfer goes in the opposite direction as expected. The sum of the Gibbs energy change due to reaction and mass transfer should always remain below zero as is shown in **Figure 3.8.** The Gibbs energy analysis showed that the total Gibbs energy of the reactor and the

Gibbs energy of each phases is progressing towards a minimum. Furthermore, the Gibbs free energy of the mixture for each phase was less than the energy of the mixture calculated before the reaction and mass transfer start at each time step.

3.4. Conclusions

The results of the simulation showed that the biphasic reactor for upgrading bio-oils could be effectively modeled and simulated using the mass transfer limitation approach. Further, the Gibbs energy plot showed that both reaction and mass transfer is thermodynamically possible in both phases. The integration of Aspen Plus in our modeling and simulation module was successful. Temperature dependent and independent pure substance and mixture thermo-physical properties were readily calculated.

The optimization results showed that only a small fraction of the interfacial area is available for mass transfer of components between the two phases. However, the effect of small interfacial area for mass transfer diminishes with time because the relative concentration of p-cresol and 4-MECH approaches equilibrium distribution ratio as the reaction time progress.

Table 3.1. Prototype reactor operating conditions

Operating Conditions	
Temperature °C	150
Pressure	400 psi H_2
Catalyst Type	5% Ru/SWNT MCM-41
Catalyst weight	15 mg
Reaction time, min	30 - 90
Reaction volume, ml	Decalin: 25 ± 0.1
	Water: 25 ± 0.1
	p-BAL: 150 ± 0.5 mg
Reactor Volume, ml	100

Table 3.2. RMSE comparison for simulation result of biphasic reactor modeling with phase equilibria and mass transfer.

Model type	RMSE (mmol/l)								
	Water phase				Organic Phase				Overall
	p-BAL	p-BOL	p-cresol	4-MECH	p-BAL	p-BOL	p-cresol	4-MeCH	
Biphasic-Mass Transfer	1.75	2.24	3.83	0.24	0.00	0.00	3.31	0.49	5.8

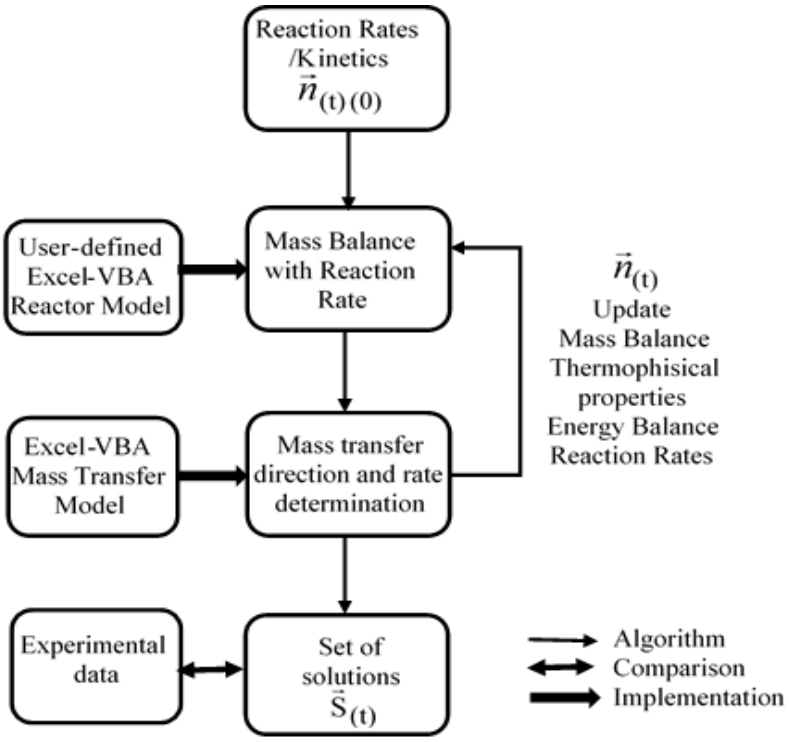

Figure 3.1. Schematic showing various steps used in modeling a biphasic reactor

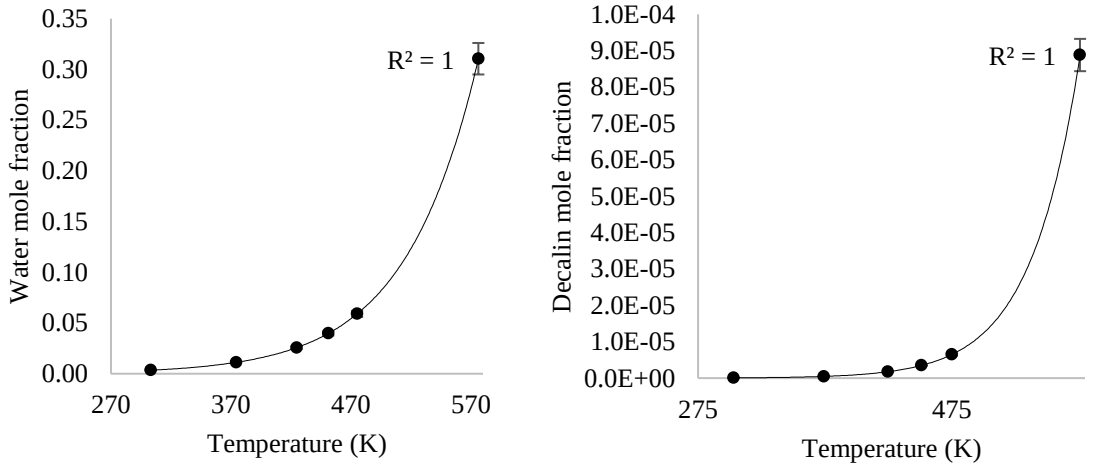

Figure 3.2. Solubility model representations for mole fractions of water in decalin rich (left) and decalin in water rich (right)

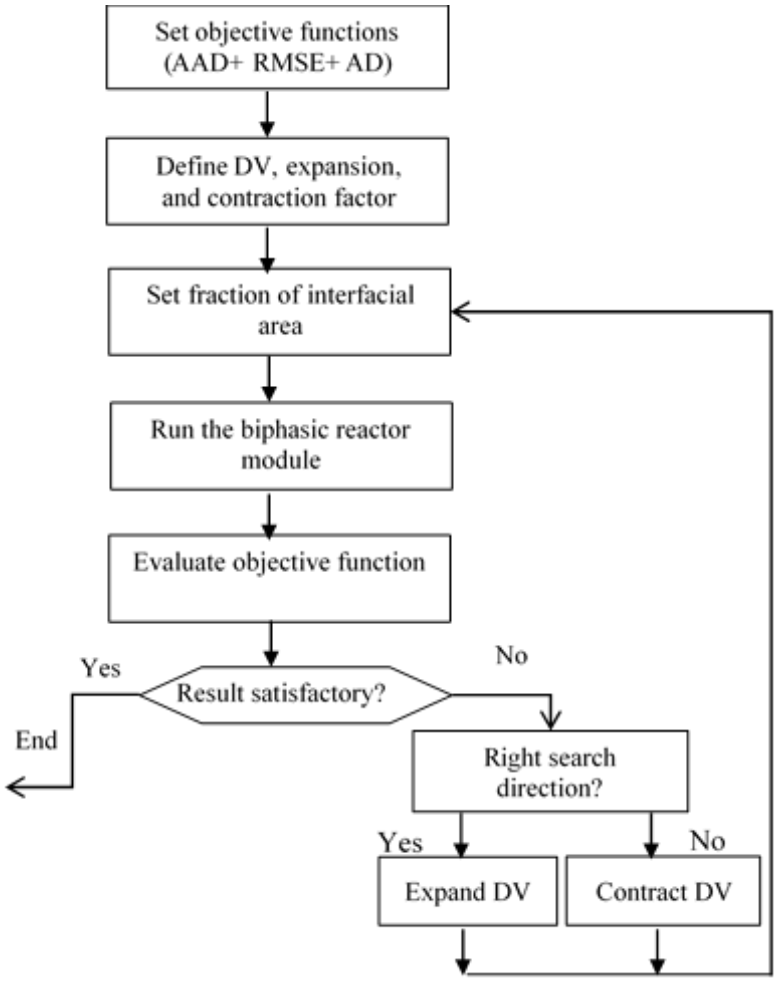

Figure 3.3. Algorithm for optimization of the mass transfer model for biphasic reactor

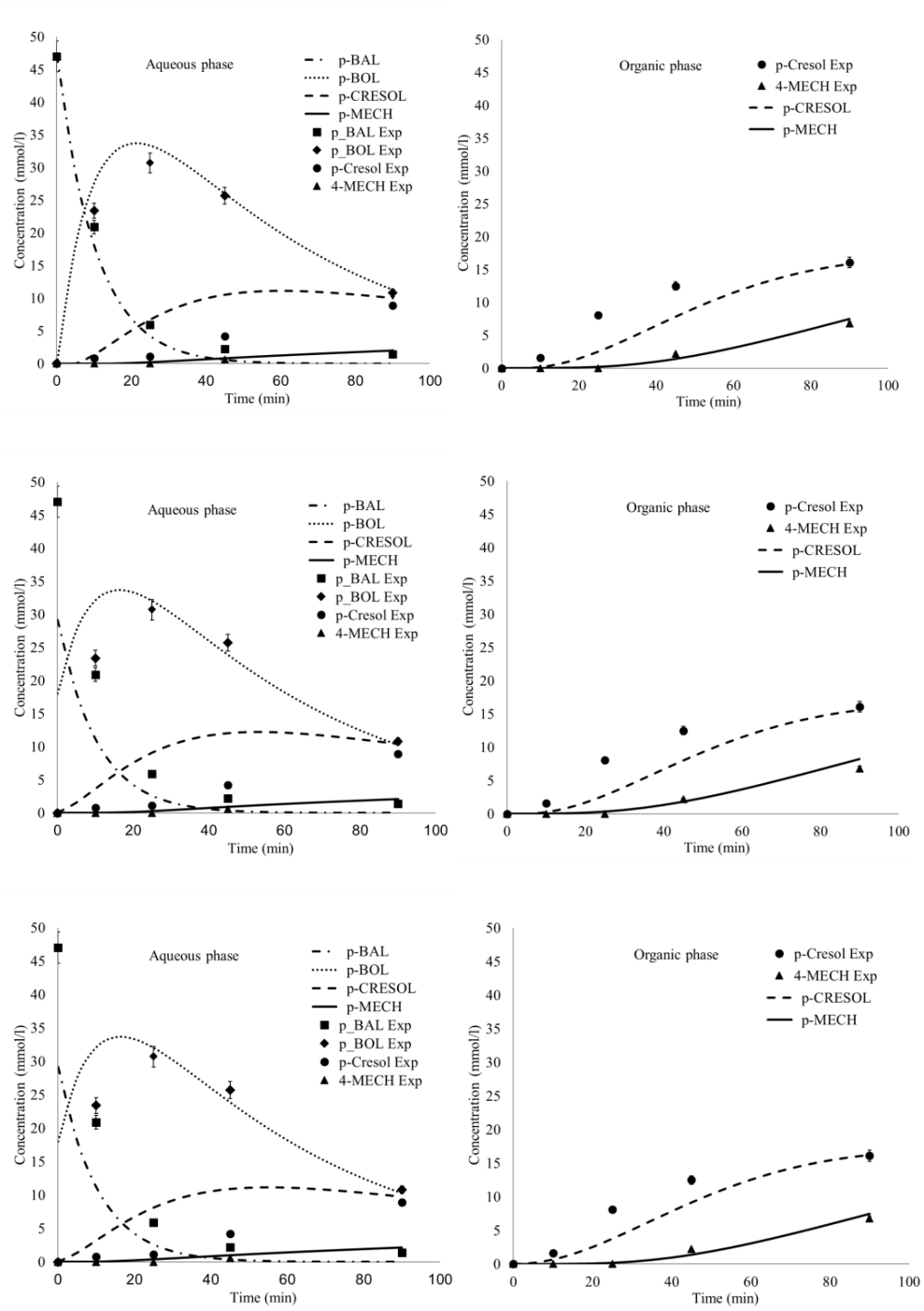

Figure 3.4. Simulation results for the biphasic reactor; before reaction starts (top), before mass transfer starts (middle), after mass transfer (bottom).

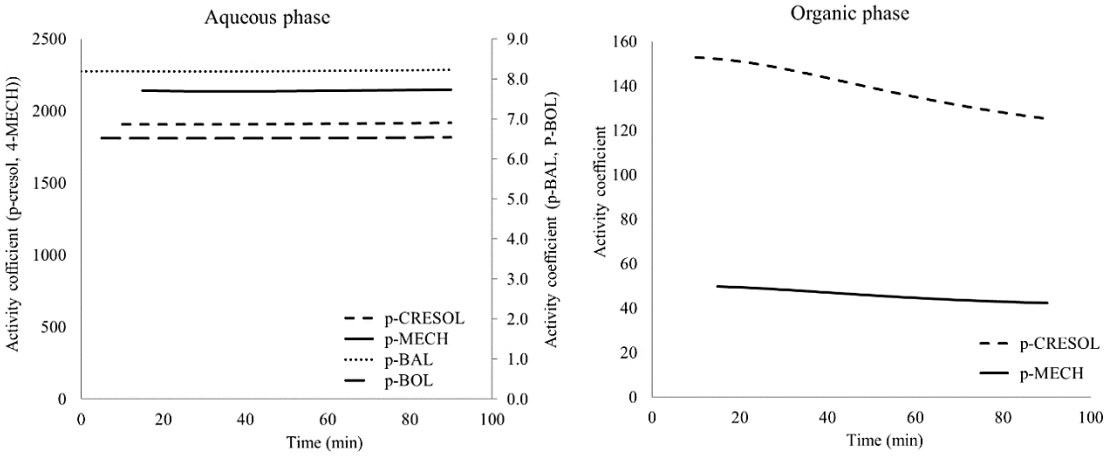

Figure 3.5. Simulation results for activity coefficient (γ) of reacting components using QSPR-Aspen Plus-Regressed NRTL parameters

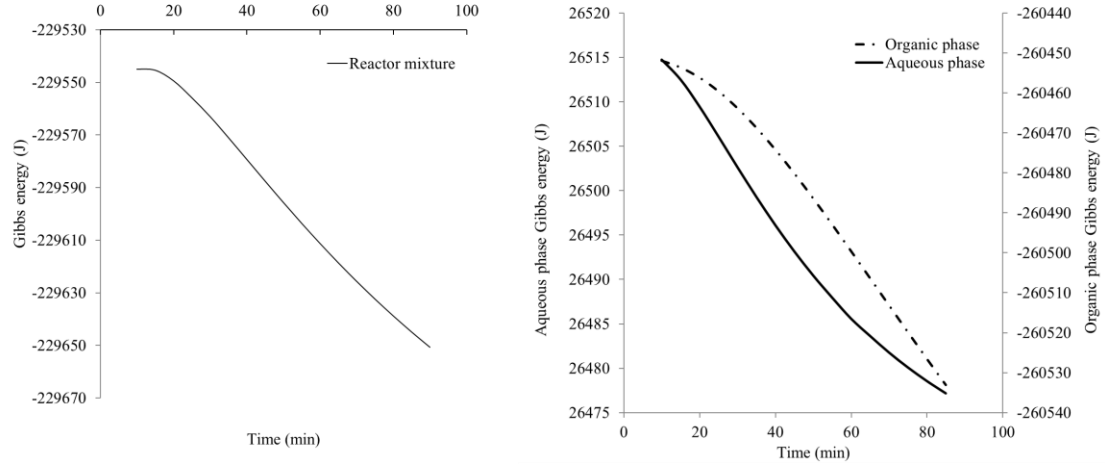

Figure 3.6. Gibbs energy plot for the reactor mixture, and aqueous and organic phase mixtures

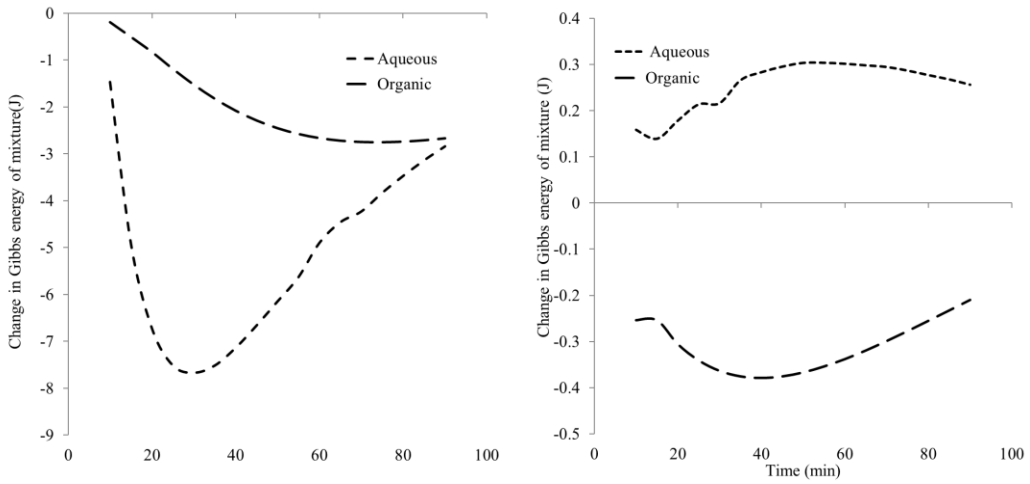

Figure 3.7. Gibbs energy change due to mass transfer (left) and chemical reaction (right).

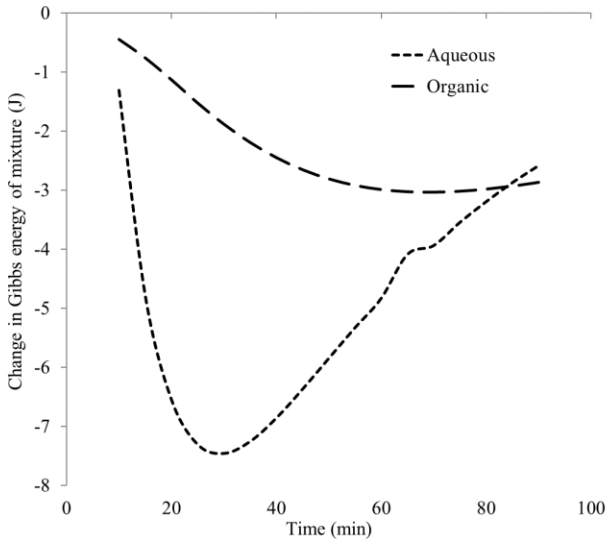

Figure 3.8. Gibbs energy change due to mass transfer (left) and chemical reaction (right).

REFERENCES

1. Crossley, S., et al., *Solid Nanoparticles that Catalyze Biofuel Upgrade Reactions at the Water/Oil Interface.* Science, 2010. **327**(5961): p. 68-72.
2. Ordomsky, V.V., et al., *Fructose Dehydration to 5-Hydroxymethylfurfural over Solid Acid Catalysts in a Biphasic System.* ChemSusChem, 2012. **5**(9): p. 1812-1819.
3. Willeman, W.F., et al., *Development of a process model to describe the synthesis of (R)-mandelonitrile by Prunus amygdalus hydroxynitrile lyase in an aqueous–organic biphasic reactor.* Biotechnology and Bioengineering, 2002. **77**(3): p. 239-247.
4. Zapata, P.A., et al., *Condensation/Hydrogenation of Biomass-Derived Oxygenates in Water/Oil Emulsions Stabilized by Nanohybrid Catalysts.* Topics in Catalysis, 2012. **55**(1): p. 38-52.
5. Fogler, H.S., *Elements of Chemical Reaction Engineering* Forth edition ed. 2006.
6. Madon, R.J., J.P. O'Connell, and M. Boudart, *Catalytic hydrogenation of cyclohexene: Part II. Liquid phase reaction on supported platinum in a gradientless slurry reactor.* AIChE Journal, 1978. **24**(5): p. 904-911.
7. Sitthisa, S., et al., *Kinetics and mechanism of hydrogenation of furfural on Cu/SiO2 catalysts.* Journal of Catalysis, 2011. **277**(1): p. 1-13.
8. Gonzo, E.E. and M. Boudart, *Catalytic hydrogenation of cyclohexene.* Journal of Catalysis, 1978. **52**(3): p. 462-471.
9. Rioux, R.M. and M.A. Vannice, *Hydrogenation/dehydrogenation reactions: isopropanol dehydrogenation over copper catalysts.* Journal of Catalysis, 2003. **216**(1–2): p. 362-376.
10. M. Negash, C.E.O., S. Gebreyohannes, T. N. Pham, and D.R. J. Faria, B. J. Neely, K. A. M. Gasem, *Biphasic Reactor Modeling and Simulation: Hydrogenation of p-Hydroxybenzaldehyde.* Computers and Chemical Engineering, 2016. **xx**(xx): p. xx.
11. Resasco, D.E., *Carbon nanohybrids used as catalysts and emulsifiers for reactions in biphasic aqueous/organic systems.* Chinese Journal of Catalysis, 2014. **35**(6): p. 798-806.
12. Melgarejo-Torres, R., et al., *Mass transfer coefficient determination in three biphasic systems (water–ionic liquid) using a modified Lewis cell.* Chemical Engineering Journal, 2012. **181–182**: p. 702-707.
13. Rudose, R.Z. and G. Lisa, *The determination of individual mass transfer coefficients in liquid-liquid extraction.* Chem. Ind. , 2003. **57**(9): p. 393-398

14. Tudose, R.Z. and G. Apreotesei, *Mass transfer coefficients in liquid–liquid extraction.* Chemical Engineering and Processing: Process Intensification, 2001. **40**(5): p. 477-485.
15. Pugazhenthi, G. and A. Kumar, *Modeling of the Mass Transfer Effect in Biphasic Enzyme Membrane Reactor for Hydrolysis of Olive Oil*, in *International Journal of Food Engineering*. 2008.
16. Kundu, A., et al., *Mass Transfer Characteristics in Gas-liquid-liquid System.* The Canadian Journal of Chemical Engineering, 2003. **81**(3-4): p. 640-646.
17. Kalaichelvi, P. and T. Murugesan, *A correlation for overall mass transfer coefficients in rotating disc contactors.* Bioprocess Engineering, 1998. **19**(5): p. 381-384.
18. Hu, Y., et al., *Modeling of a biphasic membrane reactor catalyzed by lipase immobilized in a hydrophilic/hydrophobic composite membrane.* Journal of Membrane Science, 2008. **308**(1–2): p. 242-249.
19. Handlos, A.E. and T. Baron, *Mass and Heat Transfer from Drops in Liquid-Liquid Extraction.* Aiche Journal, 1957. **3**(1): p. 127-136.
20. 2016, A.P., *Physical property calculation. Process Simulation Software.* .
21. Renon, H. and J.M. Prausnitz, *Local compositions in thermodynamic excess functions for liquid mixtures.* AIChE Journal, 1968. **14**(1): p. 135-144.
22. Zapata, P., et al., *Condensation/Hydrogenation of Biomass-Derived Oxygenates in Water/Oil Emulsions Stabilized by Nanohybrid Catalysts.* Topics in Catalysis, 2012. **55**(1): p. 38-52.
23. Faria, J., M.P. Ruiz, and D.E. Resasco, *Phase-Selective Catalysis in Emulsions Stabilized by Janus Silica-Nanoparticles.* Advanced Synthesis & Catalysis, 2010. **352**(14-15): p. 2359-2364.
24. Ruiz, M.P., et al., *Nanostructured Carbon–Metal Oxide Hybrids as Amphiphilic Emulsion Catalysts.* ChemSusChem, 2011. **4**(7): p. 964-974.
25. Rioux, R.M. and M.A. Vannice, *Hydrogenation/Dehydrogenation Reactions: Isopropanol Dehydrogenation overCopper Catalysts.* Journal of Catalysis, 2003. **216**(1–2): p. 362-376.
26. Sitaraman, R., S.H. Ibrahim, and N.R. Kuloor, *A Generalized Equation for Diffusion in Liquids.* Journal of Chemical & Engineering Data, 1963. **8**(2): p. 198-201.
27. Apreotesei Lisa, G., R.Z. Tudose, and H. Kadi, *Mass transfer resistance in liquid–liquid extraction with individual phase mixing.* Chemical Engineering and Processing: Process Intensification, 2003. **42**(11): p. 909-916.

CHAPTER IV

MODELING EFFECTS OF SOLVENT TYPE AND WATER CUT ON EMULSION CHARACHTERSTICS USING QUANTITIAVE STRUCTURE PROPERTY RELATIONSHIP (QSPR)

4.1. Introduction

Predicting the characteristics of emulsions is important, as emulsions appears as intermediate and final products in many industrial processes with diverse applications such as pharmaceutics, petroleum and biofuel processing [1]. Emulsions, which either are found naturally or produced by various techniques, have many important characteristics of practical significance such as droplet size, emulsion fraction and emulsion type [2, 3]. Given the surfactants used, temperature and mixing conditions remain the same, there seems to be a strong correlation between the type of organic solvent used and the droplet size of the discontinuous phase, the emulsion fraction and the emulsion type [4-6]. ADS also depends on particle type and particle concentration used for emulsification and stabilization [7]. Water fraction also has a strong correlation with droplet size and type of emulsions [6, 8]. Prior knowledge on the effects of the factors that determines emulsion properties is important in formulating emulsions with the desired characteristics. Models developed for emulsion properties can be used to reduce the number of experiments required to formulate an emulsion with the desired properties thereby saving time, energy and material consumption. For example, the formulation and use of relevant emulsions in

biphasic reactors may improve selectivity and yield the in specific phases, and promote higher component phase distribution of products to the desired phase [9, 10].

Capturing the relationship between these emulsion properties with the physical properties of emulsions and operating parameters with simple theoretical models and correlations is difficult due to the complex nature of emulsions properties. Many theoretical equations and experimental correlations have been developed to establish the relationship between the various factors and emulsion properties [3, 4, 6, 11-13]. The majority of emulsion property correlations in the literature accounts effects of operating parameters and water cut on the drop size distribution and viscosity of emulsions. However, models capable of predicting effects of solvent and water cut variations on average droplet size, emulsion fractions and emulsion type are rare.

Quantitate structure property relationship (QSPR) based models could be used to capture the complex relationship between molecular structure of solvents and emulsion properties. QSPR techniques have been successfully used in modeling different physical and thermodynamic properties in biphasic mediums such as partition coefficient [14] and activity coefficient [15]. Therefore, it is imperative to suggest the use of QSPR models for prediction of emulsions characteristics such as drop size, emulsion type, and emulsion fraction. For models developed with relatively small number of experimental data, K-fold or Leave-One-Out Cross-Validation (LOO CV) can be used to test the generalization error of predictive models [14, 16]

The objective of this study is to develop a linear and non-linear quantitative structural property relationship (QSPR) model between the molecular descriptors of the solvents used, water fractions and emulsion characteristics such as droplet size, emulsion type and emulsion fraction.

4.2. Materials and Methods

4.2.1. Available data

This section discusses the data collection and the methods used for model development. Experimental data for emulsion properties shown in **Table 4. 1** and **4**. **2** were collected from our collaborators in the University of Oklahoma (OU) and Oklahoma State University (OSU) center for interfacial reaction and engineering (CIRE) [17] research group, respectively. The emulsions in **Table 2** were developed using Aerosil R974 (0.5 Wt%) at a mixing speed of 5000 RPM using utlraturrax T25 homogenizer for five minutes and allowed to settle for 24 hours. Optical microscopy is used to quantify average droplet size distributions. The reported values of ADS are cumulative values for 80% the droplets taken at four different values of water cut. **Figure 4.1** shows sample droplet distribution for toluene and p-xylene at 40% water cut with 10X magnification. The experimental data on **Table 4.1** shows the effects of solvent type on droplet size, emulsion fraction, and type of emulsion, whereas the data on **Table 4.2** also includes effects of water cut on droplet size of the emulsions.

The solvents used in the experiments were classified based on structure and functional groups in order to help distribute the molecules in to model training data and test data sets proportionally. The data can be grouped in different ways and combinations as straight chain and cyclic, presence or absence of C-C double bond, presence or absence of functional groups containing oxygen and chlorine, and presence and absence of branched chains. The structure and functional groups and branches used to classify the solvents can be seen in the structures of the molecules shown in Table 1. Twenty-five total molecular solvents are used in both experiments. Cyclopentane is included only in the data from OSU, whereas the other seven solvents in Table 2 are also included in the OU experiential data.

The experimental data were closely analyzed to see if there are visible patterns and outliers in the data. Droplet size data for alpha-tetralone in **Table 4.1** was excluded as an outlier because of the exceptionally higher diameter. The drop size response to the water fraction percentage in **Table 4.2** seems logarithmic or linear for cyclic hydrocarbons, whereas exponential pattern was observed for branched cyclic hydrocarbons. The structures of the solvents are shown in **Table 4.1**. Observation of **Table 4.1** and graphical representation of the data (**Figure 4.2**) reveal that ADS values always increase with water fraction. Further, as the water fraction increases, the non-linearity of ADS with water cut appears to increase. Algorithm for the QSPR linear models development

The QSPR model development has three mail steps; descriptor generation, descriptor reduction and model analysis. **Figure 4.3** shows the algorithms used for developing the linear QSPR regression models with and without non-linear transformation of descriptors. The first step is to assemble the molecular structures of solvents using ChemBioDraw Ultra 12.0 in ChemOffice®[18] software. Then, a Python energy minimization code based on Genetic Algorithm (GA) search for the lowest energy conformation in Open Babel [19] was used to find the optimum configuration of the molecules. Then, a commercial software DRAGON [20] was used to generate 2864 molecular descriptors. Constant descriptors and descriptors with strong correlation were removed by using orthogonalization. Descriptors were first ranked based on the individual coefficient of determination (R^2) value (**Equation 4.1**). Then, sequential regression analysis (SQR) was performed to develop the multi linear regression model (**Equation 4.2**). Starting from the descriptor with the highest R^2 value, more descriptors were progressively added until the improvements in the sum of squared error (SSE) stops to show significant change. The transformation of descriptors

$$R^2 = 1 - \left(\frac{n-1}{n-p}\right)\frac{\sum_i (x_{EXP}^i - x_{PRED}^i)^2}{\sum_i (x_{EXP}^i - \bar{x}_{EXP}^i)^2} \quad \textbf{(4.1)}$$

$$y_{Predicted} = x_1 + x_2 * D_1 + x_3 * D_2 + x_4 * D_3 + \ldots \quad \textbf{(4.2)}$$

Where,

X_{exp} *is value for experimental data*

X_{pred} *is prediction value*

W is coefficients for the linear equations

D is best descriptor value

n is number of data points

P is number of parameters

Ten best ensemble models were populated and the top most frequently appeared descriptors were selected from the pool in order to enhance the reproducibility of descriptor selection. Using the best descriptors was used to show if the non-linear relationship between the descriptors and emulsion properties could improve the model predictions and the process will be repeated until reliable model prediction in obtained.

4.2.2. Data classification

The molecules used for emulsion development which are listed in **Table 4.1** and **4.2**, are classified in to aliphatic and cyclic, presence of carbon-carbon double bond, presence of single and double ring, presence if branched chain, and presence of oxygenated and chlorinated functional groups. In both cases, the first step in the model development was to divide the droplet size and emulsion fraction data randomly in to a training (80%) and test sets (20%). The data division was performed so that a proportional number of molecules from each group and from

each water cut points goes to the training set, internal test set (validation data) and external test set during randomization.

4.2.3. Prediction models for ADS and EF

The final step in the model development process was building the prediction model using the best descriptors obtained in the previous step. The data was divided in to five groups (k-fold) and 80% goes to training while 20% is used as test set. LOO CV was used for both droplet size and emulsion fraction using the same descriptors used for model development. In LOO CV model, all the 23-experimental data except one was used to train each of the QSPR linear model and the remaining one data was used as a test set. This procedure was repeated 23 times until each data in the data set had a chance to be used as a test set. Then, all the results of the training data representation of the 23 ensemble models were averaged. Each of the linear models employed the same set of descriptors but may have resulted in different coefficients.

4.2.4. Prediction model for effects of water cut on ADS

The same procedure was followed when building the model for effects of water cut on drop average drop size experimental data. Here, the percentage of water cut was added to the existing sets of the best descriptors obtained in the ADS model development. Further, as shown in **Table 4.2** above, there seems to be significant deviation from a linear relationship between the water cut and average drop size for cyclic and cyclic branched hydrocarbons, respectively. To account this non-linearity, nonlinear exponential transformation of descriptors was tested so that the models essentially remains linear but the relationship between descriptor values and ADS is non-linear.

4.2.5. Descriptor reduction

The sequential regression analysis was performed by adding one descriptor and evaluating the model performance with the best descriptors already selected The data division and

sequential regression analysis were repeated until no significant change was observed in minimizing the objective function (OF), which is the SSE. The procedure is repeated for ten times to generate an ensemble of ten models. All the best descriptors from each models in the ensemble were populated, and the most repeated descriptors were selected from the pool in to enhance the reproducibility of descriptor selection. The same procedure was used for the descriptor reduction of all the four emulsion properties models developed in this paper.

4.2.6. Prediction model for ET

A perceptron neural network was developed using the Neural Network toolbox in Matlab [21] for emulsion type, oil in water (O/W) and water in oil (W/O), modeling. Numerical values, i.e. 1 and 0, were assigned for emulsion types of O/W and W/O, respectively. Log sigmoid (logsig) was used as a transfer function in developing the ANN model. Scaled conjugate gradient back propagation (trainscg) [22] was used to train the network parameters with the objective of minimizing the sum of squared error until validation error starts to increase. **Figure 4.4** shows the graphical representation of the neural network model. The final weights and bias resulting from the network training were used to draw the boundary decision line.

Where,

D is descriptor

w is weights of the network

b is bias of the network

n is pure linear transfer function network output

a is classification of network outputs using logsig transfer fun.

4.1. Results and discussion

The coefficient of determination (R^2) was used to evaluate the performance of all the models. The highest R^2 value obtained was for the ET modeling followed by ADS and EF. The model for effects of water cut for ADS returned the lowest R^2 value. The R^2 values obtained by our models for model representation and model prediction are comparable to those reported in the literatures for QSPR models with smaller or comparable data size to our work [23, 24]

4.3.1. Average droplet size modeling

The ADS training data set representation and test set prediction by the best model returns a coefficient **of** determination values of 0.96 and 0.94, respectively with five descriptors. **Figure 4.5** shows comparisons of experimental data against model representation and prediction. Comparison of the results with literature values suggests that a prediction performance with coefficient of determination value 0.94 for the test set could be practically helpful in choosing the solvents when developing an emulsion where ADS is an important characteristic.

The average values for the ensemble models representation of the training, where all the data have a chance to be used as a test set is shown in **Figure 4.5.** The results are comparable to the best model yielding slightly lower values of root mean square error (RMSE) 2.51 to that of the best model, which has resulted in RMSE value of 2.55. The ADS QSPR linear model validation by LOO CV. has also returned closely equal values of R^2 for model representation and prediction. **Figure 4.7** shows the averaged representations and prediction results of all the 23 models used in

LOO-CV for average droplet size. The ensemble model representation and the prediction have a coefficient of determination values 0.96 and 0.92, respectively.

4.3.2. Emulsion fraction modeling

The EF model representation and prediction returned slightly lower R^2 than the ADS model. **Figure 4.8** shows comparisons of experimental data against EF model representation, and prediction, respectively .The results show that the QSPR EF model could have a practical significance since there is a good agreement between the experimental and predicted values of the emulsion fraction with a coefficient of determination values of 0.93 and 0.91 for training and test set data respectively. **Figure 4.9** shows the average values of the representation of experimental emulsion fraction data using an ensemble of five QSPR models where all the data had a chance to be included in the test set .The results are comparable to those of the best model. The Ensemble model, however, has a relatively lower RMSE value of 3.8 than the RMSE values of the best model, which is 3.9.

The EF model was also tested with LOO-CV. The LOO-CV average returned values of representation and predictions sets comparable R^2 values to the ADS model. **Figure 4.10** shows the comparison of experimental data against model results with R^2 values of 0.95 and 0.91 for ensemble model representation and prediction, respectively.

4.3.3. Emulsion type modeling

The emulsion type model was able to classify emulsion type with 100% accuracy with only two descriptors. **Figure 4.11** shows that the model classification of emulsion types in to two distinct classes with the two types of descriptor used for building the model. The figure shows all the data point used as a training, validation and test set. The black line represents the decision line and the red and the square and letter x markers represents oil in water and water in oil emulsions, respectively. The descriptor type SM15 EA for dichloromethane has unique value than the other group members in the Water in oil emulsions. This is because dichloromethane is the only straight chain hydrocarbon with functional group that contains Chlorine atoms. This implies that,

although the model was capable of accurate classification, more representative molecules with diverse functional groups should be included to build a robust ET model.

Figure 4.12 shows the resulting performance during the model training. The minimum validation error indicated by the circle on the graph was obtained at the 27^{th} epoch. The model was able to classify all the training set (70%), validation set (15%), and test set (15%) with 100% success rate.

4.3.4. Modeling effects of water cut on average droplet size

The modeling the effects of water cut on ADS showed that water cut is the most important factor (when varied in 10%wt) than other molecular descriptors. **Figure 4.13** showed the R^2 value for the model representation of training data and prediction of test set is 0.82 and 0.75 respectively. This performance was obtained with five descriptors water cut being the top descriptor in influencing the drop size of the emulsions. . Comparative value of representation and prediction is obtained using the LOO-CV **(Figure 4.14**). The relationship between water cut and droplet size was found to be non-linear. Using the exponential transformation of water cut as one of the descriptor in the descriptor set increases model representation and prediction R^2 value in to 0.88 and 0.84 as shown in **Figure 4.15.**

4.3.5. Descriptors used for model development

Table 4.3 shows the list of best descriptors used in all the four different models in this paper. Most of the descriptors provide information about the 2D atomic coordinates of the molecule and encode information on the effective position of fragments and substituents in the molecular space [20, 25]. The next significant descriptor in the list is a 3D-MoRSE (Molecular Representation of Structures based on Electron diffraction type descriptors [26]. The three parameters used to quantify the 3D-MoRSE descriptor are pair-wise interatomic distance, weighting by some atomic properties such as atomic mass and charge and the scattering

parameters representing the angle frequency in the radial function (I am collecting more literatures to update this paragraph). Water cut was found to be the most significant factor in determining the ADS of an emulsion. Therefore, it is important to look for solvent type for preferable ADS if only specific water cut variation is not possible for different reasons.

4.2. Conclusions

A linear relationship between molecular descriptors and emulsion fraction emulsion type and ADS was enough to build a model with acceptable comparable coefficient of determination in the literature for the other biphasic mediums property QSPR models such as partition coefficient and aqueous phase solubility [23, 24]. However, the relationship between water cut and drop size appears to be non-linear as prediction improvement was obtained with non-linear transformation of water cut. As demonstrated by the ET model, nonlinear models such as ANN may have returned a better result if large number of data points were provided for EF and ADS so that degree of freedom ratio have been achieved to develop a two-layer feed forward ANN models.

The descriptor value for spectral moment of order 15 from edge adjacency matrices for dichloromethane was zero unlike the other values for other solvents that delivered water in oil emulsions. Further, the prediction values of ADS and EF show %AAD deviations higher than 10% for lower molecular weight and solvents with functional groups that contain halogens such as chlorine and oxygen atoms. This show collecting more data for these groups of molecules are required to build a robust model and for a better result. The use of populating ensemble models in selecting the best descriptors increased the reproducibility of the descriptor reduction step.

Table 4.1. Effect of solvent type on emulsion properties

No	Organic phase	Structure[17]	ET	EF (% vol.)	ADS (μm)
1	hexane		O/W	39.5	20.1
2	heptane	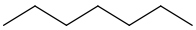	O/W	38.2	21.7
3	octane	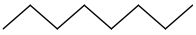	O/W	81.1	43.6
4	nonane		O/W	47.4	18.9
5	decane		O/W	50.0	22.8
6	undecane		O/W	44.7	27.0
7	dodecane		O/W	76.3	38.7
8	tridecane		O/W	38.5	18.6
9	tetradecane		O/W	65.8	35.0
10	3-methylpentane	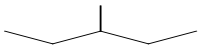	W/O	61.4	23.7
11	1-dodecene		O/W	46.2	24.3
	cyclopentane		-	-	-
12	cyclohexane		O/W	75.0	40.1
13	methylcyclohexane		W/O	60.5	18.1
14	decalin		W/O	69.7	20.8
15	toluene		W/O	65.8	40.0
16	o-xylene		W/O	56.4	34.2
17	m-xylene		W/O	65.8	36.2
18	p-xylene		W/O	71.8	39.8
19	tetralin		W/O	83.3	39.0
20	1-methylnaphtalene		W/O	78.9	42.5
	alpha-tetralone	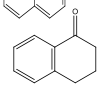	W/O		
21	Dichloromethane	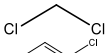	W/O	67.6	65.2
22	1,2-dichlorobenzene		W/O	38.5	21.4
23	methyl laurate	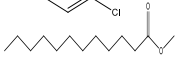	W/O	56.6	7.5

Table 4.2. Effect of water fraction on droplet size of the emulsion

No	**Solvent**		**Emulsion droplet size (μm)**			
			Water cut			
	Name	Structure	10wt%	20wt%	30wt%	40wt%
1	decalin		12.1	13.2	15.5	17.1
2	tetralin		12.0	16.8	19.0	20.0
3	cyclopentane	cyclic	13.4	17.2	20.2	23.5
4	cyclohexane		18.2	20.6	22.1	23.5
5	1-methylnapthalene		11.1	13.1	13.3	15.2
6	toluene	cyclic	12.7	14.2	15.2	24.8
7	p-Xylene	branched	13.9	14.2	15.4	24.8
8	o-Xylene		16.5	16.8	18.0	20.9

Table 4.3. Five best descriptors used in the QSPR model for emulsion fraction

No	Descriptor Name	Descriptor description	Type of descriptor
		Descriptors for ADS model	
939	MATS8s	Moran autocorrelation of lag 8 weighted by I-state	2D autocorrelations
105	MAXDP	maximal electrotopological positive variation	Topological indices
2083	Mor24s	signal 24 / weighted by I-state	3D-MoRSE descriptors
2464	R4s	R autocorrelation of lag 4 / weighted by I-state	GETAWAY descriptors
88	ICR	radial centric information index	Topological indices
		Descriptors for EF model	
939	MATS8s	Moran autocorrelation of lag 8 weighted by I-state	2D autocorrelations
345	WiA_H2	average Wiener-like index from reciprocal squared distance matrix	GETAWAY descriptors
1891	Mor24u	signal 24 / unweighted	2D Atom Pairs
2063	Mor04s	signal 04 / weighted by I-state	Walk and path counts
2474	R5s+	R maximal autocorrelation of lag 5 / weighted by I-state	3D-MoRSE descriptors
		Descriptors for ET model	
1237	SM15_EA	Spectral moment of order 15 from edge adjacency mat.	Edge adjacency indices
101	PW3	Path/walk 3 - Randic shape index	Topological indices
		Descriptors for effect of WF on EF model	
	Water %vol	-	Water fraction
105	MAXDP	maximal electrotopological positive variation	Topological indices
2083	Mor24s	signal 24 / weighted by I-state	3D-MoRSE descriptors
2464	R4s	R autocorrelation of lag 4 / weighted by I-state	GETAWAY descriptors
88	ICR	radial centric information index	Topological indices

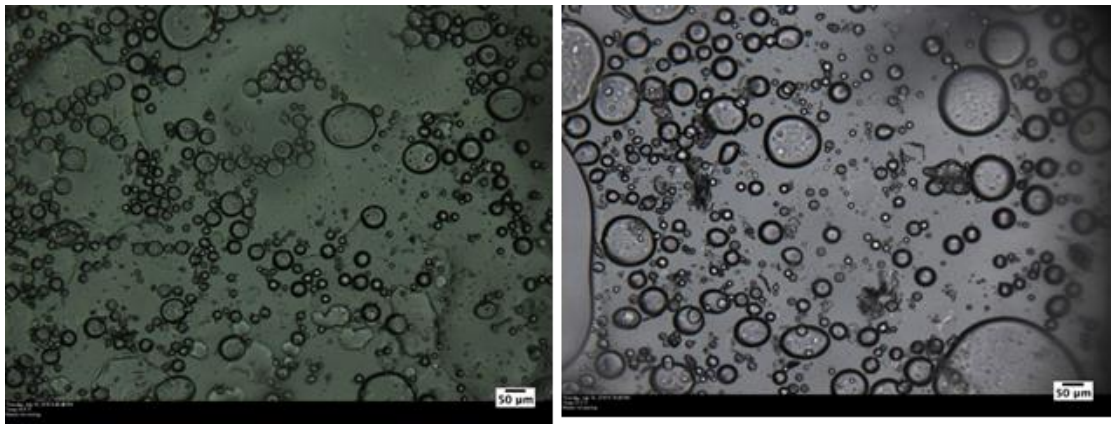

Figure 4.1. Microscope image of toluene ((left) p-xylene (right) (40wt%water)

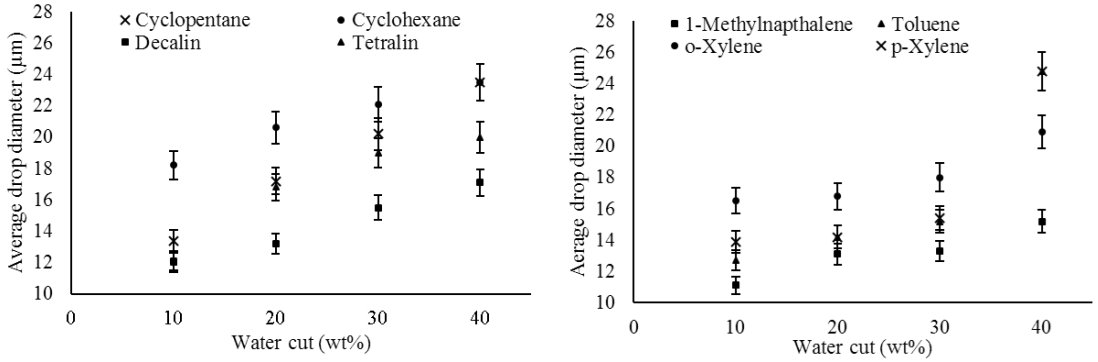

Figure 4.2. Graphical representation of experimental data for effect of water cut on drop size. for cyclic hydrocarbon (left). cyclic branched hydrocarbon (right).

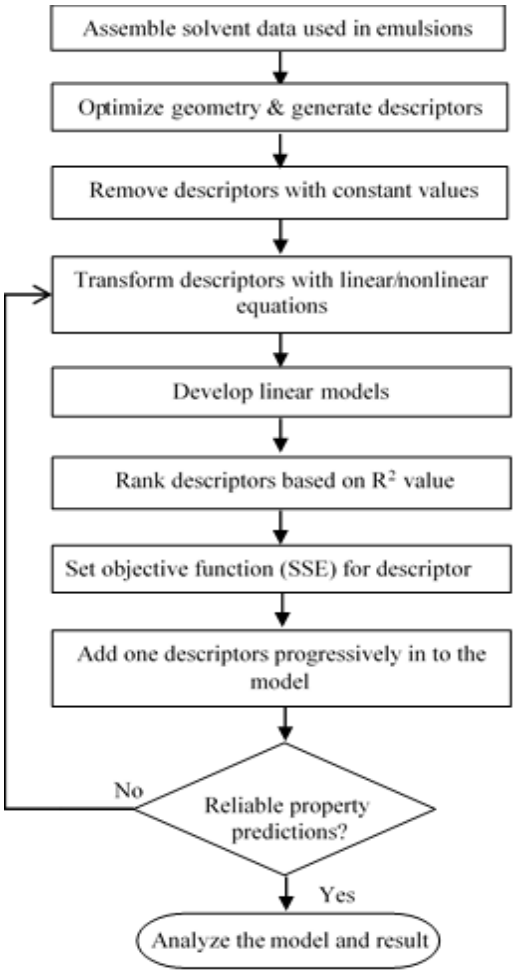

Figure 4.3. Flowchart for the algorithm of SQR model for emulsion properties

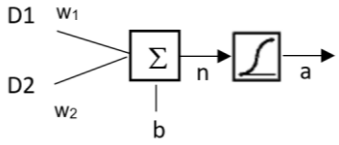

$$a = f(n) = \frac{1}{1+e^{-n}}$$

Figure 4.4. Graphical representation of a feed forward perceptron network.

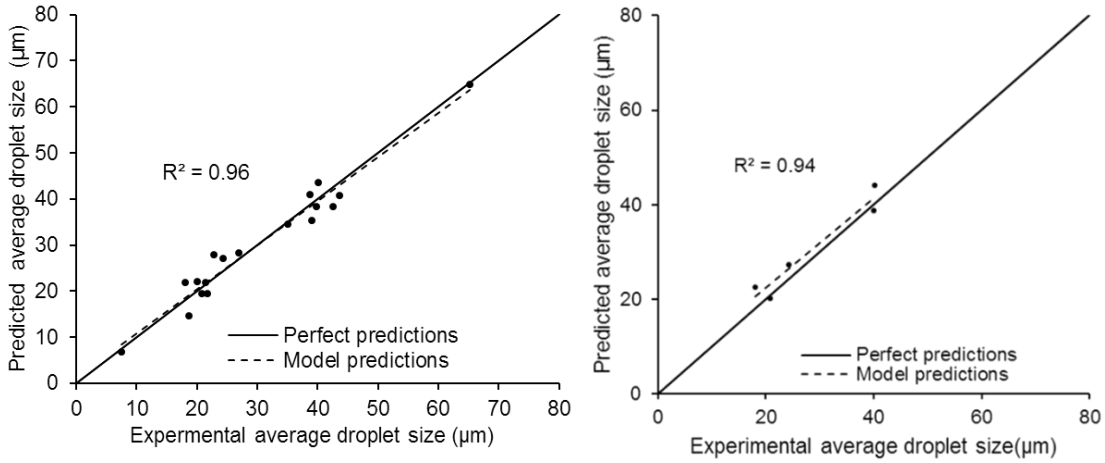

Figure 4.5. QSPR drop size model representation (left) and prediction (right)

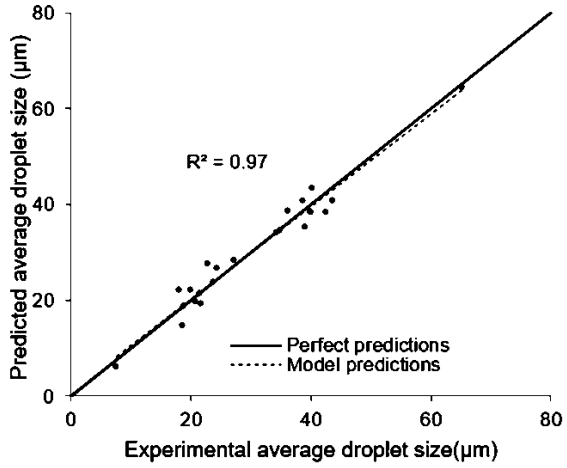

Figure 4.6. Comparison of ensemble ADS model representations against experimental data

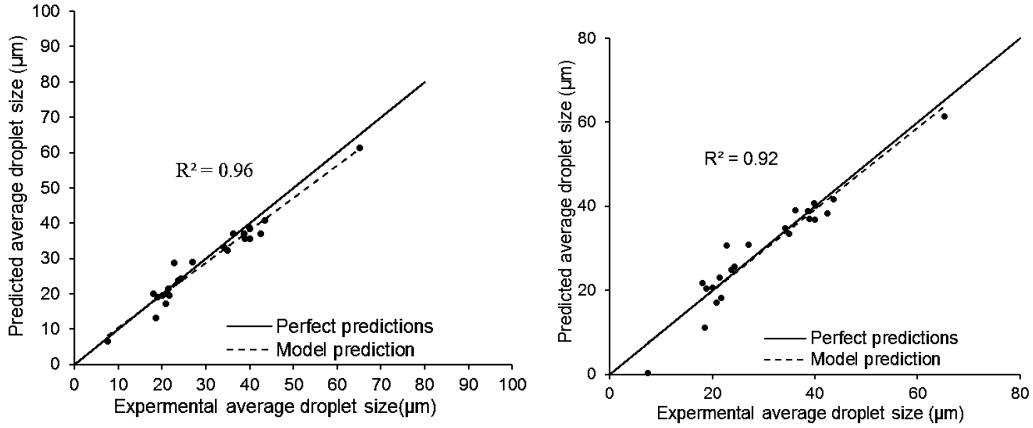

Figure 4.7. Comparison of QSPR ADS model predictions with experimental data using best using LOO –CV for Ensemble training average (left) and Ensemble test set (right)

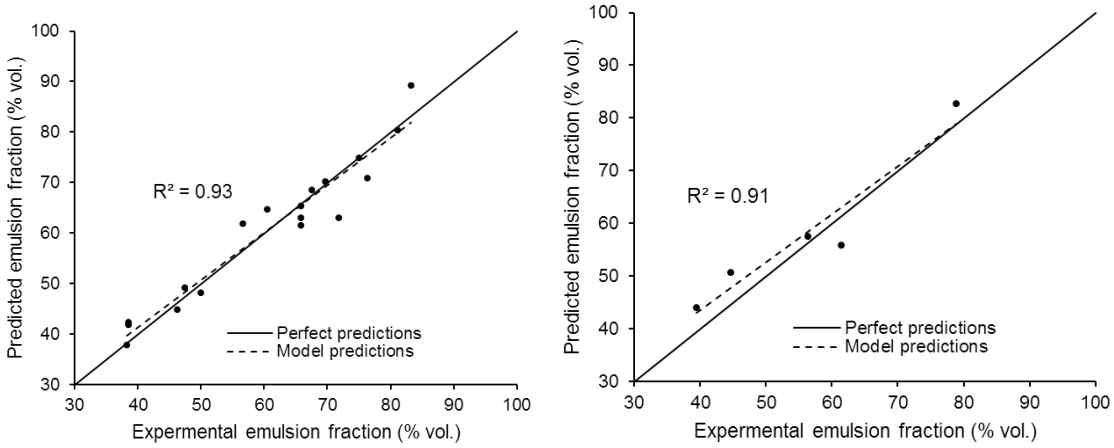

Figure 4.8. Comparison of QSPR emulsion fraction model predictions with experimental data using best model. Training data set (left). Test data set (right).

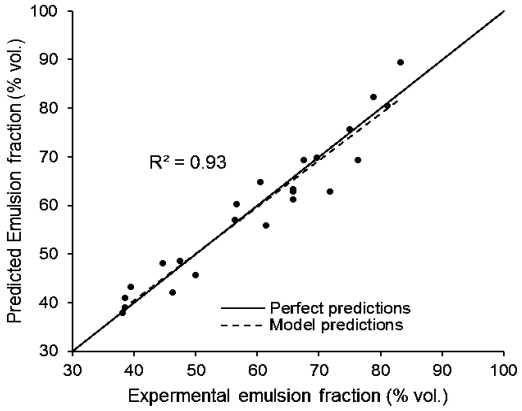

Figure 4.9. Comparison of EF ensemble model prediction against experimental data

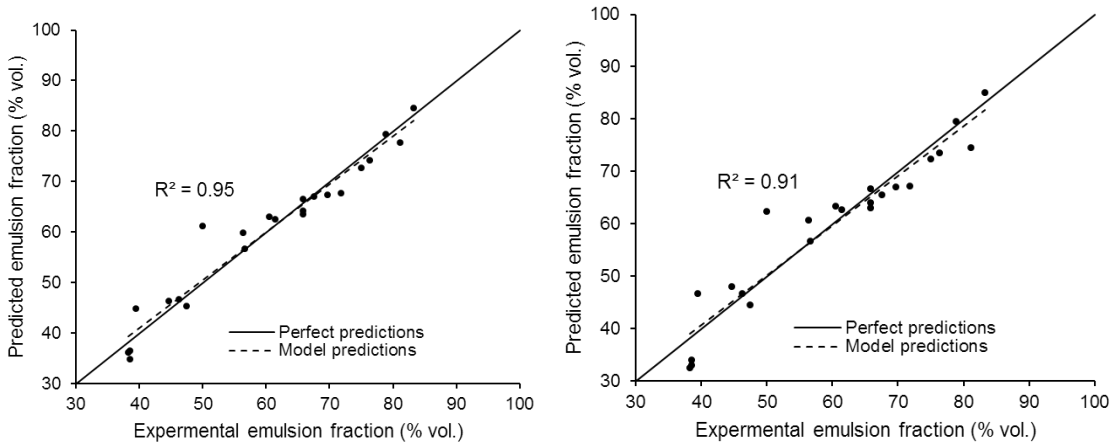

Figure 4.10. Comparison of EF experimental data with representation (left) and prediction (right) using ensemble models with leave-one out cross validation

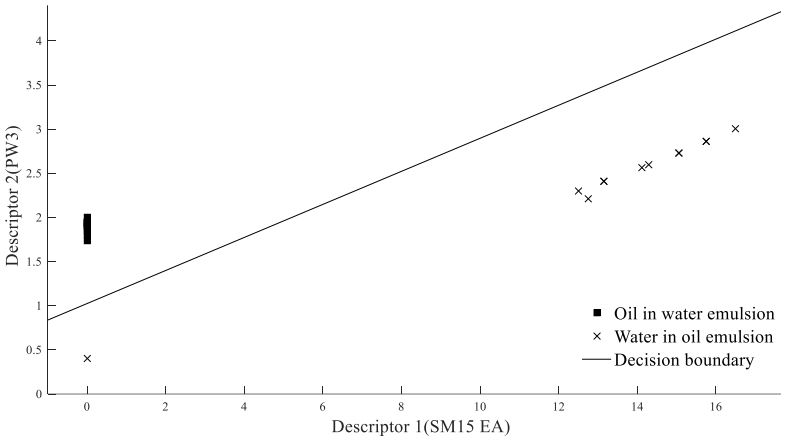

Figure 4.11. Output of the perceptron neuron emulsion type model.

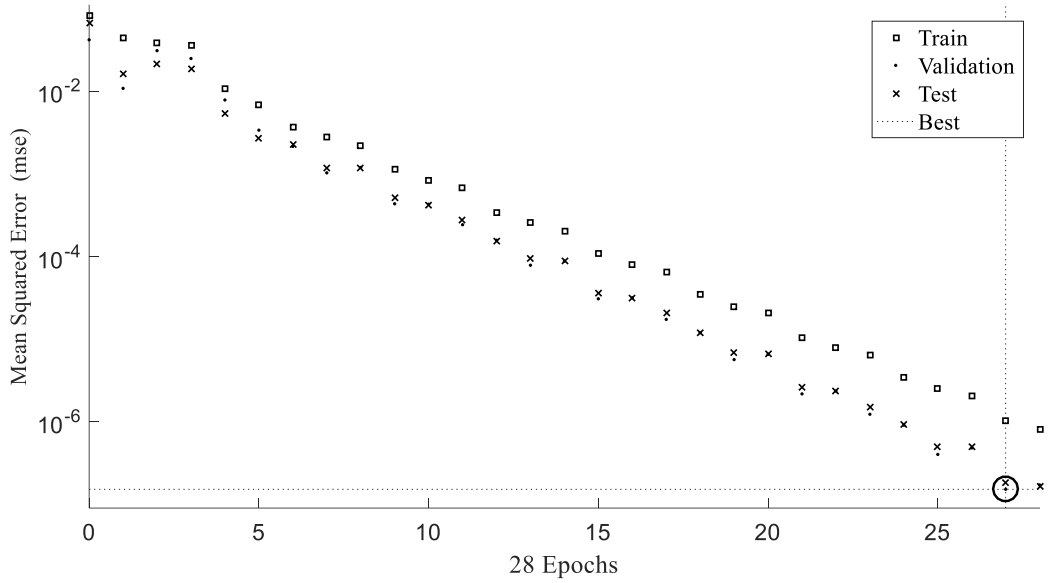

Figure 4.12. Training performance of the perceptron network using training data 70%.

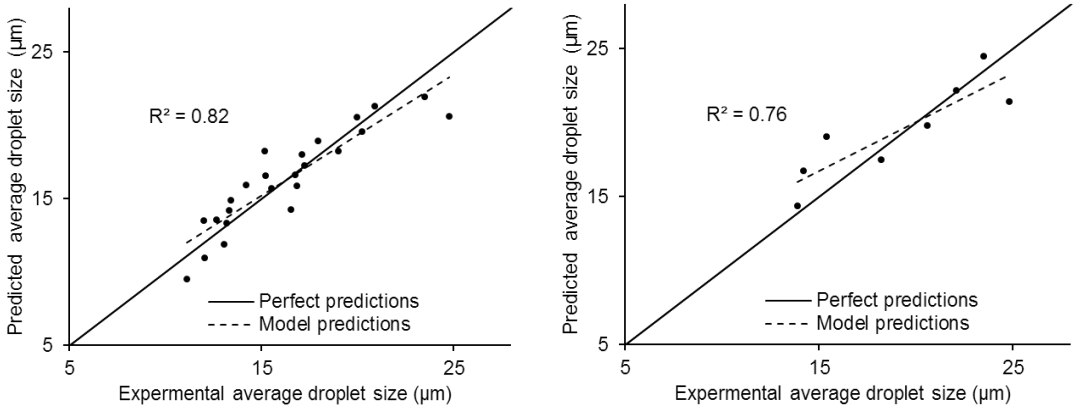

Figure 4.13. Model results for effects of water cut on ADS

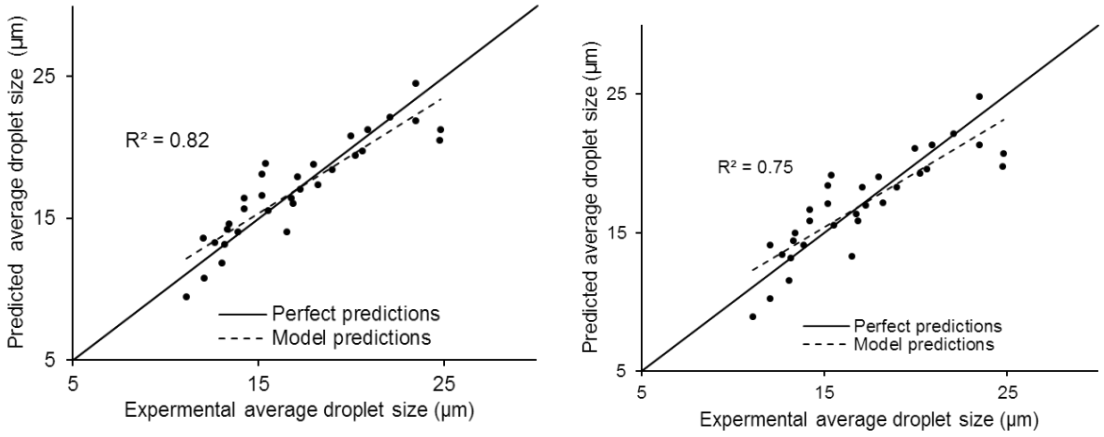

Figure 4.1. LOO-CV results for effects of water cut on ADS

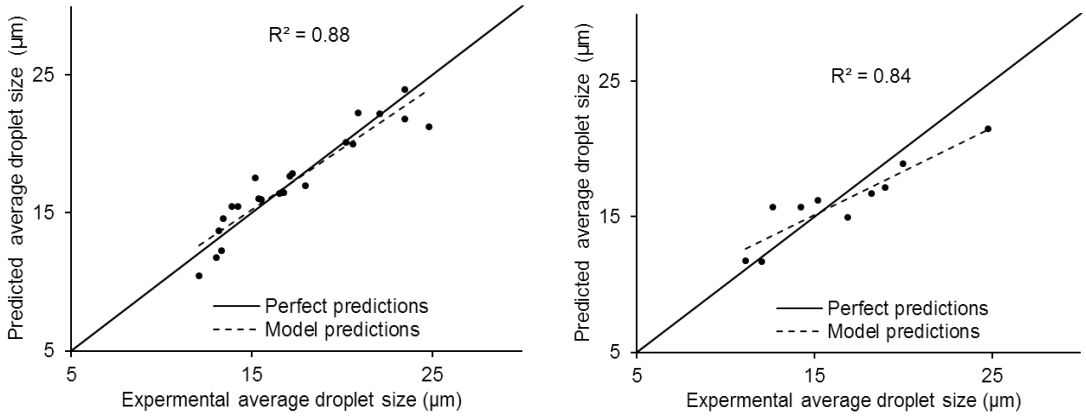

Figure 4.2. Model results for effects of water cut on ADS with exponential transformation of water cut

REFERENCES

1. Schramm, L.L., *Emulsions Foams and Suspensions. Findamental and Applications.* 2005, KGaA, Weinheim: WILEY-VCH Verlag GmbH & Co. .
2. Zalazar, A.L., M.F. Gliemmo, and C.A. Campos, *Data on the physical characterization of oil in water emulsions.* Data in Brief, 2016. **9**: p. 96-99.
3. Chanamai, R. and D.J. McClements, *Prediction of emulsion color from droplet characteristics: dilute monodisperse oil-in-water emulsions.* Food Hydrocolloids, 2001. **15**(1): p. 83-91.
4. Raikar, N.B., et al., *Prediction of emulsion drop size distributions with population balance equation models of multiple drop breakage.* Colloids and Surfaces A: Physicochemical and Engineering Aspects, 2010. **361**(1–3): p. 96-108.
5. Aichele, C.P., et al., *Characterization of water-in-crude-oil emulsions in a complex shear field.* Experimental Thermal and Fluid Science, 2014. **53**: p. 190-196.
6. Fingas, M.F., *Water-in-Oil Emulsions: Formation and Prediction.* Journal of Petroleum Science Research (JPSR) Volume 3 Issue 1, January 2014, 2014. **3**(1).
7. Nallamilli, T., E. Mani, and M.G. Basavaraj, *A Model for the Prediction of Droplet Size in Pickering Emulsions Stabilized by Oppositely Charged Particles.* Langmuir, 2014. **30**(31): p. 9336-9345.
8. Souza, W.J., et al., *Effect of water content, temperature, and average droplet size on the settling velocity of water-in-oil emulsions.* Brazilian Journal of Chemical Engineering, 2015. **32**: p. **455-464**.
9. Blumenthal, L.C., et al., *Systematic Identification of Solvents Optimal for the Extraction of 5-Hydroxymethylfurfural from Aqueous Reactive Solutions.* ACS Sustainable Chemistry & Engineering, 2016. **4**(1): p. 228-235.
10. Peters, M., et al., *Systematic Approach to Solvent Selection for Biphasic Systems with a Combination of COSMO-RS and a Dynamic Modeling Tool.* Engineering in Life Sciences, 2008. **8**(5): p. 546-552.
11. Nasery, S., et al., *Prediction of the viscosity of water-in-oil emulsions.* Petroleum Science and Technology, 2016. **34**(24): p. 1972-1977.
12. Ankur Gupta, V.N., T. Alan Hatton, and Patrick S. Doyle, *Kinetics of the Change in Droplet Size during Nanoemulsion Formation.* Langmuir 2016. **32**(11551−11559).
13. Fridjonsson, E.O., L.S. Flux, and M.L. Johns, *Determination of mean droplet sizes of water-in-oil emulsions using an Earth's field NMR instrument.* Journal of Magnetic Resonance, 2012. **221**: p. 97-102.

14. Alves de Lima Ribeiro, F. and M.M.C. Ferreira, *QSPR models of boiling point, octanol–water partition coefficient and retention time index of polycyclic aromatic hydrocarbons.* Journal of Molecular Structure: THEOCHEM, 2003. **663**(1–3): p. 109-126.
15. Gebreyohannes, S., et al., *Improved QSPR Generalized Interaction Parameters for the Nonrandom Two-Liquid Activity Coefficient Model.* Fluid Phase Equilibria, 2013. **339**: p. 20-30.
16. Evgeniou, T., M. Pontil, and A. Elisseeff, *Leave One Out Error, Stability, and Generalization of Voting Combinations of Classifiers.* Machine Learning, 2004. **55**(1): p. 71-97.
17. CambridgeSoft, *ChemBioOffice 11.0*. 2009.
18. The Open Babel Package, *Python 2.3*. 2011.
19. Talete src., *DRAGON for windows and linux 5.5*. 2010.
20. *Neural Network Toolbox for MATLAB.* 2016.
21. Møller, M.F., *A scaled conjugate gradient algorithm for fast supervised learning.* Neural Networks, 1993. **6**(4): p. 525-533.
22. Ghasemi, J. and S. Saaidpour, *QSPR Prediction of Aqueous Solubility of Drug-Like Organic Compounds.* Chemical and Pharmaceutical Bulletin, 2007. **55**(4): p. 669-674.
23. Katritzky, A.R., et al., *Aqueous Biphasic Systems. Partitioning of Organic Molecules: A QSPR Treatment.* Journal of Chemical Information and Computer Sciences, 2004. **44**(1): p. 136-142.
24. Klein, D.J., *Topological Indices and Related Descriptors in QSAR and QSPR Edited by James Devillers & Alexandru T. Balaban. Gordon and Breach Science Publishers: Singapore. 1999. 811 pp. 90-5699-239-2. $198.00.* Journal of Chemical Information and Computer Sciences, 2002. **42**(6): p. 1507-1507.
25. Devinyak, O., D. Havrylyuk, and R. Lesyk, *3D-MoRSE Descriptors Explained.* Journal of Molecular Graphics and Modelling, 2014. **54**: p. 194-203.

CHAPTER V

SOLVENT SELECTION FOR BIPHASIC REACTORS

5.1. Introduction

Selection of appropriate solvent for biphasic reactors is important for improved interfacial surface area available for mass transfer, solubility in the organic phase and partition coefficient of solutes between the two immiscible phases in the reactor. The two immiscible phases in the biphasic reactors, commonly aqueous and organic, are usually found in the form of emulsions stabilized by different types of surfactants. Biphasic reactors are usually used to create an opportunity where a specific chemical reaction is taking place in the aqueous phase and mass transfer separates one or more products to the organic phase [1, 2]. Different techniques could be employed to enhance selectivity, yield and rate of reactions and increase quality of products due to timely product separation in the biphasic reactor. The rate of mass transfer between the droplets and the continuous phase depends on the property of emulsions such as, droplet size, emulsion fraction, emulsion type, partition coefficient, solubility and mass transfer coefficient [3-5]. These emulsion properties are mainly dependent on the type of solvents used to formulate the emulsion in the biphasic reactors. Therefore, in formulating an emulsion, selection of solvent type should be given due consideration to get higher solubility, partition coefficient, surface area or a combination of these parameters.

Different studies have been conducted on selection of solvents for enhanced product separation in biphasic reactors and liquid-liquid solvent extraction [6, 7]. Such studies mainly

consider partition coefficient as a means for solvent screening because higher partition coefficient deliver higher separation capacity of aqueous phase chemical reaction products by the organic solvents. These techniques mainly used COMSO-RS for partition coefficient and mass transfer constant of products between the aqueous an organic phase of the biphasic reactor [6, 7]. However, the effect of other emulsion properties such as total interfacial surface area available for mass transfer, type of emulsion and the fraction of emulsion created in the biphasic medium should be investigated to get a comprehensive assessment. In a situation where there is no complete freedom for selection of solvent based on partition coefficient only, availability of interfacial area and emulsion type can play a role specially for molecules with low mass transfer constants and partition coefficients and reaction systems with low residence time.

In this work, a solvent screening mechanism based on emulsion type, emulsion fraction and droplet size is proposed. Further, partition coefficients and mass transfer constants were also considered and included in the overall solvent selection criteria. QSPR based linear and non-linear artificial neural network (ANN) models were used in chapter four to characterize emulsion properties. These QSPR models were adopted in building the selection algorithm used to implement our solvent screening strategy. Experimental regressed liquid-liquid equilibrium data and *a priori* prediction by UNIQUAC Functional group Activity coefficient (UNIFAC) in Aspen Plus was used to evaluate partition coefficients solutes in the aqueous-organic solvents of the biphasic reactor used as a case study in chapter two and three [8].

Solvents, which are used commonly for upgrading biofuel products in a biphasic reactor, and with similar structural and functional groups in our emulsion, models are used for evaluation. The solvents assessed in the literature that are used in bio oil upgrading in a biphasic reactor are decalin [9, 10], dodecane [11] and toluene[12], methylisobutylketone [13, 14] and dichloromethane [15] among others.

5.2. Methods

5.2.1. Preselection of solvents

Table 5.1 shows the solvents selected for evaluation. There two set of solvents; solvents which are commonly used for bio oil upgrading which are listed in the introduction section and solvents which are added to the list based on their similarity in structure with the solvents used for building the emulsion property models. There are 13 molecular solvents, six of which have experimental data on emulsion properties.

5.2.2. Solvent screening algorithm

The procedure developed for the selection of solvents for the biphasic reactor is presented in **Figure 5.1**. The first step in the algorithm was to collect and assemble solvents data from literature with a potential of making a solvent in a biphasic reactor for a specific and intended purpose. In this chapter, the goal was to select a solvent capable of increasing selectivity and yield of the biphasic reactor in upgrading a bio-oil in to a biofuel. The specific upgrading reaction of hydrogenation of p-hydroxybenzaldehyde in to 4-methyl cylohexanol was used as a case study.

Therefore, higher organic phase solubility, partition coefficient, interfacial area and mass transfer coefficient was the desired objectives in the order given. Then evaluation of the solvent and emulsion characteristics will be performed and order of priority given to solvent and emulsion properties the solvents will be ranked for analysis.

5.2.3. Emulsion property model development

The same procedure used in Emulsion model development in **Chapter 4** was used to evaluate emulsion properties of solvents collected from the literature. The same descriptors were used in the emulsion model development. The training sets and test sets are listed **Table 5.2** and **5.1** respectively.

5.2.4. Calculation of partition coefficients

Partition coefficients (K_p) and the ratio of solutes concentration between the organic phase and aqueous phase at equilibrium as shown in the following equation.

$$K_p = \left(\frac{C_O}{C_W} \right)_{equilibrium} \quad \textbf{(5.1)}$$

Where C_o and C_w represents concentration of solutes in the organic and water phases respectively. The NRTL LLE model in Apsen Plus is used to evaluate the equilibrium concentration of the solutes, p-cresol and 4-methylcelohexanol, in the biphasic reactor used as a case study. The biphasic reactor operating temperature, pressure, and concentration at the end of the reactor operations are used in evaluating the equilibrium concentrations. Five sets of experimental regressed NRTL binary liquid-liquid equilibrium data were used to evaluate partition coefficient of p-cresol between the organic solvents and water. The sources of the experimental regressed binary parameter data are disused in the results section. For the remaining solvents, *a priori* prediction by UNIFAC in Aspen Plus was used to estimate the liquid-liquid binary parameters.

5.2.5. Calculation of diffusion and mass transfer constant

The following parameters were considered in evaluating the rate mass transfer of reaction products or solutes in the biphasic reactor

a. influence of the direction of solute transfer

b. mixing condition of the biphasic reactor

c. average droplet size of the emulsions

d. diffusion coefficients of the solutes in the organic and aqueous phase solvents.

e. partition coefficients

For systems involving the interaction between polar and nonpolar components, correlation by Sitaraman et al [16] is the recommend method in the literature for estimating diffusion coefficients as given by **Equation 2**.

$$D_{AB} = 16.19 * 10^{-14} \left(\frac{M_B^{1/2} \Delta H_B^{1/3} T}{\mu_B V_A^{1/2} \Delta H_A^{0.3}} \right)^{0.93} \quad \textbf{(5.2)}$$

Where

A stands for solute

B stands for solvent

M is molecular weight of solute (g)

ΔH is change of enthalpy of vaporization (J/M)

μ is dynamic viscosity (cP)

V is molecular volume of the solute (m^3) and

T is temperature of the solution (K)

Calculation of mass transfer constant of solute A in Solvent B can be performed using empirical correlations. Tudose and Apreotesei [4] uses **Equation 3** to estimate the overall mass transfer coefficient for a water/acetone/carbon tetrachloride ternary system in a Lewis cell where acetone was allowed to diffuse from water to carbon tetrachloride and vice versa.

$$S_h = b \, \mathrm{Re}^p \, S_c^{\,n} \left(\frac{D_{AW}}{D_{AO}} \right)^2 \phi^r \quad \textbf{(5.3)}$$

Where,

The Sherwood number is calculate as,

$$S_h = \frac{dk_{mW}}{D_{AW}}$$

The Schmitt number is calculate as,

$$S_C = \frac{\gamma_A}{D_{AW}},$$

The Reynold number is calculate as,

$$Re = \frac{nd^2\rho}{\mu}$$

In the above equations,

k_m is individual mass transfer constant (m/s)

W stands for water phase

O stands for organic phase

μ is dynamic viscosity *(Pa.s)*

γ is kinematic viscosity (m^2/s)

n is stirrer speed (rpm)

d is impeller diameter (m)

ρ is density (kg/m^3)

Apreotesei et al [17] furthered the work so as to generalize by including two additional ternary systems (water-acetone-chloroform, and water-acetone-toluene) in the experiment in their bid to make a generalized mass transfer coefficient correlation which will be used for both cases of mass transfer direction change and at different mixing condition. **Table 5. 3**shows the effects of mass transfer direction on the mass transfer constant calculations included in the work of Apreotesei et al [17].

The overall mass transfer was calculated using the two-film theory and evaluated by **Equation 5.4 and 5.5.**

(c) when the mass transfer direction is from oil phase to water phase

$$\frac{1}{K_{mA_{(O/W)}}} = \frac{1}{k_{mA_{(O)}}} + \frac{\phi_{(A)}}{k_{mA_{(W)}}} \quad \textbf{(5.4)}$$

(d) when the mass transfer direction is from water phase to oil phase

$$\frac{1}{K_{mA_{(W/O)}}} = \frac{1}{\phi_{(A)} k_{mA_{(O)}}} + \frac{1}{k_{mA_{(W)}}} \quad \textbf{(5.5)}$$

Where

$C_{A(Oil)}$ *is concentration of A in the oil phase (mol/m^3)*

ϕ *is partition coefficient of species between the oil phase and water phase*

$K_{m(O/W)}$ *is mass overall mass transfer coefficient of species in when mass transfer is from oil phase to water phase (m/s)*

$k_{m(O)}$ *mass transfer coefficient of species in the oil phase (m/s)*

One of the above two equations can be used depending on the direction of mass transfer. If component A is being transferred from the organic phase to aqueous phase, then equation two can be used. If the opposite is true, then equation one will be used.

5.3. Results and discussion

5.3.1. Emulsion property modeling results

The average drop size, emulsion fraction and emulsion type for the thirteen solvents were evaluated using the emulsion property models developed in the previous chapter. The best descriptors selected in the previous step were used and model training is performed here only to estimate new coefficient for the linear model and weights biases for the ANN emulsion type model. **Figure 5. 2** shows the comparison between the experimental data for average droplet size and emulsion fraction against model predictions of the six solvents for which experimental data available. The experimental data shown in **Table 5. 1** was used as a training set when developing the model. A coefficient of determination of 0.96 and 0.94 was obtained for ADS and EF predictions. A better prediction performance than that was obtained in chapter is achieved because some of the solvents selected for evaluation were used as a training set in the model development. The results for emulsion type models predictions for these six solvents are presented in **Table 5. 4** The emulsion type model as able to classify with 100% success rate.

Decalin and tetralin showed the best emulsion properties. Decalin has the lowest average droplet size while tetralin showed the highest emulsion fraction with moderate average drop size. All the three types of emulsion are water in oil. 1-dodecene, cyclopentane and hexadecane; hydrocarbons without branched chain showed oil in water emulsion type which is preferred type of solvents if the separation is from the organic phase to aqueous phase. Table 5. 4 also shows emulsion property model predictions for the seven solvents that are collected from the literature. All the 23 experimental data points used for training the model in this case.

5.3.2. Estimation of partition coefficients

Table 5. 5 shows partition coefficient prediction by the liquid-liquid equilibrium NRTL thermodynamic model. Regressed LLE binary parameters was obtained for the interaction between p-cresol and five solvents. The results showed that there is a big difference between the partition coefficient predicted by UNIFAC and regression. Therefore, only five of the solvents with binary interaction parameters available from experimental data are considered for final analysis.

The rank of solvents based on partition coefficients revealed that decalin is the best solvent followed by 1,2 dichlorobenzene, tetralin, toluene, and o-xylene. However, the regressed binary interaction experimental data for decalin-water-p-cresol are obtained from the University of Oklahoma for a temperature range of 30-60 °C. Therefore, extrapolation was used to estimate binary parameters at 150°C. Whereas, for the remaining solvents the reactor temperature in the range of the experimental data used for binary parameters regression.

5.3.3. Estimation of mass transfer constants

The diffusivity of p-cresol and 4-MECH in all of the thirteen solvents were estimated using the Sitaraman correlation. All the physical properties used for calculations of the correlations were estimated by using Aspen plus. **Table 5. 6** the molecular diffusivity of p-cresol and 4-methylcyclohexanol in each solvents selected for screening. All the thermos-physical parameters at the reactor operating conditions calculated by Aspen Plus are also presented. Table 5. 7 shows results for individual mass transfer coefficients of p-cresol in the five solvents with a partition coefficient value obtained from prediction of equilibrium concentration using regressed binary parameters in Aspen Plus.

The ranking of solvents based on the overall mass transfer coefficients showed that the best solvent in this case is tetralin followed by toluene and o-xylene. Decalin and 1,2 dichlorobenzene decalin returned the lowest value.

5.4. Conclusion

The results of the emulsion characteristics showed that there is a significant difference in the total estimated interfacial area of droplet size created in the emulsions. Further, emulsion type was also found to be different for different classes of emulsions. Mass transfer is generally preferred and faster when the mass transfer direction is from the droplet phase in to the continuous phase. Therefore, the utility of emulsion type modeling is demonstrated in this study. Partition coefficient estimation showed that decalin is the best solvent among the five solvents followed by 1,2 dichlorobenzene, tetralin, toluene, and o-xylene. Whereas, tetralin was found to be the best solvent in terms mass transfer coefficient. This work showed that different solvents exhibit different qualities for use in biphasic reactors. Mass transfer coefficients and emulsion type, emulsion fraction and droplet size might be more important factors that partition coefficients in selecting solvents for separation depending on the reactor operating conditions. This work, therefore, adds values to the existing solvent selection procedures based on partition coefficients and solubility.

Table 5. 1. Solvents selected for evaluation of mass transfer coefficient for BPR

No	Organic phase	Structure[18]	ET	EF (%vol.)	ADS (μm)
	With experimental emulsion data				
1	1-dodecene		O/W	46.2	24.3
2	decalin		W/O	69.7	20.8
3	toluene		W/O	65.8	40.0
4	o-xylene		W/O	56.4	34.2
5	tetralin		W/O	83.3	39.0
6	dichloromethane	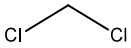	W/O	67.6	65.2
	No experimental emulsion data				
1	cyclopentane		-	-	-
2	2-methyltetrahydrofuran	 -	-	-	-
3	1,1-dichloroethane	 -	-	-	-
4	1,2-dichloroethane	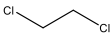 -	-	-	-
5	methyl isobutyl ketone	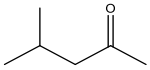	-	-	-
6	chlorobenzene	 -	-	-	-
7	hexadecane		-	-	-

Table 5.2. Solvent database used for building emulsion property model

No	Organic phase	Structure	ET	EF (% vol.)	ADS (μm)
1	hexane		O/W	39.5	20.1
2	heptane		O/W	38.2	21.7
3	octane		O/W	81.1	43.6
4	nonane		O/W	47.4	18.9
5	decane		O/W	50.0	22.8
6	undecane		O/W	44.7	27.0
7	dodecane		O/W	76.3	38.7
8	tridecane		O/W	38.5	18.6
9	tetradecane		O/W	65.8	35.0
10	3-methylpentane		W/O	61.4	23.7
11	cyclohexane		O/W	75.0	40.1
12	methylcyclohexane		W/O	60.5	18.1
13	m-xylene		W/O	65.8	36.2
14	p-xylene		W/O	71.8	39.8
15	1-methylnaphtalene		W/O	78.9	42.5
16	1,2-dichlorobenzene		W/O	38.5	21.4
17	methyl laurate		W/O	56.6	7.5

Table 5.3. Effect of Reynold number and mass transfer direction on mass transfer coefficient [17]

Equation	Phase	Re	Mass transfer direction
$Sh = 54.19Re^{1.19}S_c^{1/3}\left(\frac{D_{AW}}{D_{AO}}\right)^{1/2}$	Aqueous	$Re_W < 9500$ $Re_O < 17500$	Aqu. → Org.
$Sh = 54.15Re^{1.19}S_c^{1/3}\left(\frac{D_{AW}}{D_{AO}}\right)^{1/2}$ $(0.341*\phi^2 - 1.249\phi + 1.474)$	Organic	$Re_W < 9500$ $Re_O < 17500$	Aqu. → Org.
$Sh = 111.25Re^{0.96}S_c^{1/3}\left(\frac{D_{AW}}{D_{AO}}\right)^{1/2}$	Organic	$Re_W < 10300$ $Re_O < 17500$	Org. → Aqu
$Sh = 231.60Re^{0.95}S_c^{1/3}\left(\frac{D_{AW}}{D_{AO}}\right)^{1/2}$ $(0.0074\phi^2 - 0.011\phi + 1.091)$	Aqueous	$Re_W < 10300$ $Re_O < 17500$	Org. → Aqu

Table 5. 4. Emulsion property model results for target solvents

No	Organic phase	Structure [18]	ET		EF (% vol.)			ADS (μm)		
			Exp	Pred	Exp	Pred	%AD	Exp	Pred	%AD
		With experimental emulsion data								
1	1-dodecene	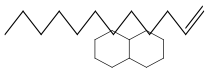	O/W	O/W	46.2	46.7	1.1	24.3	25.6	5.3
2	decalin		W/O	W/O	69.7	67.1	3.7	20.8	17.0	18.3
3	toluene		W/O	W/O	65.8	64.0	2.7	40.0	36.9	7.8
4	o-xylene		W/O	W/O	56.4	60.6	7.4	34.2	34.7	1.5
5	tetralin		W/O	W/O	83.3	85.0	2.0	39.0	36.9	5.4
6	dichloromethane	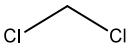	W/O	W/O	67.6	65.6	3.0	65.2	61.4	5.8
		No experimental emulsion data								
1	cyclopentane		-	O/W	-	67.6		-	34.7	
2	2-methyltetrahydrofuran	 -	-	W/O	-	58.5		-	37.8	
3	1,1-dichloroethane	 -	-	W/O	-	66.3		-	25.9	
4	1,2-dichloroethane	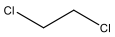 -	-	W/O	-	66.8		-	27.3	
5	methyl isobutyl ketone	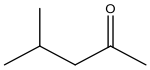	-	W/O	-	68.0		-	35.2	
6	chlorobenzene	 -	-	W/O	-	63.7		-	34.7	
7	hexadecane		-	O/W	-	38.4		-	27.3	

Table 5. 5. Partition coefficient estimation using UNIFAC and regression by Aspen Plus

Solvents		Partition coefficients values				
		a priori prediction (25°C)		Regressed from Experiment data (150°C)		
		p-cresol	4-MECH	p-cresol	4-MECH	Data source
decalin	Water	3.6	22.7	1.9	6.3	OU(extrapolated)
hexadecane	Water	38.7	49.5	-	-	-
Chlorobenzene	Water	44.3	54.6	-	-	-
MIBK	Water	252.2	56.1	-	-	-
1,2 dichlorobenzene	Water	364.3	53.3	1.4	-	NIST
1,1 dichlorobenzene	Water	35.3	96.3	-	-	-
cyclopentane	Water	35.5	42.6	-	-	-
1-dodecene	Water	20.2	18.5	-	-	-
toluene	Water	78.2	95.2	0.8	-	Aspen VLE
tetralin	Water	61.8	75.1	1.0	-	Aspen VLE
2-methyltetrahydrofuran	Water	No phase split		-	-	-
dichloromethane	Water	22.0	76.0	-	-	-
o-xylene	Water	89.6	96.7	0.8	-	NIST

Table 5. 6. Diffusivity calculation results for p-cresol and 4-MECH in all solvents using the Sitaraman correlation

Component	Parameters estimated using Aspen Plus				Calculated diffusivity (D_{AB}) m^2/s of	
	MB (g)	μ_B (cP) (150°C)	ΔH_A (J/mole)	ΔH_B (J/mole)	p-cresol	4-MECH
p-cresol(A)			51337.4			
4-MECH(A)			49301.6			
water	18.0	0.17		38218.5	3.0E-09	3.0E-09
decalin(B)	138.3	0.56		42113.1	2.6E-09	2.7E-09
hexadecane(B)	226.4	0.53		66263.8	4.0E-09	4.0E-09
Chlorobenzene(B)	112.6	0.25		35493.7	4.8E-09	4.8E-09
MIBK(B)	100.2	0.20		32867	5.6E-09	5.6E-09
1,2 dichlorobenzene (B)	99.0	0.26		27856	4.0E-09	4.1E-09
1,1 dichlorobenzene (B)	99.0	0.18		22799.4	5.4E-09	5.5E-09
cyclopentane (B)	70.1	0.16		20927.1	4.9E-09	5.0E-09
1-dodecene (B)	168.3	0.29		48945.2	5.5E-09	5.5E-09
toluene (B)	92.1	0.19		30760	5.5E-09	5.5E-09
tetralin (B)	132.2	0.46		43125.1	3.1E-09	3.1E-09
2-methyltetrahydrofuran (B)	86.1	0.14		24561.8	6.5E-09	6.5E-09
dichloromethane(B)	84.9	0.18		21233.8	4.9E-09	5.0E-09
o-xylene (B)	106.2	0.23		36480.8	5.0E-09	5.1E-09

Table 5.7. Results of mass transfer coefficient calculations for mass transfer from the aqueous phase to organic phase.

Solvents	*Re*	*Sc*	D_{AB} (m/s^2)	*Kp*	*Sh*		k_m *(m/s)*		
	p-cresol	p-cresol	p-cresol	p-cresol	Water	Organic	Water	Organic	Overall
water	9500	93.9	3.E-09						
decalin	9500	108.3	3.E-09	1.9	3.E+06	4.E+07	0.09	1.22	0.05
1,2 dichlorobenzene	9500	70.4	4.E-09	1.4	2.E+06	2.E+07	0.08	1.21	0.05
toluene	9500	51.2	6.E-09	0.8	2.E+06	3.E+07	0.06	1.79	0.08
tetralin	9500	90.8	3.E-09	1	2.E+06	5.E+07	0.09	1.97	0.09
o-xylene	9500	56.3	5.E-09	0.8	2.E+06	3.E+07	0.07	1.87	0.08

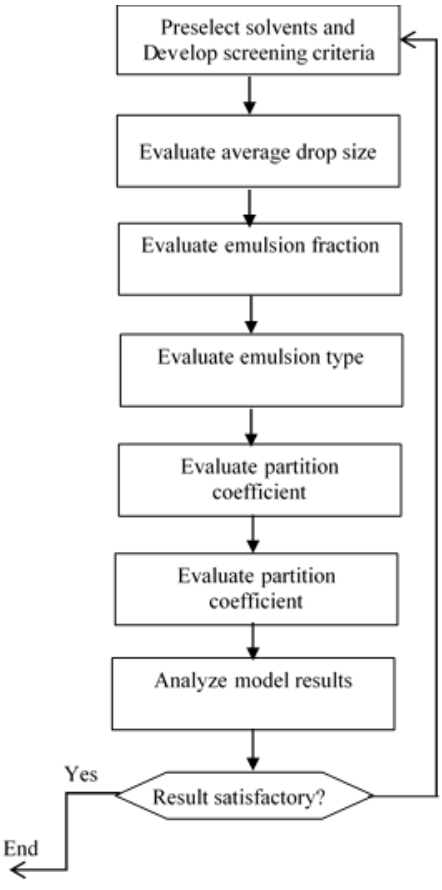

Figure 5.1. Algorithm for solvent selection and screening for biphasic reactor

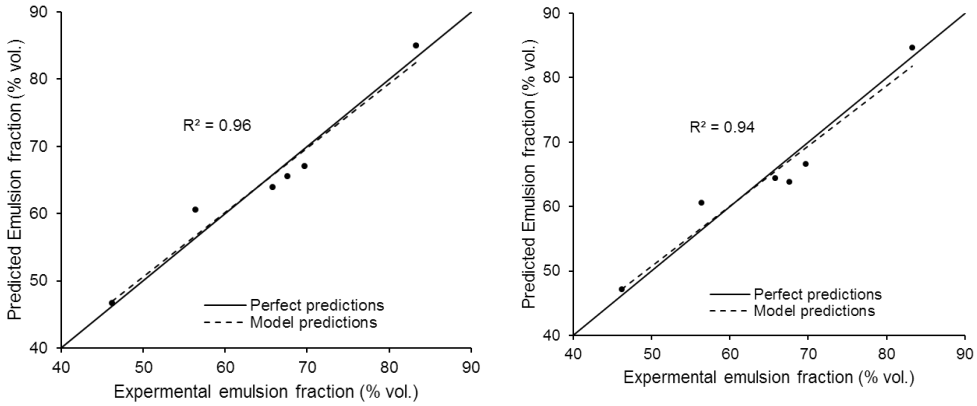

Figure 5.2. Comparison of experimental data against model prediction for ADS and EF of solvents

REFERENCES

1. Wachsen, O., K. Himmler, and B. Cornils, *Aqueous Biphasic Catalysis: Where the Reaction Takes Place.* Catalysis Today, 1998. **42**(4): p. 373-379.
2. Fridjonsson, E.O., L.S. Flux, and M.L. Johns, *Determination of mean droplet sizes of water-in-oil emulsions using an Earth's field NMR instrument.* Journal of Magnetic Resonance, 2012. **221**: p. 97-102.
3. Melgarejo-Torres, R., et al., *Mass Transfer Coefficient Determination in Three Biphasic Systems (Water–ionic liquid) Using a Modified Lewis Cell.* Chemical Engineering Journal, 2012. **181–182**: p. 702-707.
4. Tudose, R.Z. and G. Apreotesei, *Mass Transfer Coefficients in Liquid–liquid Extraction.* Chemical Engineering and Processing: Process Intensification, 2001. **40**(5): p. 477-485.
5. Tudose, R.Z. and G. Lisa, *The determination of individual mass transfer coefficients in liquid-liquid extraction.* Hemijska industrija 2003. **57**(9): p. 393-398.
6. Peters, M., et al., *Systematic Approach to Solvent Selection for Biphasic Systems with a Combination of COSMO-RS and a Dynamic Modeling Tool.* Engineering in Life Sciences, 2008. **8**(5): p. 546-552.
7. Blumenthal, L.C., et al., *Systematic Identification of Solvents Optimal for the Extraction of 5-Hydroxymethylfurfural from Aqueous Reactive Solutions.* ACS Sustainable Chemistry & Engineering, 2016. **4**(1): p. 228-235.
8. Yerramsetty, K.M., B.J. Neely, and K.A.M. Gasem, *A Non-Linear Structure-Property Model For Octanol-Water Partition Coefficient.* Fluid phase equilibria, 2012. **332**: p. 85-93.
9. Faria, J., M.P. Ruiz, and D.E. Resasco, *Phase-Selective Catalysis in Emulsions Stabilized by Janus Silica-Nanoparticles.* Advanced Synthesis & Catalysis, 2010. **352**(14-15): p. 2359-2364.
10. Zapata, P., et al., *Condensation/Hydrogenation of Biomass-Derived Oxygenates in Water/Oil Emulsions Stabilized by Nanohybrid Catalysts.* Topics in Catalysis, 2012. **55**(1): p. 38-52.
11. Dumont, E., Y. Andrès, and P. Le Cloirec, *Effect of organic solvents on oxygen mass transfer in multiphase systems: Application to bioreactors in environmental protection.* Biochemical Engineering Journal, 2006. **30**(3): p. 245-252.
12. Mahfud, F.H., et al., *The application of water-soluble ruthenium catalysts for the hydrogenation of the dichloromethane soluble fraction of fast pyrolysis oil and related model compounds in a two phase aqueous–organic system.* Journal of Molecular Catalysis A: Chemical, 2007. **277**(1–2): p. 127-136.

13. Saha, B. and M.M. Abu-Omar, *Advances in 5-hydroxymethylfurfural production from biomass in biphasic solvents.* Green Chemistry, 2014. **16**(1): p. 24-38.
14. Chheda, J.N., Y. Roman-Leshkov, and J.A. Dumesic, *Production of 5-hydroxymethylfurfural and furfural by dehydration of biomass-derived mono- and poly-saccharides.* Green Chemistry, 2007. **9**(4): p. 342-350.
15. Mahfud, F.H., F. Ghijsen, and H.J. Heeres, *Hydrogenation of fast pyrolyis oil and model compounds in a two-phase aqueous organic system using homogeneous ruthenium catalysts.* Journal of Molecular Catalysis A: Chemical, 2007. **264**(1–2): p. 227-236.
16. Sitaraman, R., S.H. Ibrahim, and N.R. Kuloor, *A Generalized Equation for Diffusion in Liquids.* Journal of Chemical & Engineering Data, 1963. **8**(2): p. 198-201.
17. Apreotesei Lisa, G., R.Z. Tudose, and H. Kadi, *Mass transfer resistance in liquid–liquid extraction with individual phase mixing.* Chemical Engineering and Processing: Process Intensification, 2003. **42**(11): p. 909-916.
18. CambridgeSoft, *ChemBioOffice 11.0*. 2009

CHAPTER VI

CONCLUSIONS AND RECOMMENDATIONS

The conclusions and recommendations drawn from this dissertation are discussed in this chapter. The overall objectives of this project were to represent biphasic reactors with a mathematical model, devise a simulation platform for the biphasic reactors, and to develop predictive models for emulsion properties and solvent selection. This work successfully demonstrates the efficacy of modeling biphasic reactors with a combined phase equilibria and mass transfer approach. Further, predictive models for emulsion properties and solvent selection were developed and the solvent properties. The predictive models for emulsions and solvents can be used to facilitate solvent selection for improved biphasic reactor performance. Specific conclusions and recommendations drawn from each chapter are discussed below

6.1. Conclusions

i. Modeling and simulation of biofuel upgrading catalytic biphasic reaction at the water/oil interface; a phase equilibria approach

Biphasic reactor model representing simultaneous liquid phase heterogeneous reaction and component phase distribution was successfully simulated and validated using available experimental data. The LLE phase equilibria model offers a better representation of the experimental biphasic reactor data. The following conclusions were drawn from this work:

i. An algorithm proposed for the modeling and simulation of a biphasic reactor was implemented successfully and validated using available experimental data.

ii. Five LLE binary parameters were regressed from the experimental ternary equilibrium data for water/decalin/p-cresol and waster/decalin/4-methylcylohexanol. Further, the linear regression of the binary parameters from the two ternary equilibrium data available from collaborators at the University of Oklahoma showed that the binary parameters were linearly dependent on temperature. The remaining 10 out of 15 NRTL binary parameters were obtained by *a priori* prediction using the QSPR-NRTL and UNIFAC models.

iii. Assessment of the effect of liquid-liquid equilibrium (LLE) binary parameters on phase behavior modeling shows that only regressed parameters should be used to provide reliable LLE predictions. In the absence of regressed LLE binary data, however, a priori prediction by QSPR-NRTL and UNIFAC models could offer an alternative method. The results of this work showed the advantage of using a priori-prediction for binary parameter estimation especially when the solute has a limited solubility in one of the two solvents. This reduced the need for additional experimental ternary equilibrium data without affecting significantly the results of the model.

iv. The kinetic models developed using the Eley-Rideal mechanism fit the experimental kinetic data. The kinetic parameters for both reaction rate and adsorption equilibrium constants were estimated successfully by using non-linear regression.

v. The successful integration of Aspen Plus and Excel-VBA using Aspen Simulation Workbook offered a unique advantage for calculation of both temperature dependent and temperature independent thermo-physical properties of pure substances and mixture with greater accuracy and speed. The modeling and simulation strategy of the biphasic reactor was successfully validated with a case study of biphasic reactor data obtained from collaborators at the University of Oklahoma.

vi. The activity coefficient test revealed that activity coefficients remain nearly constant throughout the period of the reaction and only concentrations were used for expression of the kinetic model. The Gibbs energy test showed that the mixture Gibbs energy for each phase and the overall phase minimizes as the reaction proceeds, supporting the assumptions that the system is progressing toward a local equilibrium at the interface and a global equilibrium in the overall reactor.

ii. Modeling and simulation of biofuel upgrading catalytic biphasic reaction at the water/oil interface; a mass transfer approach

A mass transfer model, instead of the thermodynamic NRTL model, was used for representing the component phase distribution in the biphasic reactor model in this chapter. The same kinetic model used in the first chapter was used to represent the heterogeneous liquid phase reaction. This more rigorous approach better explains the phase selectivity of reactions in the biphasic reactor and offers a direct expression of emulsion properties such as interfacial area and partition coefficient in the component phase distribution model unlike the previous approach. Optimization of mass transfer parameters was necessary to match predictions obtained by the previous approach. The following conclusions were drawn from this work.

i. An alternative algorithm proposed for the modeling and simulation of a biphasic reactor was implemented successfully and validated using available data. The results of the simulation showed that the biphasic reactor for upgrading bio-oils could also be modeled and simulated effectively using the mass transfer limitation approach.

ii. The integration of Aspen Plus in the simulation module was successful and provided convenient estimation of thermos-physical parameters.

iii. Optimization based on direct heuristic search was successfully implemented to estimate the fractional interfacial area available for mass transfer. The results of the simulation

showed that only a small fraction of the theoretical interfacial area between the two phases is available for mass transfer.

iv. The modeling of the biphasic reactor with mass transfer limitation showed that biphasic reactors could offer selectivity of reaction in the desired phase, separation of products with increased organic phase solubility, and continuation of the upgrading process in the presence of component phase-distribution. The modeling and simulation strategy of the biphasic reactor based on the mass transfer limitation approach was validated with a case study of biphasic reactor data obtained from collaborators at the University of Oklahoma.

v. The Gibbs energy test showed that the mixture Gibbs energy for each phase and overall reactor approaches a minimum as the reaction proceeds. Further, the total Gibbs energy change for each time step is shown to be negative supporting the assumption of simultaneous reaction and mass transfer in developing the biphasic reactor model. The activity coefficient test revealed that activity coefficients remain nearly constant throughout the period of the reaction and only concentrations were used for expression of the kinetic model.

iii. Modeling effects of solvent type and water cut on emulsion characteristics using quantitative structure-property relationship

A quantitative structure-property relationship (QSPR) model for best descriptor selection and linear and non-linear ANN model development for emulsion properties was developed and implemented successfully. The model was validated using experimental data. Further, Leave One Out Cross Validation was used to evaluate the generalization error of the models and approximately comparative results were obtained. The following conclusions were drawn from this work.

i. The molecular 2D and 3D structures of the solvents used in the experiential database were drawn and optimized. Approximately 2684 descriptors were generated with CODESSA and used for model development.

ii. The use of populating ensemble models in selecting the most frequently appearing uncorrelated descriptors for the final model development increases the reproducibility of the descriptor reduction step. Five descriptors were selected for the final model for average drop size and emulsion fraction while two descriptors were selected for emulsion type modeling.

iii. For average drop size and emulsion fraction modeling, a satisfactory result was obtained using a multi linear regression QSPR model in capturing the relationship between molecular descriptors and structures as reflected in the property of interest. The results showed that an average absolute percentage deviation less than 10% for all the QSPR models.

iv. For emulsion type modeling, a pattern classification artificial neural network model based on a simple feed forward perceptron was sufficient to provide classification with a 100% success rate.

v. Water fraction was found to be the most significant descriptor in determining average drop size of the emulsions with a non-linear relationship. This result showed that the effect of water fraction on average drop size should be assessed when selecting a solvent for emulsion development.

iv. Predictive models for solvent selection for biphasic reactor

By using the emulsion property models developed in chapter 4, and theoretical estimation of mass transfer constants and partition coefficients, the potential utility of a solvent selection strategy for biphasic rectors was demonstrated. Specific conclusion drawn from this chapter include the following:

i. The results of the emulsion characteristics show that there is a significant difference in the total estimated interfacial area of droplet size created in the emulsions.
ii. Emulsion type modeling shows different groups of solvents result in different emulsion types. The developed model facilitates identifying solvents that provide a continuous phase for organic solvents.
iii. The results of emulsion property modeling demonstrates the importance of biphasic reactor solvent selection for the enhanced mass transfer of components between the two phases in the reactor.

6.2. Recommendations

i. The main objective of the bio-oil upgrading experiment was to upgrade p-hydroxybenzaldehyde to p-cresol and 4-methylcyclohexanol and consequent transfer of the products from the water phase to the organic phase or vice versa. Therefore, a strategy implemented for selecting a solvent with a higher interfacial area, mass transfer constant, and partition coefficient should be supported and validated with experimental data.
ii. In the current reaction under consideration, the reactor was a batch reactor with 90 minutes residence time which gives components enough time to distribute between the two phase. Therefore, the phase equilibria model is recommended to represent such types of biphasic reactors for better accuracy. A mass transfer model, however, might be more useful in different scenarios such as low residence time due to different reactor configuration and relatively higher reaction and lower mass transfer rate.
iii. The solvent screening strategy was employed only for solvents with similar structures and functional groups to those used to build the emulsion property models. In order to build a robust solvent screening and design strategy based on evolutionary based genetic algorithm and artificial neural network QSPR emulsion property models, a large database

of emulsion properties should be collected. This work didn't include evaluation of some properties of solvents which might affect the performance of solvents such as boiling points, organic and aqueous phase solubility. Additional models for these properties could be developed and included in the development of predictive models for solvent selection.

APPENDICES

Appendix A. Regression of NRTL binary parameters

Regression of NRTL binary parameters using experimental ternary equilibrium data was performed and the results are presented in this supplemental material. Ternary equilibrium mole concentration data (Table SM1) for p-cresol and 4-MECH in a water/decalin system and solubility data (Table A.1) for water and decalin were collected at OU. Table A.2 and Figure SM1 show the solubility model results from regressing the experimental solubility data. Tables A.3 and SM4 show the equilibrium mole fraction calculated using the equilibrium concentration data and the solubility model. The mole fraction data were used to regress NRTL binary parameters at 30-60 ºC. The regressed NRTL binary parameters were used to develop a linear regression model, and NRTL binary parameters at the reactor temperature of 150 ºC were predicted and used in the simulations.

The NRTL binary parameters were found to be linearly dependent on temperature. Tables A.5 and A.6 show NRTL binary parameters regressed at each temperature, initial values used for regression, and prediction at 150°C using the regression model. Regression results for average values in the range of 30-60°C is also provided in the same table. The linearity of the regression model can be observed in Figures A.2 and A.3. Aspen Plus V8.2 was used for regression.

The regression results were highly sensitive to the initial values. Therefore, a good representative value was used to initialize the regression. The regression was performed first at 60ºC, and the values obtained at this temperature were used to initialize regression at 50ºC.

A similar procedure was followed for regressions at 40ºC and 30ºC. The tolerance and the number of iterations used were $1.0*10^{-08}$ and 500, respectively.

Table A.1. Experimental data and model representation for solubility of water and decalin

Experimental concentration data (mol/l)						
water/decalin/p-cresol system						
Temp (°C)	Organic phase			Aqueous phase		
	p-cresol	water	decalin	p-cresol	water	decalin
30	0.104	0	-	0.087	-	0
40	0.109	0	-	0.082	-	0
50	0.118	0	-	0.071	-	0
60	0.123	0	-	0.068	-	0
water/decalin/4-MECH system						
Temp (ºC)	Organic phase			Aqueous phase		
	p-cresol	water	decalin	p-cresol	water	decalin
30	0.0244	0	-	0.0119	-	0
40	0.0266	0	-	0.0106	-	0
50	0.0273	0	-	0.0092	-	0
60	0.0280	0	-	0.0085	-	0

Table A.2. Experimental data and model representation for solubility of water and decalin

Temperature (K)	Decalin mole fraction (water-rich)	Water mole fraction (decalin-rich)
Experimental Data		
374.15	4.10E-07	9.7E-03
424.65	2.00E-06	2.5E-02
451.15	-	4.1E-02
475.15	7.70E-06	5.4E-02
576.15	8.80E-05	3.1E-01
Model Representations		
303.15	7.62E-08	3.5E-03
374.15	4.78E-07	1.1E-02
424.65	1.77E-06	2.6E-02
451.15	3.50E-06	4.0E-02
475.15	6.52E-06	5.9E-02
576.15	8.88E-05	3.1E-01

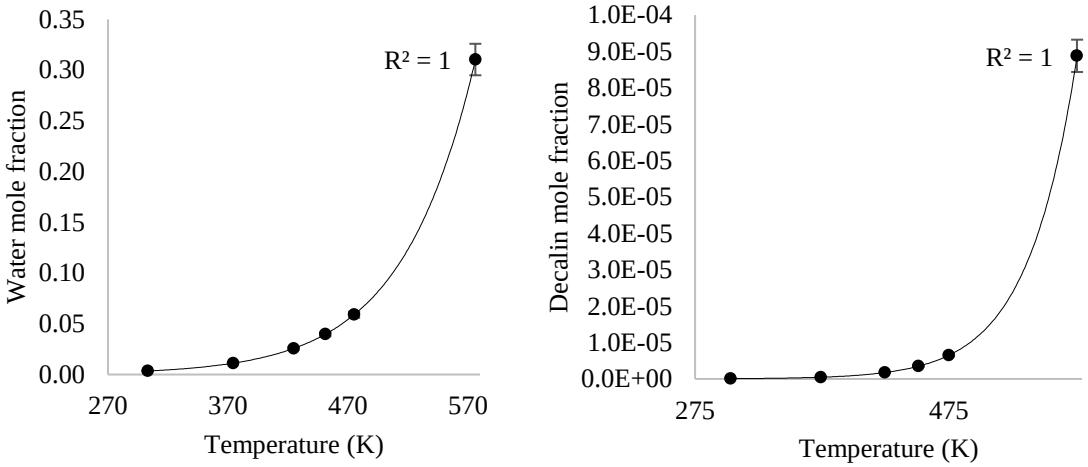

Figure A.1. Solubility model representation for decalin and water

Table A.3. Ternary mole fraction data for water/decalin/p-cresol system

	Organic phase			Aqueous phase		
T (°C)	p-cresol	water	decalin	p-cresol	water	decalin
30	0.01602	3.14E-03	0.9808	0.00160	0.99840	8.65E-09
40	0.01692	3.71E-03	0.9794	0.00152	0.99848	1.14E-08
50	0.01845	4.39E-03	0.9772	0.00133	0.99867	1.49E-08
60	0.01937	5.19E-03	0.9754	0.00128	0.99872	1.96E-08

Table A.4. Ternary mole fraction data for water/decalin/4-MECH system

	Organic phase			Aqueous phase		
T (°C)	4-MECH	water	decalin	4-MECH	water	decalin
30	0.00377	3.34E-03	0.9929	0.000216	0.9998	8.67E-08
40	0.00415	3.96E-03	0.9919	0.000195	0.9998	1.14E-07
50	0.00429	4.69E-03	0.9910	0.000170	0.9998	1.50E-07
60	0.00443	5.55E-03	0.9900	0.000161	0.9998	1.97E-07

Table A.5. Results of NRTL binary parameter regressions for the water/decalin/p-cresol system

System	Comp1	Comp2		A12 & A21 values (α_{12} = 0.2)					
				Regressed				Predicted	Regressed
			Initial value	30°C	40°C	50°C	60°C	150°C	30-60°C
1	p-cresol	water	3258	4893	4774	4567	4521	3300	3258
	water	p-cresol	2423	2375	2385	2394	2410	2512	2423
2	p-cresol	decalin	-593	-475	-485	-498	-507	-604	-193
	decalin	p-cresol	2677	3128	3111	3091	3081	2936	2677
3	water	decalin	4588	5521	5533	5545	5579	5737	4588
	decalin	water	1508	1639	1630	1618	1603	1498	1508

Table A.6. Results of NRTL binary parameter regressions for the water/decalin/4-MECH system

System	Comp1	Comp2		A12 & A21 values (α_{12} = 0.2)					
				Regressed				Predicted	Regressed
			Initial value	30°C	40°C	50°C	60°C	150°C	30-60°C
1	4-MECH	water	3185	3283	3161	2932	2881	1556	3185
	water	4-MECH	2639	2407	2419	2421	2435	2509	2639
2	4-MECH	decalin	-96	-121	-135	-153	-153	-261	-96
	decalin	4-MECH	2251	2103	2086	2080	2062	1949	2251
3	water	decalin	4467	4392	4445	4497	4547	5005	4467
	decalin	water	1500	1511	1501	1487	1470	1349	1494

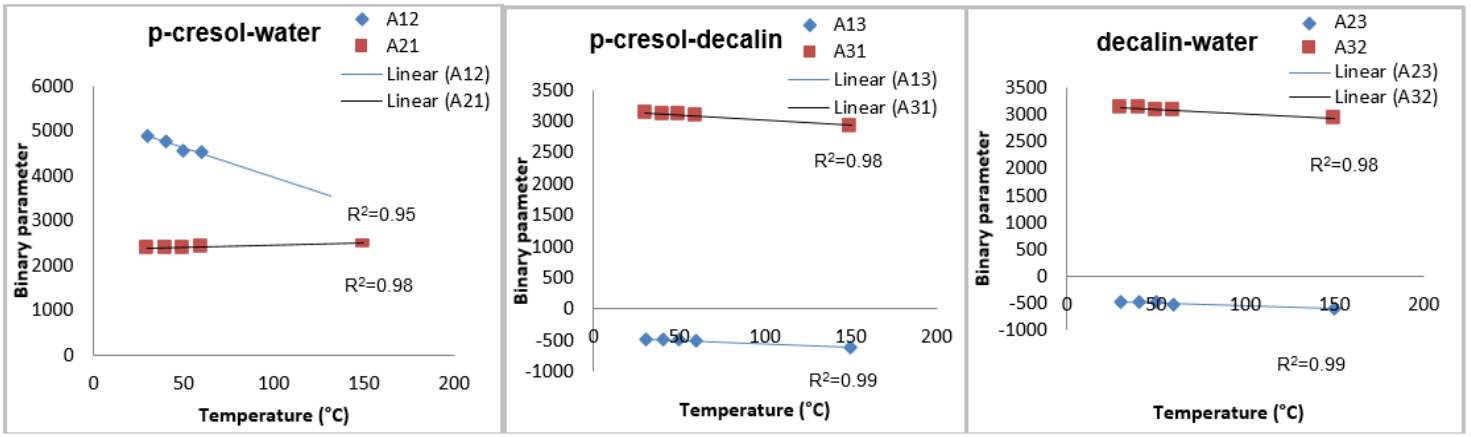

A. Regression results for the water/decalin/p-cresol system

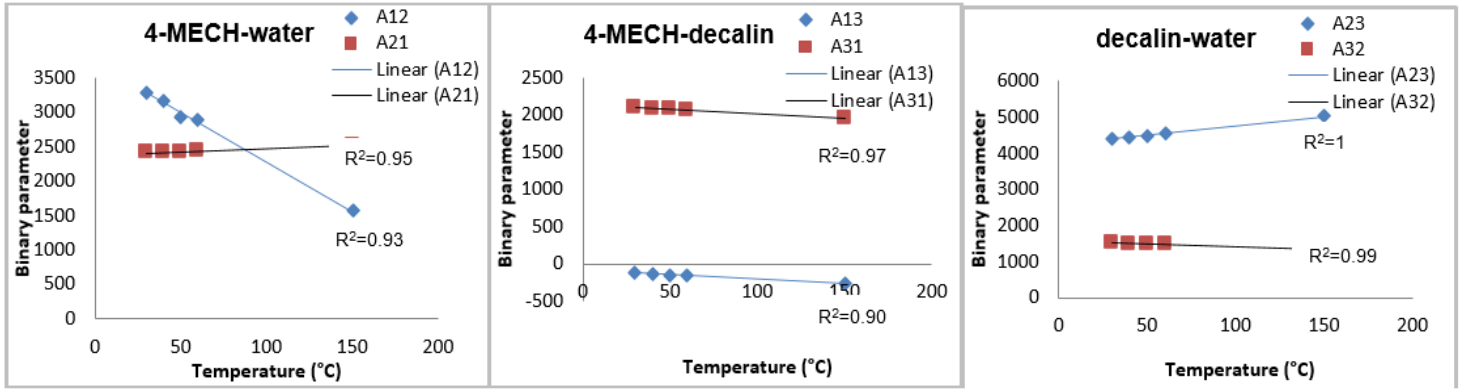

B. Regression results for the water/decalin/4-MECH system

Figure A. 2. NRTL binary parameters model prediction at 150°C

Appendix B. A priori prediction of NRTL parameters

For the combination of binary compounds lacking experimental data, QSPR and UNIFAC were used to predict NRTL binary parameters at 25°C. The results of the *a priori* predictions are shown in **Table B.1**.

Table B.1. *A priori* predicted NRTL binary parameters at 25°C

			UNIFAC($\alpha_{12} = 0.2$)		QSPR($\alpha_{12} = 0.3$)	
System	Comp. 1	Comp. 2	A12	A21	A12	A21
1	decalin	water	2101.6	3617.5	1524.6	1109.1
2	decalin	p-BAL	1492.9	980.9	1150.5	488.7
3	decalin	p-BOL	1083.7	524.8	1217.6	1499.4
4	decalin	p-cresol	650.5	112.1	963.6	1445.1
5	decalin	4-MECH	764.2	42.2	1013.7	1106.0
6	water	p-BAL	1210.3	-262.0	1617.3	-437.2
7	water	p-BOL	1132.8	-275.5	1999.2	-331.6
8	water	p-cresol	1333.2	-176.4	2201.8	-341.6
9	water	4-MECH	1800.8	209.7	1248.3	-113.6
10	p-BAL	p-BOL	97.1	-42.9	742.6	159.7
11	p-BAL	p-cresol	654.7	-424.5	603.2	106.3
12	p-BAL	4-MECH	1186.1	-570.3	682.5	18.9
13	p-BOL	p-cresol	954.4	-571.7	571.5	137.3
14	p-BOL	4-MECH	1333.4	-676.3	782.0	60.0
15	p-cresol	4-MECH	-274.0	-400.4	594.2	-71.3

Appendix C. Molar Enthalpy and Molar Gibbs Energy change for each reactions

The heat of reaction and Gibbs energy change based on molar values for the three reactions and the biphasic reactor mixtures calculated using Aspen Plus are shown in Tables SM8 and SM9, respectively.

Table C.1. Molar Heat of reaction for each reaction

Reaction	Molar Enthalpy (J/mole) at 150°C and 400 psi							Heat of reaction (J/mole)
	decalin	water	p-Bal	p-BOL	p-cresol	4-MECH	hydrogen	
	-186083	-275770	-262519	-318423	-160274	-373955	3633	
Reaction 1	-	-	262519	-318423	-	-	-3633	-59537
Reaction 2	-	-275770	-	318423	-160274		-3633	-121254
Reaction 3	-				160274	-373955	-10899	-224580

Table C.2. Molar Gibbs energy change for each reaction

Reaction	Molar Gibbs Free energy (J/mole) at 150°C and 400 psi							Gibbs energy change (J/mole))
	decalin	water	p-Bal	p-BOL	p-cresol	4-MECH	hydrogen	
	183823	-218392	-129673	-82934	-1247	-67386	10953	
Reaction 1	-	-	129673	-82934	-	-	-10953	35786
Reaction 2	-	-218392	-	82934	1247	-	-10953	-145164
Reaction 3	-	-	-	-	-1247	-67386	-32859	-101492

Appendix D. Best descriptor values used for the emulsion property model

Table D.1. Best descriptor values for all models for all molecules listed in Table 4.1.

No	88 ICR	101 PW3	105 MAXDP	345 WiA_H2	939 MATS8s	1235 SM13_EA	1891 Mor24u	2063 Mor04s	2083 Mor24s	2464 R4s	2474 R5s+
1	1.585	0.214	0.232	0.433	0	0	0.537	3.624	0.659	1.807	0.055
2	1.95	0.219	0.246	0.38	0.372	0	0.12	4.587	-0.016	1.978	0.062
3	2	0.223	0.256	0.339	-0.278	0	0.445	3.472	0.439	1.949	0.056
4	2.281	0.226	0.264	0.306	0.105	0	0.569	5.21	0.533	1.922	0.047
5	2.322	0.229	0.27	0.279	0.005	0	0.367	5.301	0.314	2.143	0.055
6	2.55	0.231	0.275	0.257	0.004	0	0.458	11.645	0.346	2.115	0.048
7	2.585	0.232	0.279	0.238	0.004	0	0.248	5.362	0.001	2.322	0.04
8	2.777	0.234	0.282	0.221	0.003	0	0.927	10.46	0.89	2.194	0.038
9	2.807	0.235	0.285	0.207	0.003	0	0.42	7.878	0.228	2.236	0.04
10	1.459	0.281	0.278	0.45	0	10.833	0.13	1.108	0.137	2.744	0.071
11	0	0.25	0	0.522	0	0	-0.102	0.016	-0.206	2.082	0.058
12	0.863	0.274	0.36	0.458	0	11.367	0.081	2.475	0.126	2.744	0.063
13	1	0.284	0.167	0.409	0	12.382	-0.128	-0.447	-0.079	2.044	0.121
14	1.5	0.288	0.12	0.409	0	12.226	-0.134	-0.455	-0.03	2.029	0.118
15	1.495	0.342	0.157	0.334	0	14.291	-0.172	-0.443	-0.053	2.21	0.105
16	1	0.319	1.466	0.411	0	13.048	0.022	-0.196	-0.112	1.844	0.201
17	2.79	0.255	3.797	0.198	-0.042	11.038	0.034	6.882	-0.929	3.324	0.145
18	2.585	0.232	0.719	0.238	-0.018	0	0.527	6.864	0.289	2.233	0.087
19	1.522	0.326	0.06	0.362	0	13.646	0.19	5.431	0.312	3.195	0.036
20	0.863	0.274	0.083	0.458	0	11.367	-0.048	-1.237	0.069	1.834	0.109
21	1	0.319	0.12	0.411	0	13.048	-0.128	-0.395	-0.068	2.444	0.143
22	1.522	0.326	0.258	0.362	0	13.646	-0.173	1.005	-0.14	2.452	0.067
23	1.495	0.342	4.286	0.334	0	14.291	0.076	3.966	0.697	4.104	0.37
24	0	0.25	0	0.625	0	8.875	-0.212	-0.121	-0.397	1.419	0
25	1	0.277	1.333	0.531	0	11.568	0.167	-3.264	0.52	1.24	0.104

APPENDIX E. Rate equations using Euler's method

The rate equations using Euler's method was derived as follows.

$$C_{A-OIL}(t_1) = C_{A-OIL}(t_0) + \Delta t\left(-\frac{k_1 K_A C_{A-Oil}(t_0)}{\Theta_V(t_0)} - k_{pA_{-1}} C_{A-Oil}(t_0) + k_{pA_1} C_{A-Water}(t_0) \right) \quad \text{(E.1)}$$

$$C_{A-Water}(t_1) = C_{A-Water}(t_0) + \Delta t\left(-\frac{k_1 K_A C_{A-Water}(t_0)}{\Theta_V(t_0)} + k_{pA_{-1}} C_{A-Oil}(t_0) - k_{pA_1} C_{A-Water}(t_0) \right) \quad \text{(E.2)}$$

$$C_{B-Oil}(t_1) = C_{B-Oil}(t_0) + \Delta t\left(\frac{k_1 K_A C_{A-Oil}(t_0)}{\Theta_V(t_0)} - \frac{k_2 K_B C_{B-Oil}(t_0)}{\Theta_V(t_0)} - k_{pB_{-1}} C_{B-Oil}(t_0) + k_{pB_1} C_{B-Water}(t_0) \right) \quad \text{(E.3)}$$

$$C_{B-Water}(t_1) = C_{B-Water}(t_0) + \Delta t\left(\frac{k_1 K_A C_{A-Water}(t_0)}{\Theta_V(t_0)} - \frac{k_2 K_B C_{B-Water}(t_0)}{\Theta_V(t_0)} + k_{pB_{-1}} C_{B-Oil}(t_0) - k_{pB_1} C_{B-Water}(t_0) \right) \quad \text{(E.4)}$$

$$C_{C-Oil}(t_1) = C_{C-Oil}(t_0) + \Delta t\left(\frac{k_2 K_B C_{B-Oil}(t_0)}{\Theta_V(t_0)} - \frac{k_3 K_C C_{C-Oil}(t_0)}{\Theta_V(t_0)} - k_{pC_{-1}} C_{C-Oil}(t_0) + k_{pC_1} C_{C-Water}(t_0) \right) \quad \text{(E.5)}$$

$$C_{C-Water}(t_1) = C_{A-Water}(t_0) + \Delta t\left(\frac{k_2 K_B C_{B-Water}(t_0)}{\Theta_V(t_0)} - \frac{k_3 K_C C_{C-Water}(t_0)}{\Theta_V(t_0)} + k_{pC_{-1}} C_{C-Oil}(t_0) - k_{pC_1} C_{C-Water}(t_0) \right) \quad \text{(E.6)}$$

$$C_{D-Oil}(t_1) = C_{D-Oil}(t_0) + \Delta t\left(\frac{k_3 K_C C_{C-Oil}(t_0)}{\Theta_V(t_0)} - k_{pD_{-1}} C_{D-Oil}(t_0) + k_{pD_1} C_{D-Water}(t_0) \right) \quad \text{(E.7)}$$

$$C_{D-Water}(t_1) = C_{D-Water}(t_0) + \Delta t\left(\frac{k_3 K_C C_{C-Water}(t_0)}{\Theta_V(t_0)} + k_{pD_{-1}} C_{D-Oil}(t_0) - k_{pD_1} C_{D-Water}(t_0) \right) \quad \text{(E.8)}$$

$$\Theta_V = 1 + K_A C_{A-Total} + K_B C_{B-Total} + K_C C_{C-Total} + K_D C_{D-Total} + K_{H_2}^{1/2} P_{H_2}^{1/2} \quad \text{(E.9)}$$

VITA

Menelik Negash

Candidate for the Degree of Doctor of Philosophy/Education

Dissertation: MODELING BIPHASIC REACTORS, EMULSIONS AND SELECETION OF SOLVENTS

Major Field: Chemical Engineering

Biographical:

Education:

Completed the requirements for the Doctor of Philosophy in your major at Oklahoma State University, Stillwater, Oklahoma in July 2017.

Completed the requirements for the Master of Science in Chemical Engineering at Addis Ababa University, Addis Ababa, Ethiopia in September 2010.

Completed the requirements for the Bachelor of Science in Chemical Engineering at Bahir Dar University, Bahir Dar, Ethiopia July 2004.

Experience:

- Research and Teaching Assistant, School of Chemical Engineering, Oklahoma State University, Stillwater, OK. January 2014-December, 2016.
- Assistant Production Manager, Dakasos Sankale Lime Factory, Ambo, Ethiopia. September, 2009-August, 2010.
- Lecturer, Bahir Dar University, Bahir Dar, Ethiopia. September 2010-August 2013,
- Graduate Assistant, School of Chemical and Food Engineering, Bahir Dar University, Bahir Dar, Ethiopia. July 2004-August 2007.

Professional Memberships:

- American Institute of Chemical Engineers (2014-present)
- National Society of Black Engineers (2014-present)
- Ethiopian Society of Chemical Engineers (2005-Present)